CELL PATTERNING FOR SPATIALLY

STANDARDIZED CELL BIOLOGY
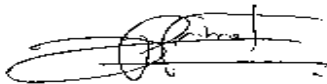
By
FRIMAT JEAN-PHILIPPE

Bachelor of Science
University of Edinburgh
Edinburgh, Scotland
2004

Master of Science
The University of Manchester
Manchester, England
2006

Submitted to the 'Fakultat Chemie' at the 'Technische Universität Dortmund', Germany in partial fulfillment of the requirements for the Degree of DOCTOR OF PHILOSOPHY, October 2010

Declaration

The work in this thesis is based on research carried out at the Leibniz-Institut für Analytische Wissenschaften -ISAS-e.V., Department of Miniaturisation, Dortmund, Germany. The work presented herein is my own work, unless referenced to the contrary in the text.

_____

Dortmund, November 2010

Acknowledgments

I owe my deepest gratitude to my supervisor, **Dr Jonathan West**, whose unwavering encouragement, guidance, enthusiasm and support has enabled me to be the scientist that I am today. I can never thank him enough.

I would like to thank **PD Dr Joachim Franzke** for his continuous support and without whom this thesis would not have been possible.

I am also grateful to Prof Dr Jan Hengstler and Dr Christoph Van Thriel (from IfaDo) for their support and valuable discussions on the development of the network formation assay project.

Special thanks to Heike Hardelauf with whom I have worked very closely for 2 years.

The completion of this thesis would not have been possible without the help from Dr Peter Jacob, Dr Raffael Kettler, Dr Dirk Janasek, Dr Cristina Cadenas, Sarah Waide, Julia Sisnaiske, Uli Marggraf, Ya-Yu Chiang, Marco Becker, Antje Michels, Silke Kittel, Norman Ahlman, Alex Bauer, Susanne Funken, Sasidhar Maddula, Melissa Mariani, Maria Becker, Peter Lampen, Magnus Eickmeyer and the ISAS workshop team.

Lastly, I offer my regards and blessings to my dearest ISAS colleagues: Ann-Kathrin Stark, Chandrasekhara Hariharan and Marc Vaudel.

"Simplicity is the ultimate sophistication"

Leonardo da Vinci

Abstract

The onus in modern cell biology is on the development of reproducible, The onus in modern cell biology is on the development of reproducible,

develop cell patterning capabilities that are accessible to biologists and to demonstrate new and innovative analytical methods based on the spatial control of cell positioning for widespread cell biology applications as well as fundamental research applications.

Plasma stencilling methods for cell patterning were developed which are simple, rapid, inexpensive, reproducible, effective and potentially universal cell line patterning techniques. PDMS micropatterning techniques were also developed to achieve a high resolution patterning capability over large areas and with absolute freedom of design while remaining efficient, cheap, simple and highly reproducible. These features make these methods accessible and desirable to biologists and microengineers alike. As a result from these developments, novel bio-analytical platforms were produced and innovative assays are presented. Cell patterning using these novel techniques was successfully used for the parallel and mass production of 3D spheroids, with high reproducibility and excellent control of the uniformity of spheroid size. A spatially standardized analytical display for high throughput neurotoxicity screening is also presented where cell patterning offers a route to standardize the neurite outgrowth lengths. In addition, a microfluidic system was also used to efficiently pattern and couple single cells by differential resistance pathway principles and validates the concept of using the natural behaviour of cells for mechanical operations within microengineered environments.

Taken together, this thesis demonstrates that it is possible to exploit cell micropatterning technologies for the realization of spatially standardized, highly reproducible and quantitative cell biology assays for both fundamental research and commercial applications.

Contents

1

Introduction

1.1 Background

Spatial organisation can be observed throughout the natural world and is essential to its proper function. From the direction and length of atomic bonds (10^{-11} to 10^{-15} meters) to the interactions of galaxies within the universe (10^{15} to 10^{18} meters), the presence of spatial organisation is critical for the establishment and understanding of the physical laws. In biology, cellular processes (10^{-6} to 10^{-9} meters) are also spatially organized. However, experimental methods for controlling spatial parameters during cell culture are largely non-existent and instead researchers rely on acquiring vast amounts of microscopy image data followed by careful interpretation using statistics. This thesis considers the application of microtechnologies for the development of new cell biology assays to provide exquisite spatial control.

Cell-matrix interactions are a key feature in cell biology and by understanding the required surface cues it is possible to select appropriate materials for cell patterning. The microenvironment of cells is key in deciding whether a cell will live or die, whether a cell can divide or not, whether a cell will produce insulin or not and lots of other behavioural responses. In other words, cell-matrix interactions dictate a cell's fate by triggering specific cellular pathways in response to specific stimuli. Extra cellular matrix (ECM) proteins found in living tissues orchestrate cell attachment and migration, providing a scaffold surface for cells to grow. Typically cell adhesion occurs in four steps: cell attachment, cell

spreading, organization of the cytoskeleton and the formation of focal contacts (Schaffner P and Dard MM*, 2002). Many matrix proteins are directly responsible for cell attachment and migration (Gelse K *et al* 2003). Integrins (part of the cell-adhesion receptor family) interact with the ECM and cytosolic components to activate intracellular signalling pathways that initiate a cells response to the microenvironment (Hynes RO *et al* 2002). These interactions have determining roles in processes such as proliferation and differentiation. By replicating these cell-matrix interactions cell biology can be accurately replicated *in vitro* for all manner of experimental studies. For example, cell adhesion to surfaces can be enhanced by surface cues, such as coating biomaterial surfaces with proteins of the ECM (fibronectin, laminin or collagen) or peptides (RGDs, Scaffner P and Dard MM*, 2002). The chemical modification of surfaces has been the focus of many investigations to study cell-surface interactions and to control cell adhesion and growth on materials (Michael KE *et al* 2003, Keselowsky BG *et al* 2003, Healy KE *et al* 1996, Maheshwari G *et al* 2000, Rajagopalan P *et al* 2004, Luk YY *et al* 2000).

1.2 Microfabrication for the life sciences

Microfabrication techniques have made it possible to produce micropatterns at the same length scale as living cells. The challenge has been to tailor traditional methods developed for solid-state processing, into methods suitable for manipulating the organic and molecular materials required for cell adhesion. Using micropatterned surfaces, many studies have focused on ways to investigate cytoskeletal architecture (Théry M *et al* 2006) and cell behavioural responses to different scales and geometries of the adhesive microenvironment (Bhatia SN *et al* 1999, Chen CS *et al* 1997). Cell-surface interactions are complex and vary in relation to different materials, different chemical and topographical cues and different types of cell. In order to spatially control cell-

surface interactions, it is possible to chemically engineer patterns on surfaces by a host of techniques, most notably by ‚soft lithography' which is described below (Whitesides GM *et al* 2001, Xia YN and Whitesides GM, 1998a and 1998b).

1.2.1 Photolithographic patterning

Lithography is a term used to describe a variety of techniques where the creation of a chemical structure is made by using masked light patterns. The first step when using photolithography is to design patterns (geometric features) using software such as autoCAD and contacting a manufacturing company to write the designed patterns on a mask (typically made of a quartz plate (glass) coated with non-transparent chromium). Such masks (quartz/chromium) can have features as small as 1-2 µm, with a line resolution of 100 nm. Importantly, these features can be replicated faithfully across a substrate and between substrates. The geometric patterns on the mask are transferred onto a substrate using UV illumination techniques. In order to achieve such a transfer, a photoresist thin polymer layer (UV-sensitive polymer) is first spin coated onto the wafer. This UV-sensitive material layer is then subjected to soft baking for hardening of the photoresist layer by solvent degassing. Both the coated-mask and substrate are brought in close contact (typically using a mask-aligner). UV exposure through regions of the mask without a chrome layer leads to the local activation of the photoresist. Areas shielded by the chrome pattern on the mask remain unactivated. With positive photoresists, this results in the irradiated areas becoming soluble and easily removable whereas unexposed areas stay insoluble, allowing the formation of an inverted image of the mask. With negative photoresists, the chrome pattern on the mask is replicated in the substrates photoresist. The patterned photoresist surfaces can then be used as masks in themselves for the selective treatment of the surface, either by the addition or the removal of materials. The patterned surface is finally revealed by dissolution of the patterned photoresist layers using solvents such as acetone.

In an excellent example of photolithography for cell patterning Healy KE *et al* (1996) showed that amino-silane/alkylsilane could be successfully patterned

and used for regioselective cell adhesion. Following the technique just described, the substrate was patterned with hydrophobic alkylsilane (uncharged). The photo-resist layer was then removed by lift off for coating these unmodified areas with a hydrophilic aminosilane (charged). This study clearly demonstrated that cells exhibited a preference for hydrophilic charged surfaces (coated with aminosilane) compared to hydrophobic uncharged surfaces (coated with alkylsilane).

1.2.2 Soft lithography: Microcontact printing (µCP) and Microfluidic printing (µFP)

Soft lithography was developed by George Whitesides and is an extension of lithographic patterning. In this technique, the production of elastomeric 3-D microstructures are used for patterning surfaces with biomolecules by microcontact printing (µCP) or microfluidic printing (µFP). The ability to pattern surfaces with proteins has become an essential and powerful tool in cell biology including protein microarrays, biosensors (Templin MF *et al* 2002), tissue engineering and regenerative medicine (Tan W and Desai TA, 2004, Christman KL *et al* 2006) and cell-patterning (Chen CS *et al* 1998).

1.2.2.1 Microcontact printing (µCP)

The µCP method is simple and cheap and was originally used as a patterning system for microelectronic devices (Kumar A and Whitesides GM, 1993) and was developed by Singhvi R *et al* (1994) to print self-assembled monolayer of alkanethiolates on gold surfaces. It was then introduced by Bernard A *et al* also in 1998 to directly stamp adhesion molecules onto cell culture substrates. A great variety of substrates as well as materials that can be deposited during imprinting can be used which has led to a great µCP diversity in biological applications (Xia YN and Whitesides GM, 1998a and 1998b). The µCP process first involves creating a microstructured master by conventional photolithography. Commonly, a thick-film photoresist material termed SU-8 is used, to produce distinctive 3-D

structures with near vertical side walls. The structured substrate is then used for moulding a liquid polymer resulting in the formation of an elastomeric stamp, which corresponds to the exact replica of the master. Typically the elastomer material is poly(dimethyl)-siloxane (PDMS). The mould (or liquid polymer) is then thermally cured allowing it to become hard and is then disassociated from the master, creating the elastomeric stamp (Figure 1.2.1(a)). Oxygen/air plasma treatment is often used on the stamp to increase the surface free energy for enhanced absorption (especially when PDMS is used).

It is important to note that the material used for creating the elastomeric stamp can impose a limitation in the topographical designs that can be replicated (Bietsch A and Michel B, 2000). The molecules to be printed are transferred to the stamp by a process often referred to as 'inking'. Typically the molecules, such as proteins, are dissolved in a buffer and aliquoted onto the microstructured surface of the PDMS stamp, or instead the inverted stamp is placed and floats on the buffer. During inking the molecules are transferred onto the microstructured surface. Once inked with the molecule of choice the microstructured stamps are first dried and then brought into contact with a substrate, with the transfer of molecules by physisorption acting to print the molecular pattern on the substrate. The elastomeric nature of the stamp enables excellent conformal contact with the substrate for good pattern transfer. Using this approach, functional proteins or synthetic peptides can be printed for the alteration of the surfaces adhesive properties (Figure 1.2.1(b 1-3)). For example, adhesion promoting proteins of the extra cellular matrix (ECM) (fibronectin (Lehnert D *et al* 2004), laminin (Lauer L *et al* 2001, Klein CL *et al* 1999), poly-L-lysine (James CD *et al* 1998) or synthetic peptides containing the ECM binding sites such as Arg-Gly-Asp (RGD) sequences (Scaffner P and Dard MM, 2002) have been printed as self assembled monolayers to produce geometrically controlled patches for cell patterning. The intervening spaces in between adhesion proteins printed by µCP can then be passivated with molecules, such as serum albumin, which resist cell adhesion in order to confine the cell adhesion pattern. In an alternative way, molecules which resist protein adsorption and cell adhesion, notably

poly(ethylene glycol) (PEG) (Singhvi R *et al* 1994, Mrksich M *et al* 1997, Chen CS *et al* 1998) (Figure 1.2.1(b 4)), can be patterned by µCP and cell adhesion proteins or peptides can subsequently be used to backfill the intervening spaces.

An important observation regarding the conservation of protein/peptide functionality during the printing process was demonstrated by Graber DJ *et al* (2003). In this study, they have reported a long list of different stamped proteins and peptides used in biological experiments after successful printing, which retained their full properties. Furthermore, another approach to print both cell-adhesive and cell non-adhesive structures can be achieved by printing supported lipid bilayers. Different cell-adhesion properties can be achieved depending on lipid composition, as shown by Hovis JS *et al* (2001). Although functionality of molecules that have been patterned on the stamp have been demonstrated, a major problem is that the stability of these molecules are not sufficient for long-term cell-biology experiments, especially when these are not covalently bound to the substrate. As suggested by different groups, techniques exist to overcome this issue. For example, chemical activation of polymeric surfaces (Lahann J *et al* 2002 and Hyun J *et al* 2001) and silanization of glass or silicon oxide coated surfaces can offer ways to form covalently linked patterns to stabilize the printed molecules (Cornish T *et al* 2002, Wheeler BC *et al* 1999 and Scholl M *et al* 2000).

However, limitations exist when using µCP techniques. Such limitation includes the control of ligand density (when cell-culture media is added on the substrate, exchange and degradation of the printed molecules are likely to occur) (Nelson CM *et al* 2003). Importantly, it remains challenging to produce patterns of uniform quality in a reproducible fashion. Pattern reproducibility across chip and between chip to chip and batch to batch is problematic as reported by Fink J *et al* 2007.
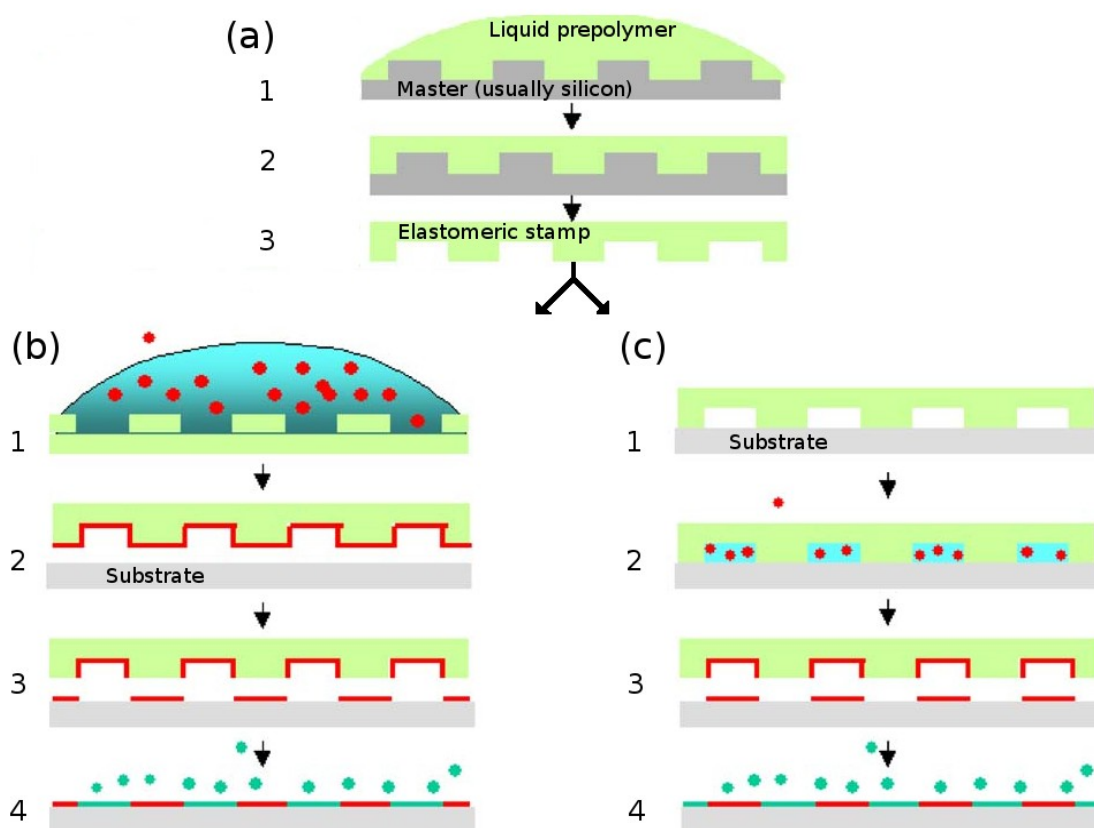
Figure 1.2.1: Schematic of the microcontact printing (µCP) and microfluidic patterning (µFP) techniques. The two methods share the common procedure of creating a stamp of suitable structural dimensions. **(a)** A liquid pre-polymer is casted on the structured master surface (1). After curing 2) the elastomeric stamp is ready for use (3). **(b)** In µCP the stamp is inked with the solution containing the (bio)molecules to be printed (1). The biomolecules are transferred by printing onto the substrate (2). Following the removal of the stamp (3) the surface is backfilled with the second (passivating) molecular solution (4). **(c)** In µFP the stamp is first brought into tight contact with the substrate (1). The patterning solution is afterwards introduced into the channels (2), usually using capillary forces. After adsorption of the molecules of interest the stamp is removed (3) and the remaining area backfilled with a passivating solution (4). Adapted from Falconnet D *et al* 2006.

1.2.2.2 Microfluidic patterning (μFP)

Microfluidics can also be used to pattern surfaces. The approach is called microfluidic patterning (μFP), with the elastomer structured to contain microfluidic channels for injecting and routing the molecular ink across a substrate. As before, molecule transfer results in the formation of a pattern on the substrate. Fluid can easily be applied by pressure, capillary forces or electro-osmotical driven flows (Fiorini GS and Chiu DT, 2005). The process is illustrated in Figure 1.2.1(c 1-4). The chemistry as well as the different substrates that can be used are essentially the same as the ones used in μCP. One major advantage with using μFP is that patterns can be created on wet surfaces. This is of particular relevance for studying the functionality of sensitive surface printed biomolecules. Another key feature of μFP when compared with μCP is that there is a greater control in surface-ligand density. One major disadvantage of μFP is that typically, only linked network structures can be patterned, rendering the formation of dense arrays difficult. To overcome this, multi-layer microfluidic systems can be used (Anderson JR *et al* 2000) with repeated deposition of molecules in combination with rotation of the microchannel device producing the array (Delamarche E *et al* 1998).

1.2.3 Stencil-assisted patterning

In this rather simple technique, which can be regarded as an extension of μFP, a perforated membrane, termed stencil, is placed on top of the substrate so that when the stencil and the substrate are combined, only the areas of the substrate which are exposed by the through holes in the stencil are modified (whereas the remaining areas are protected by the stencil). Therefore, access to the surface/substrate is limited by the patterns defined by the stencil, and only on these areas can the substrate be chemically patterned or used for cell seeding without coating the substrate. A good example of this is reported by Folch A *et al* (2000) and Ostuni E *et al* (2000). In their studies, they have successfully used PDMS stencil (produced using photolithography) for direct cell patterning without

altering the chemistry of the substrate (Figure 1.2.2). Once the stencil is peeled off, every cell population will outgrow their pre-defined areas and such systems could be used to study cell migration and proliferation behaviours but also to generate co-cultures of different cell types. In the latter, the holes in the stencils pre-limits the areas to which the first cell type can attach and grow, but once the stencil is removed, a second type of cells can be seeded.
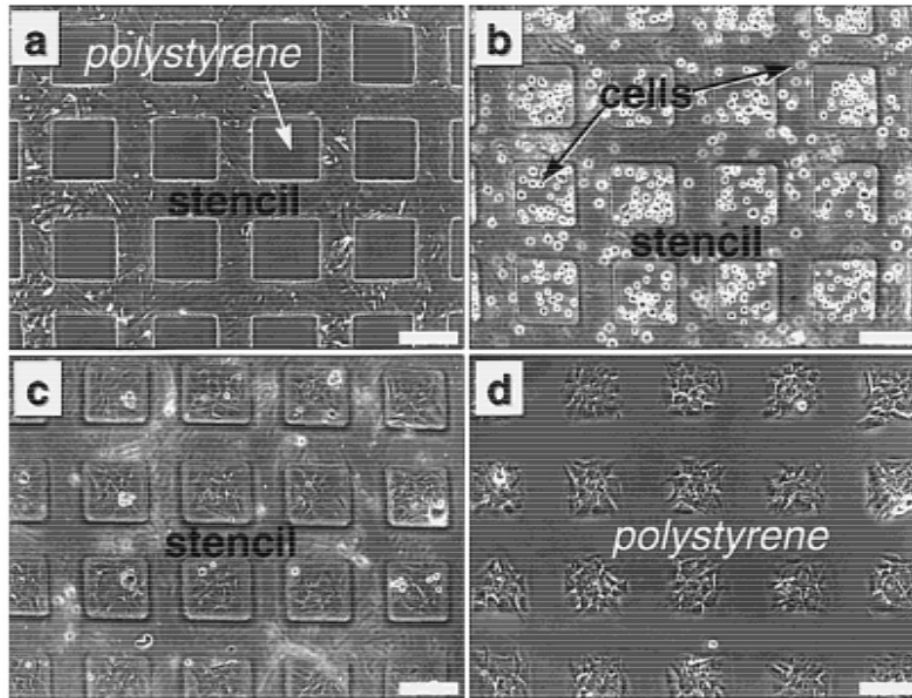
Figure 1.2.2: Sequence of phase-contrast micrographs depicting the creation of a cellular micropattern by means of a 100-µm-thick stencil containing 140-µm-side square separated by 100 µm. **(a)** The stencil is applied to a polystyrene surface and covered with seeding medium; **(b)** the cell suspension is dispensed; **(c)** cells after full attachement and spreading at the bottom of the holes (cells attached onto the stencil are out of focus); **(d)** cells after removal of the stencil. Scale bar = 100 µm. Taken from Folch A *et al* 2000.

Using this approach, Thomas CH *et al* (1999) generated a grafted interpenetrating network poly(acrylamide-co-ethyleneglycol) layer on a glass surface which resists cell adhesion. They then used O_2 plasma treatment through the stencil features (small holes), removing the cell resistant coating locally and showed that cell stability on the patterns could last for up to 60 days in culture. In

addition, any substrate material can be used with elastomeric stencils, even curved surfaces, and the immobilisation of more fragile molecules can be achieved as no organic solvents are required in the preparation.

More recently, the introduction of focused ion beam milling in stencil-assisted patterning have lead to the development of a new generation of stencils allowing both micro and nano features to be combined (Kim GM *et al* 2003). These have open the way to higher resolution protein immobilization and cell patterning and may offer great potential in biological applications. However, these methods involve the use of hard, brittle materials with small features punctured in thin (micron-scale) membranes. These materials prevent conformal contact with rigid substrates and are prone to breaking during handling.

1.2.4 Photoimmobilization and photoactivation micropatterning

In addition, chemical micropatterns for cell attachement can be created via surface-immobilized photoreactive molecules. Here the generation of patterns involves the irradiation of photoactive surfaces and the use of a photomask to utilize photons as reagents for pattern formation (Fodor SP *et al* 1991). This technique has been used to generate micron-sized architectures by controlling the deposition of a wide variety of particles such as proteins (Rozsnyai BF *et al* 1991), DNA (Pease AC *et al* 1994), cells (Dillmore WS *et al* 2004) and nanoparticles (Chen SJ *et al* 2004). The methods directly pattern the surface, eliminating the small losses in resolution associated with the additional steps used in standard photolithography. Hypolite CL *et al* (1997) used UV or laser activation of benzophenone groups to attach and immobilize the Arg-Gly-Asp (RGD) sequence to ethylene glycol modified alkanethiols.

Different methods can be used to photo-activate surfaces, as shown by Conrad PG *et al* in 2003. In this study, they used laser light photoactivation using a 20-μm-diameter beam and demonstrated the ability to generate complex as well as heterogeneous patterns. In addition, Dillmore WS *et al* in 2004 reported a scanning type of lithography involving the use of a microscope objective and a mercury lamp to activate the surface. They demonstrated that serial photo-

activation could be achieved to generate high-resolution patterns using scanning near-field optical microscopy (SNOM). The main disadvantage of this technique is that oxidation of thiols (i.e. alkanethiols) molecules may occur making this approach unsuitable for long term cell cultures. Photochemical micropatterning of carbohydrates on glass has also been achieved (Carroll GT *et al* 2006). They demonstrated that by utilizing SAMs containing phthalimide chromophores they could successfully immobilize carbohydrates on a flat substrate, irrespective of molecular weights (MWs). The immobilized carbohydrate antigens are shown to retain their ability to interact with the corresponding antibody and in addition, the photochemical nature of this technique allows large libraries of carbohydrates to be immobilized without previous derivatization (Carroll GT *et al* 2006). Other groups have shown that UV-directed light can also be used to directly pattern cells (Fink J *et al* 2007) (Figure 1.2.3).
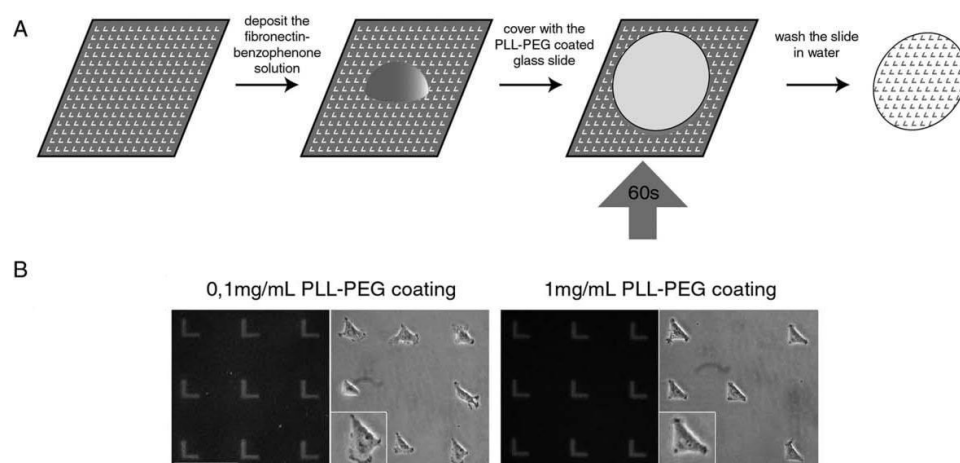
Figure 1.2.3: UV-directed light micropatterning. **(A)** Fabrication method. A droplet of the fibronectin-benzophenone grafting solution was deposed on an optical chromium photomask. A PLL-g-PEG coated glass slide was placed on the droplet. The slide was exposed to UV light (310–460 nm) through the photomask for 60 s. The glass slide was washed twice with distilled water. **(B)** Resistance of the PLL-g-PEG coating to non-specific fibronectin grafting. UV-exposure was performed with low (0.1 mg/mL, left) and high (1 mg/mL, right) concentration of the grafting solution. In the first case, the cells managed to spread out after a few hours (left). In the second case, cell spreading out of the pattern was significantly reduced (right). Taken from Fink J *et al* 2007.

1.2.5 Mechanical cell patterning

1.2.5.1 Micromechanical reconfigurable cell cultures

Other techniques exists to engineer microstructures or surfaces for cell-based assays. Hui EE and Bhatia SN (2007) have developed a silicon comb device to micromechanically control cell-cell interactions and measured intracellular communication between hepatocytes and supportive stromal cells in co-culture. Here, cell patterning onto the comb device is achieved by functionalization of the silicon with polystyrene followed by plasma treatment, resulting in a surface comparable to tissue culture. Different modes of contact can be used to dynamically monitor cell-cell interactions with temporal control (Figure 1.2.4). Cultures can be mechanically switched to initiate contact between the two cell population and they showed that hepatocytes viability is dependent on the proximity of the stroma cells.
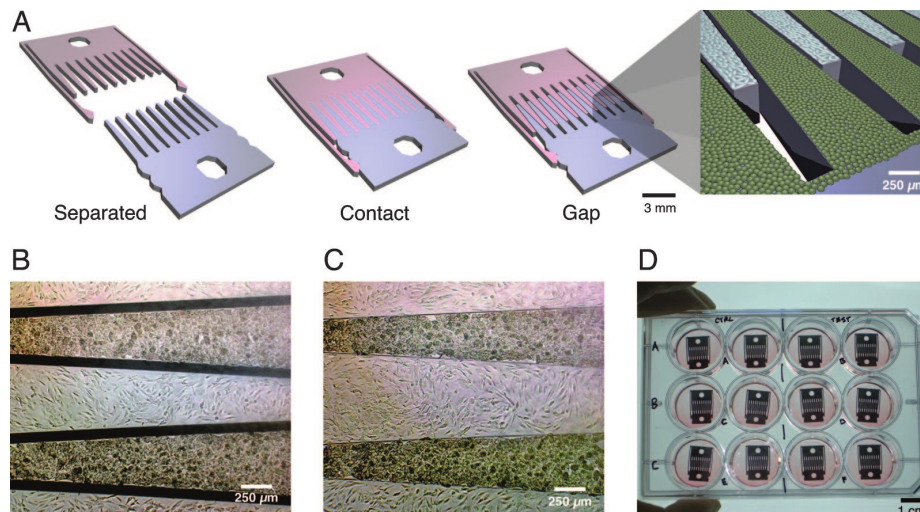
Figure 1.2.4: Micromechanical reconfigurable culture (µRC). **A:** Microfabricated silicon parts can be fully separated (Left), locked together with comb fingers in contact (Centre), or slightly separated (Right). **B and C:** Cells are cultured on the top surfaces. Sliding the parts by 1.6 mm changes the gap between the fingers by only 80 µm. Bright-field images of hepatocytes (darker cells) and 3T3 fibroblasts cultured on the comb fingers. **D:** Devices in a standard 12-well plate. Taken from Hui EE and Bhatia SN, 2007.

1.2.5.2 Electromagnetic: Optical tweezing and dielectrophoresis

Physical techniques can be used for cell positioning. As early as 1987, Ashkin A *et al* reported that in order to control the spatial organisation of living cells on surfaces, optical forces such as a focused laser light, an optical tweezer, could be used. Using this approach, controlling the movement of single cells can be achieved by applying a focused laser beam to cells or peptides that have a higher refractive index than their surroundings allowing one to trap these cells (or peptides) into „optical pockets". Cells are captured by the laser beam as they pass into the light path and it is the interfaces between two different refractive indexes (commonly referred as optical tweezers) that creates the optical force that is applied to the cells. Cell movement responses can therefore be controlled by „redirecting" the laser beam at the interface, applying a force in the order of piconewtons. Control of cell geometries can be achieved on large areas (up to 7 mm) and cell movement speed has been recorded to be as high as 50 µm/s (Odde DJ and Renn MJ, 2000). The use of optical force has also enabled the extremely efficient development of cell sorting technologies (McDonald MP *et al* 2003) and also allows patterns of different cell types to be generated with nanometer precision (Nahmias YK *et al* 2004). Optical tweezers are useful tools for parallel cell trapping (Akselrod GM *et al* 2006). Similarly multiple dielectrophoresis (DEP) traps can be used for parallel cell positioning. For example, radial DEP patterns produced with concentric stellate tip electrodes have been used for structuring hepatocytes populations to mimic liver morphology (Ho CT *et al* 2006) and an integrated circuit DEP platform has been used for programmable cell transport and trapping (Hunt TP *et al* 2007). It is important to note that although electromagnetic trapping methods presents many advantages, only cells in suspension can be positioned.

1.2.5.3 Microfluidics for cell positioning

Although the general approach to pattern cells is based on the modification of surface properties, microfluidic-based techniques are increasingly being used for

cell positioning and the development of cell based assays (Beebe DJ *et al* 2002, Takayama S *et al* 2003, Folch A and Toner M, 2000). The major goal is to have a high throughput approach for positioning small populations or single cells at desired locations. Importantly, the microfluidic array format is suitable for both adherent and suspension cell cultures. The physics governing microfluidic systems can be found in detail in two excellent reviews by Beebe DJ *et al* (2002) and Stone HA *et al* (2004). In theory, efficient miniaturization of microfluidic systems can also facilitate massive parallelization and serial processing through multiplexing (Craighead H *et al* 2006, deMello AJ *et al* 2006, El-Ali J *et al* 2006, Yager P *et al* 2006, Lanigan PMP *et al* 2008). Microfluidic platforms have also been developed for high-throughput (HTP) and parallel screening of a large number of conditions. For example, Hung PJ and Park JK (2005) have integrated a concentration gradient generator inside a microfluidic cell culture array allowing many growth conditions to be analysed in a combinatorial fashion.

Although controlling surface properties can be utilized for cell positioning inside microfluidic devices, 'fluidic trapping', the mechanical trapping of cells using fluidic differential pathways has also been used. Using this approach, cells are typically loaded within a flow and follow the fluidic path of least resistance until they get captured by sub-cellular-sized openings within the channels. Once trapped, the cell blocks the opening and diverts the streamlines to exclude subsequent cells. Following the mechanical positioning of cells by these differential fluidic pathways, various analysis can be performed. For example, Yang M *et al* (2002) have used this principle to dock HL-60 cells inside parallel dam-like structures and measured the ATP concentration threshold that induces significant intracellular calcium signalling. The fluidic differential pathways principle can also allow the sequential trapping of single cells along a row of microfluidic exits. Using this approach, Khine M *et al* (2005) have developed a polymeric microfluidic chip that can selectively immobilize and locally electroporate HeLa single cells using low applied voltages (< 1 V) and in a parallel fashion while demonstrating a higher electroporation efficiency than conventional techniques. For applications requiring high density single cell

arraying, 2-layer microstructured traps can be constructed to trap single cells by intelligent use of fluidic streamlines. A good example is the microfluidic platform for single cell arraying developed by Di Carlo D *et al* (2006) showing high-density arrays of single cells produced solely on hydrodynamic principles inside a microfluidic device (figure 1.2.5). Here arrays of single cells allows the quantification in the distribution of behavior amongst a population of individual cells for the identification of rare events otherwise masked in the overall cell population profile.
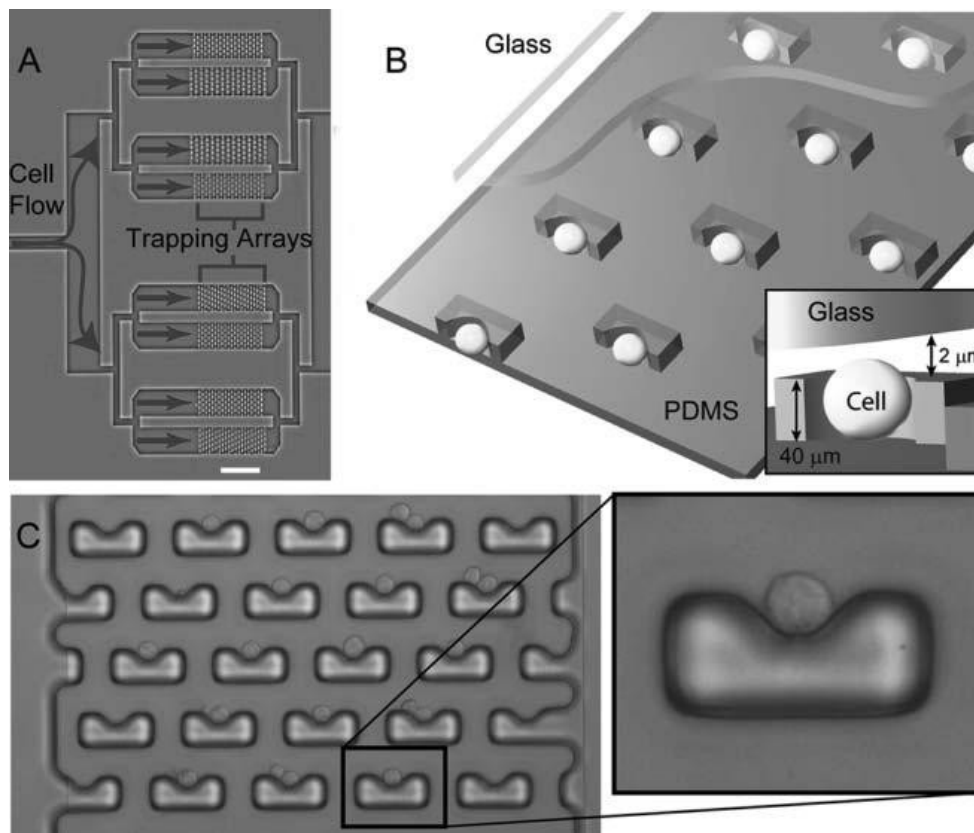
Figure 1.2.5: Single cell trapping arrays. **(A)** A photograph of the cell trapping device is shown. (Scale bar = 500 μm). **(B)** Mechanism of trapping is presented. Traps are moulded in PDMS and bonded to a glass substrate. Trap size biases trapping to predominantly one or two cells.**(C)** A high resolution bright field micrograph of the trapping array with trapped cells is shown. A magnification shows the details of the trapped cell. (Taken from Di Carlo D *et al* 2006).

Finally, using similar fluidic streamline principles as DiCarlo D *et al*, Skelley AM *et al* developed a microfluidic device for efficient cell pairing and fusion (Skelley AM *et al* 2009). In this system, a 2-layered device was used with an ingenious method to position two different cells together with single cell pairing efficiencies of up to 70%. Briefly, single cells are transported into single-cell-sized traps, followed by flow reversal to reverse park single cells in a trap positioned opposite the first trap. The second trap is sufficiently large to accommodate two cells. Introduction of second cell type leads to the fluidic pairing with the first cell type. The trap size limits more than two cells occupying the same trap. Using this device, electrical fusion of paired cells was successful, with membrane reorganization efficiencies of up to 89% and with over 50% of properly paired and fused cells over the entire device, 5-fold greater than with a commercial electrofusion (Skelley AM *et al* 2009).

1.2.6 Other methods for cell patterning

1.2.6.1 Ink-jet printing

It is also possible to directly generate chemical patterns by using ink-jet technology with the jetting of proteins or alkanethiols onto surfaces. This has been shown by many groups (Pardo L *et al* 2003, Roth EA *et al* 2004, Sanjana NE *et al* 2004 and Turcu F *et al* 2003) who have successfully demonstrated that by small modification of commercially available ink-jet printers, one could use this technology to directly print cells onto gel membranes and other types of substrates. The use of multiple nozzle devices can also allow multifunctional surfaces to be made and multiple compounds can be jetted onto the same spot. Unfortunately, the current method is limited by the nozzle diameter, the original resolution of the printer and the tensions occurring at the liquid/solid interface have a direct impact on spot size and resolution that can be generated (the smallest reported spot is ~100 µm). Nevertheless, the use of ink-jet technology in biological research and applications has the potential to generate cell arrays in a

high throughput manner. In addition, laser printing can be used for biomolecule patterning. Barron JA *et al* (2005) developed a biological laser printing (BioLP) method which is a non-contact, orifice-free technique that enables the deposition of biological molecules with a spatial accuracy of up to 5 µm. They also demonstrated the first steps towards using BioLP to engineer heterogeneous three-dimensional constructs that could be used in tissue engineering applications and cell experiments.

1.2.6.2 Laser ablation

Alternatively, laser ablation techniques could be used to design sub-cellular features of 1 µm in size. Laser ablation was used on electron beam-grafted cell-repellent polymers by Yamato M *et al* (2003) and they reported that laser-patterned fibronectin pre-coated tissue culture polystyrene could be successfully used to culture hepatocytes for up to two weeks.

1.2.6.3 Plasma patterning and glow discharged plasma deposition

Plasmas can be used to produce micropatterns on substrates by surface oxidation or material deposition that can be used for cell adhesion and patterning. Plasma is a substance similar to gas with the difference that plasma contains ionized particles. Plasma generator systems are able to ionize gases in a vacuum system by using radio frequency (RF) excitations typically in the MHz range but also at lower frequencies (KHz) as well as higher (microwave). The type of atoms in a plasma, the ratio of ionized to neutral particles and the particle energies all result in a broad spectrum of plasma types, characteristics and behaviours. The glowing gas that carries electricity between two electrodes when voltage is applied between them is termed a plasma discharge. In the context of this thesis, the use of plasma (created by radio-frequency (MHz) glow discharge) can be used to treat surfaces to impart certain characteristics but also to deposit polymeric films of various thicknesses (from a few nanometres to micrometers) on different substrates. Film deposition (such as fluorocarbon films) by RF-glow discharge has found wide applications in microelectronics, aerospace,

automotive and biomedical industries (Favia P *et al* 2003). A discharge deposition process has also been used to produce patterns of biomaterials for two-dimensional *in vitro* cell cultures (Barbucci R *et al* 2005). As demonstrated by Goessl A *et al* (2001), plasma lithography, combining plasma deposition with photolithography, can also be used to produce surfaces with contrasted properties. Essentially the final surface contained both hydrophobic cell adhesion promoting areas and hydrophilic cell repellent background. Smooth muscle cells are shown to grow on the hydrophobic cell adhesion promoting areas for at least 14 days, maintaining pattern fidelity. It is important to note that plasma lithography has limitations. For example, the production of highly stable plasma polymer layers is often regarded as complex and optimal conditions to prevent de-lamination are tedious and time consuming.

Oxygen plasma systems (low frequencies systems) have been used to produce surface oxidation patterns for cell patterning investigations by regio-selective activation. Using an oxygen rich vacuum environment (200-600 mTorr), a low frequency plasma (30 W) was used in combination with microfluidic stencils for regio-selective stripping of cell adhesion coatings (poly-l-lysine) producing molecular patterns for cell adhesion (Rhee SW et al 2005). In addition, low pressure RF oxygen plasma discharges can be used to produce oxidation patterns on partially masked hydrophobic polystyrene (Detrait E *et al* 1998). An oxygen plasma operating at 150 W and 1 Torr was also used with a stencil to produce patterns suitable for cell adhesion on a protein repelling interpenetrating polymeric network (IPN) of poly(acrylamide) and poly(ethyleneglycol) (P(AAm-co-EG)) grafted to glass substrates (Tourovskaia A *et al* 2003). In all cases, protein adsorption prior to cell seeding was required for successful cell patterning.

1.3 Cell patterning and cellular behaviour

The spatial control of cells using micropatterning techniques enabled important biological results to be obtained in the field of apoptosis (Chen CS *et al* 1997), in the control of the cytoskeletal architecture (Théry M *et al* 2006a), cell internal organization (Théry M *et al* 2006b) and division axis (Théry M *et al* 2005). As discussed previously, microfabrication and engineering of micropatterned surfaces to control cell adhesion and spreading have proven useful for providing a basic understanding of cell behaviour. It has been reported that patterning techniques can be a useful tool for the onset or inhibition of cellular differentiation processes. Two important features can be controlled with cell patterning: the size and the shape of the pattern adhesion footprint.

1.3.1 The impact of cell adhesive footprint size on cell function

The size of the adhesive footprint can be used to control certain cellular characteristics. There is evidence that controlling the cell's size using engineered micropatterned surfaces can elicit a change in the phenotype of the cells. Singhvi R *et al* (1994) showed that by controlling hepatocyte cell size on micropatterned surfaces, albumin secretion could be altered. Chen CS *et al* (1997) showed that confining cells to a restricted area for growth can elicit a forced apoptotic cascade. More interestingly, another observation was made in a study focussing on stem cell differentiation (McBeath R *et al*, 2004). When mesenchymal stem cells (MSC) are allowed to spread out they tend to differentiate into an osteoblastic phenotype whereas when they keep a round morphology they tend to differentiate into a more adipocytic phenotype (McBeath R *et al*, 2004, Gregoire FM *et al* 1998, Sikavitsas VI *et al* 2001). Chondrocyte cells *in vivo* also maintain a rounded morphology whereas when grown *in vitro*, they rapidly de-differentiate into a very flat and spread fibroblastic morphology and phenotype (Brodkin KR *et al* 2004). Similarly, the majority of the literature claims that a very flat and spread oesteoblast morphology is the sought after morphology for

biomaterials and tissue engineering scaffolds yet *in vivo* oesteoblasts maintain a more 3-dimensional morphology (Tsuang YH *et al* 1997, Sikavitsas VI *et al* 2001, Bosetti M *et al* 2007, Hamilton DW *et al* 2007, Xu JL *et al* 2008, Huang W *et al* 2007). There is therefore clear evidence that controlling the size of the cells can lead to the control of its fate and function.

1.3.2 The impact of adhesive footprint shape on gene expression

Stress levels relating to changes in cell shape and the cytoskeletal organisation (change in cellular morphology) can affect the nucleus and can subsequently disturb organelles and DNA organization and distribution leading to changes in the cell's function (Alvarez M *et al* 1997 and Maniotis AJ *et al* 1997). Although the exact impact of cell morphology related to cell function remains largely unknown, a few hypotheses have been put forward. The relation between cell shape and resulting gene expression may be due to a direct link between the cytoskeleton and the nucleus by mechanical force- i.e. mechanotransduction (Maniotis AJ *et al* 1997, Ruoslahti E and Vaheri A, 1997). Nuclear matrix proteins (NMP-1 and -2) are thought to play a key role as they can directly interact with gene promoter sequences (Bidwell JP *et al* 1998) and are part of the nuclear scaffold that is able to affect DNA supercoiling. As NMP-DNA interactions can modulate gene expression, these architectural transcription factors could have determining effects on the regulation of transcription as a result of cell and nucleus deformation.

It has also been suggested that the activity of Rho family GTPases can be influenced by the cell's morphology and various studies have demonstrated that Rho GTPases are essential to the proliferation and differentiation of cells (Hill CS *et al* 1995, Ren XD *et al* 1999, Takano H *et al* 1998 and Welsh CF *et al* 2001). Subsequently, Rho GTPases may have a cytoskeletal-dependent critical role in cellular development and cellular functions (Sordella R *et al* 2003). McBeath R *et al* (2004) also reported that the RhoA-ROCK signalling pathway mediated a commitment switch for stem cells in response to actin-myosin-generated tension and controlling RhoA activity could eliminate the need for soluble differentiation

factors. Therefore, the control of cell shape is critical for the commitment of stem cell fate. Furthermore, nuclear shape changes can be modulated via cell morphology alterations and can therefore play a role in cell growth control and influence cell-surface interactions (Thomas CH *et al* 2002).

Although little work has been done in this area to understand how cell morphology affects gene expression, differentiation, proliferation and apoptosis, it has been widely recognised that the relationship between morphology/shape, mechanotransduction via the cytoskeleton and cell adhesion are likely to play a key role in the relationship between form and function in cell-surface interactions but also in tissues and organs.

1.4 Spatially standardized cell biology

The application of micropatterning techniques has led to great advances in our understanding of the effects of size and shape on cell function. However, beyond basic science, microtechnologies remain largely untapped for addressing a large number of widespread and industrial applications.

The spatial standardization of biological cell cultures through cell micro patterning can in theory be used for the development of innovative, quantitative, rapid, inexpensive and reproducible assays in cell biology. Cell biology naturally tends towards an apparently chaotic state *in vitro* due to a lack of structure and organisation within the cell culture environment. Better control of the pattern of the adhesive environment can be used to produce well defined *in vitro* cell cultures and lead to the development of more organised cell culture systems for a better representative and biologically relevant *in vitro* system. Improving the spatial control of cells within a culture can also lead to a better reproducibility of a given experiment and allows parallelization of the same experiment for rapid high throughput screening experiments. But as mentioned previously, only very limited industrial applications have been found for such a powerful capability that has

been around and available now for over 10 years. One reason could be that the vast majority of the techniques available to produce patterns for cells are essentially developed by and used by microengineers and not biologists.

1.4.1 Microfabrication for biologists

Successful cell patterning means that cells show good adhesion on the patterned substrate with long term confinement. As described previously, there is a myriad of techniques available to pattern cells. Most of these are performed by bioengineering teams that have both the expertise and equipment to successfully produce surfaces for cell patterning. When biologists adopt such technologies, they are often faced with problems that are not mentioned in relevant publications. Or, more commonly, the type of equipment and required laboratories are simply not available to the biologists. The challenge is to develop or adapt micropatterning techniques in laboratory settings dedicated to cell biology (Fink J *et al* 2007). Nevertheless, it is increasingly common to outsource parts of the microfabrication process, most notably the masters for moulding PDMS stamps, microfluidic channels or stencils. The remaining challenges are to develop methods which are reproducible, straightforward and rapid.

Alternatively, there is scope for cell microchips to be commercially available. Compatibility with a maximum of cell culture substrates is also highly desirable. For example, patterning cells inside commercially available multi-well plates would have tremendous impact on automated analysis for high content cell based screening. The efficiency by which cells can be patterned and confined within the patterns is also highly critical. To date, no such technique exists that allows biologists to easily experiment with cell patterning. µCP is by far the simplest method to pattern cells due to the fact that no specialized equipment is needed, all reagents are commercially available, affordable, non-toxic and stable, and no expertise in chemistry is required. These attributes have favoured µCP as the technique of choice for cell patterning but still requires considerable efforts and patience for the in-house development of a reliable technique. Furthermore, drawbacks such as the degradation of the printed

molecules under cell culture conditions (Nelson CM *et al* 2003) and issues relating to pattern reproducibility across the substrate remain problematic. To further improve the uptake of cell patterning methods in laboratories dedicated to biology, novel micro patterning techniques that fulfils the above mentioned criteria are needed.

1.5 Summary of thesis

The research presented in this thesis has several aims for the development of spatially standardized, quantitative and high throughput cell biology assays. In chapter 2 a novel air plasma stencilling method was developed for producing cell adherent hydrophilic patterns on hydrophobic substrates. This simple technique is suitable for adoption by biologists within biology laboratory settings. The method is also highly appropriate for inclusion of cell patterns within microfluidic devices but is, however, not readily suited for the production of cell arrays. To address this, in chapter 3 a novel thin film PDMS printing technique based on the classical µCP method was developed which offers absolute freedom of design along with the benefits of simplicity, high resolution, reproducibility and low cost. The technique uses standard tissue culture substrate materials for cell adhesion with patterns confined using a nanoscale-thick cell repellent PDMS film. To demonstrate the potential of thin film PDMS patterning, the array format was used for the mass production of uniform 3-D tumour spheroids, showing great potential for drug discovery and screening as well as fundamental tumour biology research. Chapter 4 examines another application for the thin film PDMS micropatterns: An innovative spatially standardized neurite outgrowth analytical display called the network formation assay (NFA) was developed. The array format provides assay coordinates, defines neurite length and measures connectivity. Together these features enable the rapid and reproducible screening of the neurotoxic potential of test substances. In chapter 5, the research explored the potential of microfluidics for the highly parallel arraying of heterotypic single cell couples for the investigation of contact modes of

communication during heterotypic co-culture. A differential fluidic resistance approach was used in combination with a novel cellular valving concept for coupling single cell pairs, with the maintenance of the co-cultures dependent on the plasma stencilling method presented in the first research chapter.

Taken together, this thesis demonstrates that it is possible to exploit cell micropatterning technologies for the realization of spatially standardized, highly reproducible and quantitative cell biology assays for both fundamental research and commercial applications. The thesis presented herein is truly interdisciplinary, combining plasma technology, material patterning, surface analysis, microfluidics and cell biology for the development of spatially standardized cell cultures.

2

Plasma Stencilling Methods for Cell Patterning
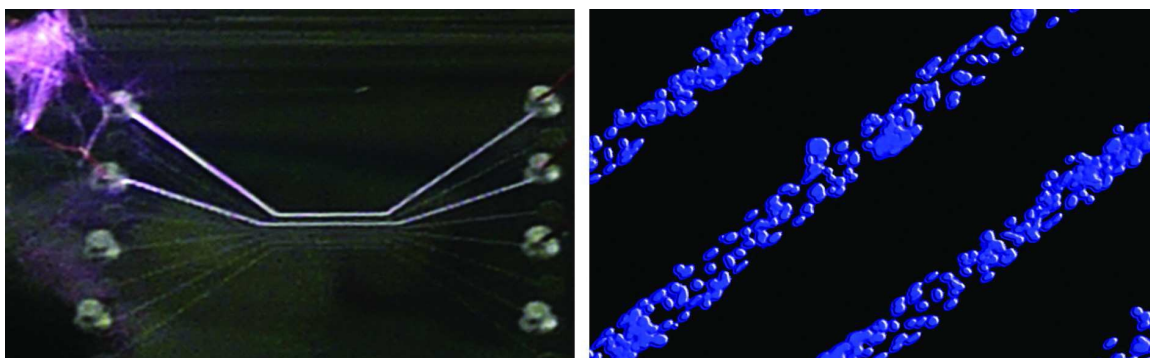
2.1 Introduction

This chapter describes the development of plasma stencilling methodologies for cell patterning. Commonly, plasmas are used for surface activation which results in charged and increased absorption properties of the treated surface and can also act as an effective surface cleaner. Typically, a plasma is generated by electrical ionization of a gas inside a vacuum. The glowing gas that carries electricity between the two electrodes when voltage is applied is termed a plasma discharge. The type of atoms in a plasma, the ratio of ionized to neutral particles and the particle energies all result in a broad spectrum of plasma types, characteristics and behaviours. Although radiofrequency (MHz) plasma generators are typically used for surface activation, dielectric barrier discharge (DBD) device which operate at lower voltages and frequencies (kHz) have also been used to produce plasma discharges. In this study, the generation of surfaces with contrasting wetting properties was achieved using an atmospheric plasma produced by a Tesla generator or by DBD systems in combination with a microengineered stencil. When using such devices, the plasma activation process through the stencil results in the regio-selective oxidation of the treated surface which leads to an increase in hydrophilicity and charging.

As described in the introduction (section 1.2), most patterning techniques involve the use of chemical or molecular coatings to generate cell adhesive and cell resistant areas. For example, through hole PDMS stencils have been used to pattern extra-cellular matrix (ECM) proteins for cell registration (Ostuni E *et al* 2000). Capillary flow has been used to load and pattern proteins and cells using microfluidic stencils in conformal contact with a variety of heterogeneous and even microstructured substrates (Folch A and Toner M*,* 1998). Following cell loading and cell adhesion to the substrate, the stencil can be removed allowing another cell type to be co-cultured in between the micropatterns. Alternatively, different cells can be loaded in different channels to produce a mixed cell culture system (Folch A and Toner M, 1998). As mentioned previously, plasma systems

have also been used in combination with microfluidic stencils for regio-selective stripping of cell adhesion coatings (poly-l-lysine) producing molecular patterns for cell adhesion (Rhee SW et al 2005). Low pressure RF oxygen plasma discharges can also be used to produce oxidation patterns on partially masked hydrophobic polystyrene (Detrait E *et al* 1998). In all cases, protein adsorption prior to cell seeding was required for successful cell patterning and plasma activation was performed under vacuum conditions. In addition the plasma activated surfaces needed modification with either cell repellent or cell adhesive molecules prior to plasma exposure.

In this study, an atmospheric pressure air plasma (30 kV at 2 MHz) was used in combination with microengineered stencils for selective oxidation of hydrophobic PDMS, methylated glass and polystyrene substrates for patterning 10 different cell lines without the need for further surface modification steps. This approach eliminates the need for coating surfaces with adhesion molecules or cell repellent species and works on the sole principle that hydrophobic PDMS is cell repellent whereas hydrophilic PDMS allows cell adhesion. This finding greatly simplifies the patterning process and is able to produce highly effective, reproducible and long term cell patterns. The use of Tesla generators for plasma ignition also obviates the need for gas supplies or vacuum conditions during plasma activation treatments. Patterning of parallel and orthogonal tracks as well as arrays was achieved using three different stencil materials: a PDMS microfluidic stencil, a polyimide stencil with micromachined through holes and a glass multi-microcapillary system functioning as a dielectric barrier discharge (DBD) system. Plasma stencilling methods are also compatible with plasma bonding techniques, where the same plasma treatment can be used for cell patterning and device sealing. This offers a simple route to undertake experiments involving cell patterning in combination with microfluidics. For example, microfluidics can be used for media perfusion, the spatial delivery of substances (Takayama S *et al* 2003), the establishment of well defined gradients, along with many other capabilities. In addition, an equation was introduced to calculate the efficiency of patterning.

2.2 Materials and methods

2.2.1 Stencil fabrication

Poly(dimethylsiloxane) (PDMS) stencils with 20 and 50 μm channel widths (15 μm deep, 20 mm long) were prepared by moulding SU-8 masters fabricated by standard photolithography methods. Photolitography uses light and a photomask to generate a pattern of photosensitive resist layer lying on top of a substrate. The resist is then cured to generate a template that can be replicated by moulding (the full process is described in chapter one, section 1.2.1: 'photolithography'). The PDMS (Sylgard® 184, Dow Corning) prepolymer was mixed with the curing agent at a ratio of 10:1 (w/w) and thoroughly degassed. PDMS was poured onto the SU-8 master and cured at 80 °C for 20 minutes. A frame was used to contain the PDMS, producing stencils with a typical thickness of ~2 mm (figure 2.2.1a). For plasma introduction, 1 mm diameter through holes were punched into the stencils, followed by a 70% ethanol wash and dried with N_2 to remove particulate debris and sterilise the surface. Cell arrays were generated using a 125 μm thick polyimide (Katco Ltd, UK) stencil with a 4 x 4 matrix of 200 μm diameter holes produced by micromilling (figure 2.2.1b).

For the production of cell arrays with smaller island diameters a dielectric barrier discharge (DBD) prototype was constructed from a 7-fold glass capillary (Hilgenberg GmbH). Each capillary has a 1 mm outer diameter and a 0.56 mm inner diameter, and were miniaturised by weight-assisted (50 g) pulling through a vacromium heating coil (HEKA Elektronik GmbH), followed by polishing with sequential grades of finer sandpaper to produce bore diameters of ~100 μm. Tungsten wires with a diameter of 100 μm were inserted into each capillary and secured ~1 mm from the capillary openings with an epoxy (figure 2.2.3).
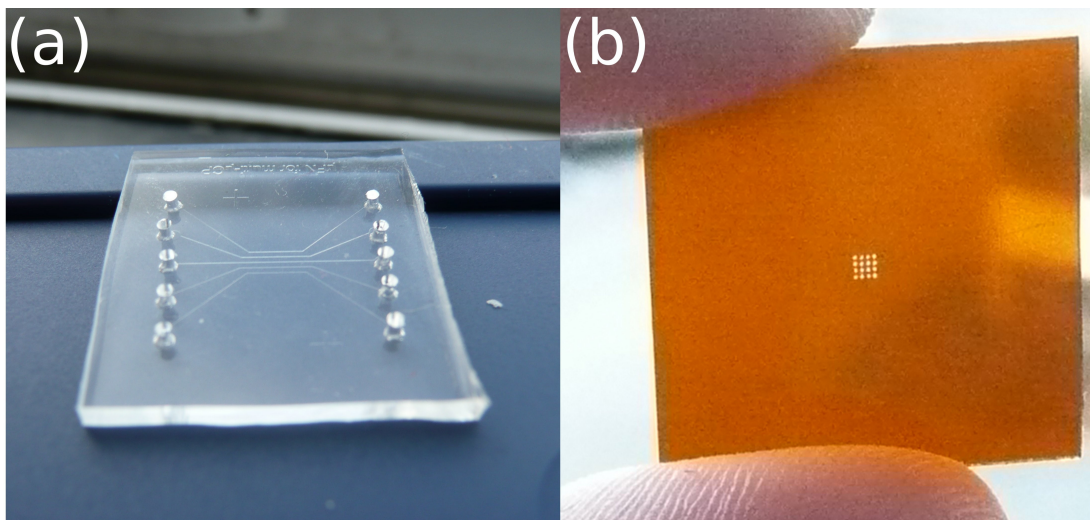
Figure 2.2.1: Stencils used for cell patterning. A typical PDMS stencil with 2 mm thickness and 1 mm diameter through holes (a). Polyimide stencil with a 4 x 4 matrix of 200 µm diameter holes (b).
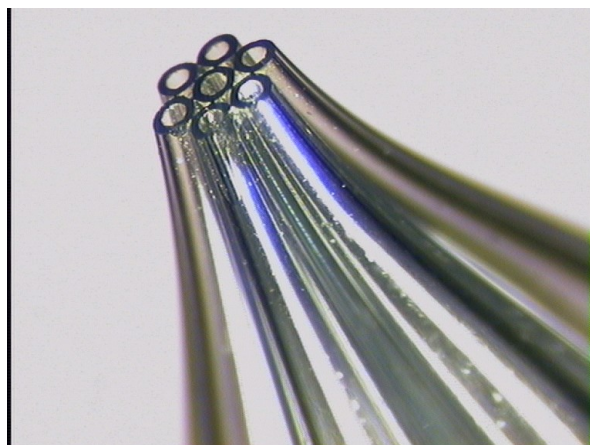
Figure 2.2.2: A 7-fold glass capillary stencil with tungsten wires inside.

2.2.2 Substrate preparation

To demonstrate the versatility of plasma stencilling, hydrophobic PDMS and bacteriological grade polystyrene (BGPS, from VWR International, Inc.) substrates were used. For ease of microscopy, thin (<400 µm) and flat PDMS-glass bilayer substrates were prepared by pressing a small volume PDMS deposit between a glass coverslip and a polystyrene surface, with curing for 10

minutes at 80 °C. Again the PDMS was sterilised with 70% ethanol followed by deionised water and dried with N_2. For certain microfluidic and optical applications glass is a preferred substrate. To extend the plasma stencilling capability methylated glass was also tested. Briefly, a 10% (v/v) dichlorodimethylsilane (DCDMS, Sigma Aldrich) in hexane mixture was prepared and heated to 50 °C to produce a silane vapour. Glass slides were exposed to the vapour for 30 minutes, followed by a short (20 s) rinse in hexane to remove unbound silanes.

2.2.3 Plasma activation

Plasma stencilling involved the use of a Tesla generator (VP23, Leybold-Heraeus Inc., USA) powered with a 30 kV, 2 MHz signal to produce an atmospheric pressure air plasma (figure 2.2.3).

Figure 2.2.3: A hand-held Tesla generator.

For stencilling the substrate was placed on a conductive surface that served as the ground electrode. As shown in figure 2.2.4, a PDMS stencil contacting the substrate was used to route the plasma through the microchannels.
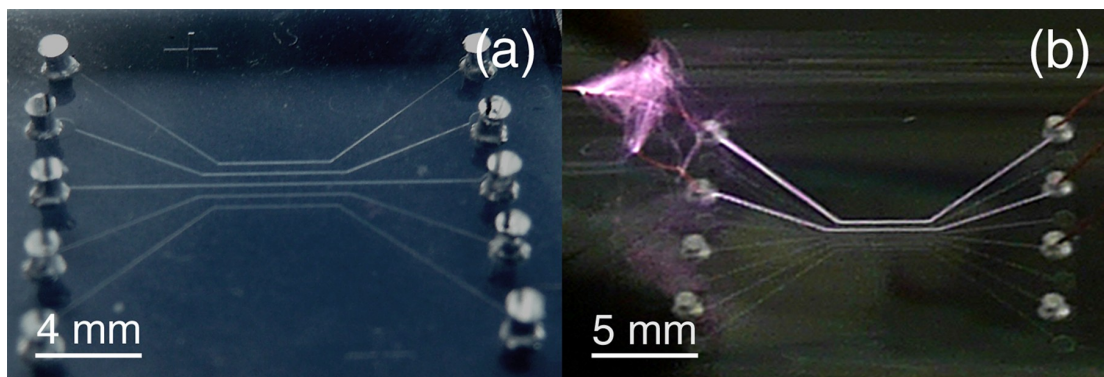
Figure 2.2.4: PDMS microfluidic stencil (a), and plasma stencilling using a Tesla generator (b). Copper wires were inserted to aid visualisation of the plasma.

Surface activation over small areas is rapid. For the generation of a microarray of hydrophilic patterns, a polyimide stencil was used for masking during a 10 s plasma activation treatment. Alternatively, and for the generation of smaller arrays, the microcapillary-based DBD prototype was operated at 4-6 kV, 35 kHz to generate parallel DBDs, again for 10 s, to selectively activate a PDMS-glass substrate. With this prototype, the PDMS-glass substrate acts as the dielectric barrier when positioned between the microelectrodes in the microcapillary array and a counter electrode. Conformal contact of the glass microcapillary array with the PDMS surface was used to enable plasma stencilling.

2.2.4 Surface characterisation

The hydrophilicity of the activated surfaces was characterised by contact angle measurements using a 1 µL sessile water droplet. In addition, surface roughness (R_{RMS}) was assessed using white light interferometry (WLI) (New View 5000, Zygo Corporation, Middlefield, USA) and by high resolution imaging using an environmental SEM (Quantam200F, FEI, operating at 90 Pa.). Chemical alterations following plasma activation of the BGPS surfaces were investigated using XPS (AXIS-HS-spectrometer Kratos, Manchester, UK). For excitation a non-monochromatic MgKα radiation source was used, with detection using a concentric hemispherical analyzer with fixed analyzer transmission. Scan surveys

were first undertaken using an 80 eV pass energy with 1 eV steps, followed by scans of the C 1s and O 1s regions with a 20 eV pass energy with 0.1 eV steps. Relative quantification factors were obtained by calibration using poly(ethylene glycol) and poly(sodium-4-styrenesulphonate) standards. Contact angle and XPS studies involved plasma treatments of a 100 mm^2 area, with treatment durations normalized to a 1 mm^2 area for comparison with white light interferometry analysis of a plasma stencilled track (50 μm x 20 mm) with a footprint of 1 mm^2.

2.2.5 Cell culture

Cell lines were purchased from ECACC (UK) or from DSMZ (Germany), and all cell culture media and consumables were purchased from Sarstedt AG & Co. (Germany) or PAA Laboratories GmbH (Germany). The 10 cell lines used in this study were human epithelial cells of colon origin (SW480, SW620, NCM460 and HT29), human keratinocytes (HaCaT), human neuroblastoma cells (SH-SY5Y), human breast cancer cells (MCF7), human fibroblasts (142BR), and poorly adherent human embryonic kidney cells (HEK293) as well as murine macrophages (J774.2). All cells were cultured under standard conditions according to the supplier recommendations. Cells were harvested using trypsin once the cultures were 80-90% confluent. Cell patterning was also tested with serum-free media supplemented with 10% (v/v) Lipumin ADCF (PAA Laboratories GmbH, Germany), a cocktail containing recombinant growth factors, synthetic hormones and other growth promoting components.

2.2.6 Cell patterning

Patterning involved seeding cells immediately after plasma stencilling and without further surface modifications. Cells were seeded in a 1 mL suspension containing 2 x 10^5 cells and incubated for 24 hours at 37 °C in a 5% CO$_2$ atmosphere. The suspension was then removed, replaced with new media and incubated for up to 15 days, with 3-4 day periodic media exchange. An inverted microscope (IX71, Olympus) was used to observe the cell patterns daily, with images recorded

using a CCD camera (Luca[EM], Andor Technology). For higher resolution imaging an environmental SEM (Quanta 200F, FEI) operating at 90 Pa was used. To quantify patterning, cells in the image were delineated for counting with ImageJ (NIH) (figure 2.2.5).
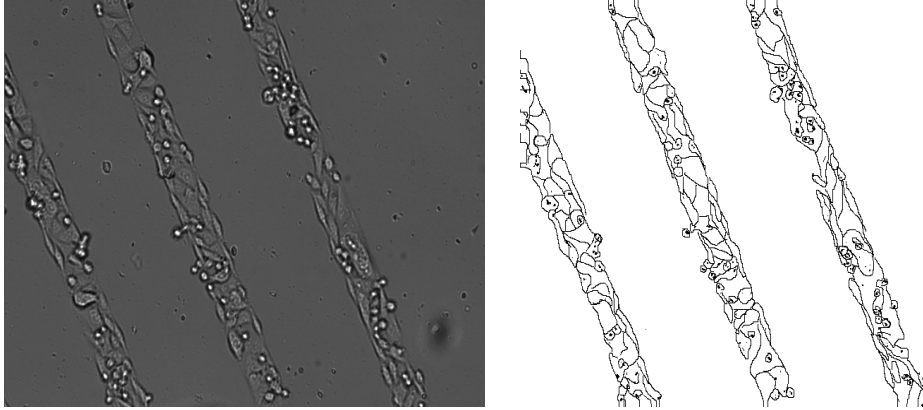
Figure 2.2.5: SW480 cells on 50 µm-wide plasma activated tracks (left). Cell delineation of the same picture using Image J (right).

Following media exchange and the removal of non-adherent cells, the patterning efficiency E_{patt} was determined. Patterning efficiency is defined as the number of cells adhering to the plasma activated area N_p relative to the number of cells adhering to an equivalent sized, untreated area N_u and was calculated according to:

$$E_{patt} = 2 \times \left(\frac{N_p}{N_p + N_u} - \frac{1}{2} \right) \times 100 \tag{1}$$

Using this equation, perfectly patterned cells have an E_{patt} of 100%, cells randomly adhering to the surface have a value of 0% and patterns of cells perfectly excluded from the activated area have a value of -100%. To fully characterise the effectiveness of cell patterning, the filling efficiency E_{fill} is required and was defined as the percentage of the activated area that was

occupied by the cells. Unless stated otherwise, these experiments were undertaken in triplicate (*n*=3).

2.2.7 Infra red ellipsometry

To investigate the effect of wettability on protein structures, human serum albumin (HSA) and collagen I were deposited onto hydrophobic and hydrophilic p-type Si(111) substrates. Silicon substrates were either plasma activated for 2 minutes to provide a hydrophilic surface (contact angle of 12.14 +/- 1.59) or vapour silanized with 10% (v/v) dichlorodimethylsilane (DCDMS, Sigma Aldrich, as described above) to provide a hydrophobic surface (contact angle of 100.64 +/-2.03). Both protein solutions were at a concentration of 50 µg/mL in 1 x PBS. In order to measure the Si/protein/solution-interface at 37°C the protein solutions had to be heated to 42°C in a dewar-glass beaker outside of the in-situ-cell. Measurements were undertaken with a Bruker Vertex 70 spectrometer (FTIR). The detector was a photovoltaic Mercury-Cadmium-Telluride (MCT) system from InfraRed Associates, Ince. The angle of incidence was 50° with the substrate having a 1.5° wedge shape in order to separate the reflection from the backside of the sample and from the Si/protein/solution-interface.

2.2.8 Packaging

Patterns can be assembled inside a microfluidic chamber by plasma bonding for the spatial delivery of substances or for simple perfusion applications. Briefly, plasma exposure to generate the pattern can also be used to activate the area surrounding the stencil. Equally, the microfluidic chamber can be separately plasma treated (5 min at 1 mbar) followed by conformal contact between activated substrate and chamber to seal the device. Through holes at the top of the chamber were created to allow insertion of media containing cells.

2.3 Results and discussion

2.3.1 Surface characterization

Cell adhesion and growth is inhibited on inherently hydrophobic PDMS (De Silva MN *et al* 2004) and polystyrene (Dewez JL *et al* 1996, Rhee SW et al 2005). In this study, these polymeric substrates have been plasma stencilled to selectively activate the surface to a hydrophilic state and enable the straightforward patterning of mammalian cells without further surface modification. Hydrophobic polymer surfaces can be made hydrophilic by plasma treatments. The plasma treatment oxidizes the surface, a process partly mediated by ozone and gaseous radicals, altering the surface properties to a hydrophilic state by adding silanol (SiOH) groups to the surface (Rhee SW et al 2005, Hillborg H *et al* 2000). In this study, a Tesla generator was used for the plasma treatment of three hydrophobic surfaces: PDMS, methylated glass and bacteriological grade polystyrene (BGPS). The Tesla generator can be used with air at atmospheric pressure, eliminating the need for a vacuum, a gas supply or the controlled deposition of polymer or molecular layers. The use of a Tesla generator operating at low voltages and frequencies has the additional potential benefit of being battery operated (Heming R *et al* 2009). Plasma treatment durations and the resulting contact angles for the three substrates are recorded in table 2.3.1. As shown from table 2.3.1, hydrophilicity increases with plasma activation time for all 3 hydrophobic polymer substrates, as demonstrated by the decrease in contact angles. BGPS surfaces were transformed to a hydrophilic state with as little as 1 s plasma exposure with contact angles decreasing from 103.7 ± 1.7° to 49.9 ± 4.4°. With PDMS, previous studies have shown that a silica film is produced as a result of surface oxidation (Kim J *et al* 2000). This process is reversible over time and the activated PDMS substrates will recover to a hydrophobic state. There is strong evidence that the mechanism of hydrophobic recovery is caused by the diffusive return of low molecular weight oligomers to the surface (Kim J *et al* 2000). To avoid this hydrophobic recovery, the plasma activated PDMS

substrates were quickly seeded with cells or, for later use, immersed in deionised water (Kim J *et al* 2000, Delamarche E *et al* 1998).

Table 2.3.1: Surface activation characterised using contact angle (CA) measurements and white light interferometry (WLI). For the CA study, substrates were treated by rastering the plasma over a 100 mm^2 area, whereas WLI was used to study the roughening of a 50 µm wide and 20 mm long plasma stencilled track with a total activation footprint of 1 mm^2. Both sets of measurements have the activation time normalised to the treatment of a 1 mm^2 area.

	poly(dimethylsiloxane)		methylated glass		bacteriological grade polystyrene (BGPS)	
activation time (s)	contact angle	roughness (R_{RMS} (nm))	contact angle	roughness (R_{RMS} (nm))	contact angle	roughness (R_{RMS} (nm))
0	106.3 ± 1.7°	16	104.8 ± 1.1°	3	103.7 ± 1.7°	19
1	60.5 ± 2.1°	61	19.8 ± 1.0°	3	49.9 ± 4.4°	29
3	29.1 ± 1.8°	140	<5°	4	31.1 ± 2.0°	267
5	9.7 ± 0.7°	233	<5°	5	23.8 ± 1.6°	284

Nevertheless, hydrophilic PDMS surfaces could be obtained with a 1s plasma exposure, with contact angles decreasing from 106.3 ± 1.7° to 60.5 ± 2.1°. For methylated glass, a dramatic drop in contact angle was observed after 1s of plasma exposure, from 104.8 ± 1.1° to 19.8 ± 1.0°. Longer plasma treatments resulted in contact angles that were too small to accurately measure. This dramatic drop may be due to the fact that vapour phase deposition of dichlorodimethylsilane (DCDMS) on glass surfaces produces self assembled monolayers (SAMs) which are easily removed during the plasma treatment due to their extreme thinness (monolayer). Previous studies have shown that deposition of DCDMS creates densely packed self assembled monolayers (Ashurst WR *et al* 2001) producing contact angles typically around 100° (Brzoska JB *et al* 1994). The methylsilane monolayer mimics the hydrophobic properties of PDMS, and during plasma activation the surface is oxidised, stripping methyl

groups and changing the surface stoichiometry from n-Si-$(CH_3)_2$-O-n to SiO_2, glass (West J *et al* 2007).

Standard tissue culture grade polystyrene, which is suitable for cell adhesion, is oxidized to obtain a contact angle of ~50° whereas BGPS (non-oxidized) is hydrophobic and resists cell adhesion (Dewez JL *et al* 1996). Differences in substrate wettability have been previously used for cell patterning (Detrait E *et al* 1998). Therefore, the regio-selective oxidation of BGPS can generate substrates with contrasting free energy patterns that could be used for cell patterning.

2.3.2 Cell patterning with SW480 epithelial cells

To selectively activate the hydrophobic surfaces, stencils were fabricated. PDMS stencils were produced with recessed microfluidic channels and simply positioned onto the hydrophobic substrates with conformal contact. Contrasting free energy patterns could be obtained by routing the plasma inside the microfluidic channels (section 2.2.3, figure 2.2.5), selectively activating the exposed hydrophobic surface areas within the microfluidic channels. This creates a surface with contrasting wettability properties. As shown in figure 2.3.1(a), an image of the shadow cast from 350-µm-wide water tracks on the surface of plasma stencilled PDMS demonstrates the selectivity of the patterning process. SW480 cells were immediately seeded on the substrates following plasma treatments and without any other surface modifications. Following overnight incubation at 37°C with 5% CO_2 and a media exchange, cells were observed to only adhere and grow on the plasma treated regions. Figure 2.3.1(b) shows SW480 epithelial cells patterned following plasma stencilling of a PDMS substrate. The use of PDMS as stencil material brings the advantage that the elastomeric nature of PDMS enables conformal contact between substrate and stencil. PDMS stencils have been used in this study to generate surface free energy patterns with high precision on PDMS, methylated glass and BGPS surfaces. Similarly, the use of PDMS as the substrate also allows the use of non-elastomeric stencils such as polyimide and polycarbonate.
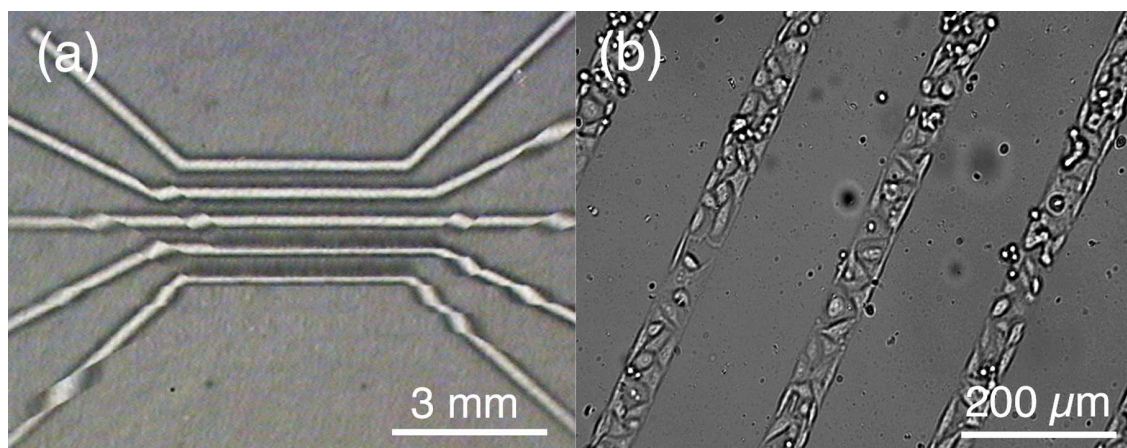
Figure 2.3.1: Wetting pattern on PDMS following plasma stencilling (a) and SW480 epithelial cell patterns on a plasma stencilled PDMS substrate (b).

2.3.2 Topographical analysis by WLI

Substrate exposure to the plasma also creates material roughening. White light interferometry (WLI) was used to analyze the level of roughening of PDMS, methylated glass and BGPS following varying plasma exposure times. Table 2.3.1 characterizes the topographical variations for the three hydrophobic substrates. Results show that with increasing plasma exposure times, roughness values (R_{RMS}) for PDMS and BGPS progressively increase to over 200 nm. Figure 2.3.2 shows the topographical roughness for BGPS with increasing plasma exposure treatments. Widening of the roughened tracks is also apparent with longer plasma exposure times. In contrast, glass substrates showed minimum roughening following plasma treatments, with only 5 nm R_{RMS} for a 5 second activation exposure. For comparison, the roughness of untreated glass was around 1.9 nm R_{RMS}. It is important to note that in combination with hydrophilicity, surface roughness has been previously reported to aid cell adhesion and growth (van Kooten TG and von Recum AF, 1999). For example, fibroblast cells (COS-7) show preferential adhesion behavior on hydrophilic and roughened substrates (Patrito N *et al* 2007). However, cells patterned equally on

methylated glass and PDMS surfaces, suggesting that wettability is the dominant parameter for cell adhesion.
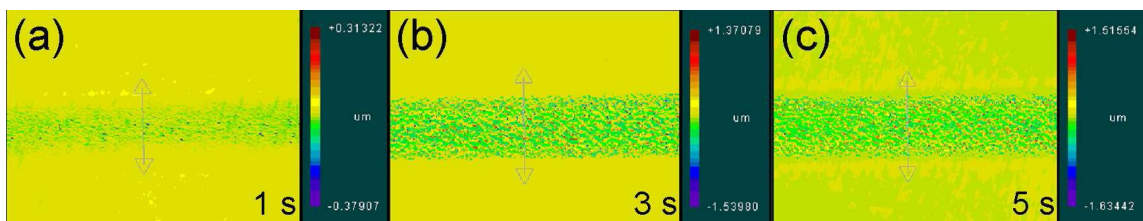
Figure 2.3.2: White light interferometry analysis of polystyrene (BGPS) surface roughening caused by plasma stencilling for 1 s (a), 3 s (b) and 5 s (c).

2.3.3 Polystyrene biocompatibility following plasma treatment

The variation in plasma exposure time (from 1 s to 5 s) did not affect cell adhesion on PDMS or methylated glass surfaces. Figure 2.3.3(a) shows SW480 cells patterned on plasma stencilled PDMS (20 µm wide tracks) with different plasma exposure times. Equally good cell patterning was obtained regardless of plasma exposure time. Similar findings were observed for methylated glass substrates. However, BGPS surfaces with longer plasma exposures showed reduced cell adhesion and pattern occupancy (Figure 2.3.3(b)).
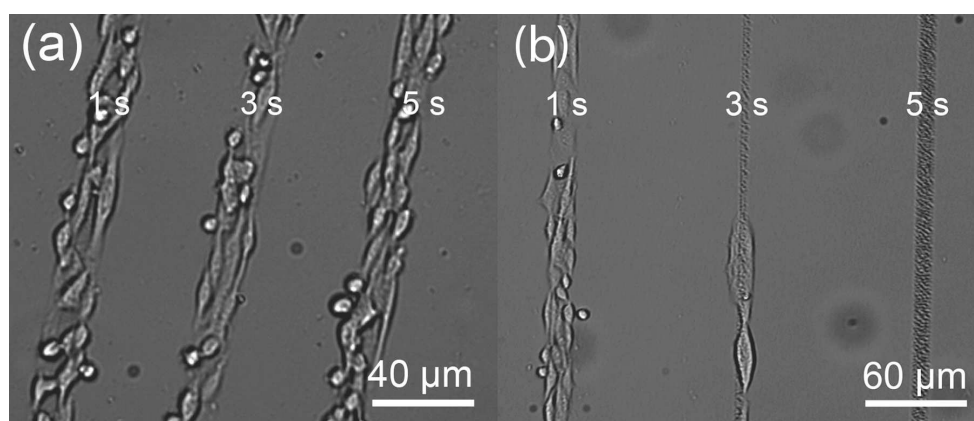
Figure 2.3.3: Effect of plasma exposure duration on SW480 epithelial cell adherence and growth on PDMS (a) and BGPS (b) substrates after 48 hours of culture.

Reduced cell adhesion on BGPS with prolonged plasma exposure in combination with the otherwise favorable hydrophilicity and roughening was investigated by XPS analysis. All C1s spectra were fitted with the same set of Gauss-Lorenzian curves on a linear background. The resulting data of the C 1s and O 1s signals for different activation periods is shown in Table 2.3.2.

Table 2.3.2: XPS data of the C 1s and O 1s signals from plasma treated BGPS surfaces for different durations.

Electron level	C 1s						O 1s
Binding energy (eV)	283-284.2	~285	~286.3	~287.8	~289.3	~290.6	~533
Probable species [27]	C-aromatic	C-C C-H	C-OH C-O-C phenol	C=O	COOH O-COO	O=COO	all
Sample							
untreated BGPS	45.0	46.7	0.8	0.0	0.0	0.2	3.1
1 s treatment	15.4	49.0	5.9	3.1	2.8	1.4	20.0
3 s treatment	13.5	45.9	6.5	2.6	3.9	1.4	23.8
5 s treatment	10.9	46.0	3.9	3.4	3.2	3.0	28.4

The data presented in Table 2.3.2 shows that the O 1s signal at ~533 eV progressively increases from 3.1 atomic percent (untreated) to 28.4 atomic percent (5 s) with longer treatment durations, indicating that oxidation is occuring. Phenolic compounds can result from polystyrene surface oxidation and these are known to cause protein denaturation and cytotoxicity. The signal intensity of the phenolic compounds (at ~286.3 eV) (Beamson G *et al* 1992) were similar for the different treatment durations indicating that phenolic compounds are not being produced at toxic levels. However, activated BGPS surfaces were analysed by scanning electron microscopy (SEM) and showed that longer plasma exposure resulted in excessive oxidation and melting of the polystyrene. As a result, oxidized polymeric nanoparticles were formed on the surface (Figure 2.3.4). These have the potential to be absorbed by cells and cause cytotoxic effects at high surface densities, rendering the surface non-biocompatible. Therefore,

plasma treatment duration is critical for patterning cells on BGPS with prolonged treatment leading to cytotoxic effects.

Glass substrates are the preferred substrate for optically demanding measurements such as Raman spectroscopy, but the additional methylation step prior to plasma exposure makes it less practical than PDMS. In addition, PDMS is also the choice material for many types of implants, indicating that with the appropriate treatments (Brohim RM *et al* 1992*,* Danino A *et al* 2001) PDMS is biocompatible. Therefore the preferred material for patterning was PDMS as it is biocompatible regardless of plasma exposure durations. Furthermore, the use of PDMS ensures conformal contact with a variety of stencil material due to its elastomeric nature and it does not require passivation with cell repellent species.
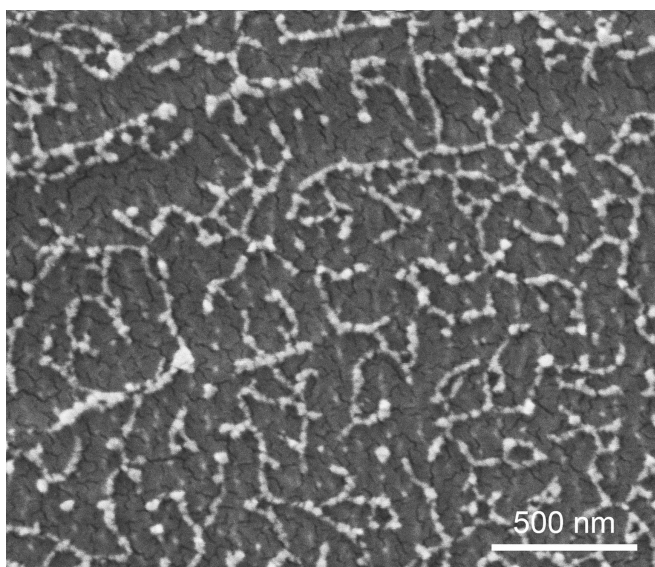
Figure 2.3.4: A SEM image of BGPS after prolonged (5 s) plasma treatment.

2.3.4 The role of serum proteins

Cell patterning is typically achieved by positioning adhesion promoting proteins (e.g. fibronectin, collagen) surrounded by cell repellent proteins (e.g. PEG) on the surface. A major advantage of the plasma stencilling approach is that it does not require molecular patterning steps prior to cell patterning, greatly simplifying the

patterning process. It is well established that surface membrane proteins are responsible for cellular interactions with its micro-environment and therefore proteins play an important role in cell adhesion. Previous experiments have shown that serum was necessary for pattern recognition and patterned growth (Kleinfeld D *et al* 1988, Detrait E *et al* 1998).

To investigate the role of proteins present in the cell culture media from the fetal calf serum (FCS), cell patterning was also tested with serum-free media supplemented with 10% (v/v) Lipumin ADCF (PAA Laboratories GmbH, Germany), a cocktail containing recombinant growth factors, synthetic hormones and other growth promoting components. The exact composition of the FCS present in the media is unknown, but is likely to include ions and salts, various growth factors such as epithelial growth factor (EGF), granulocyte colony stimulating factor (G-CSF) and neurotrophic factors, but also insulin, hormones and a mixture of extra cellular matrix (ECM) proteins. The Lipumin ADCF solution is used to replace all the components of the FCS except for the ECM proteins. Cell patterning was unsuccessful when serum proteins were absent from the cell culture media, indicating that proteins from the FCS are responsible for mediating cell adhesion on the plasma activated regions. In corroboration with these findings, other studies have shown that cell patterning could be achieved without the need for directly patterning adhesion molecules (Rhee SW et al 2005, Detrait E *et al* 1998, Patrito N *et al* 2007). It has been reported that cell adherence is enhanced on hydrophilic surfaces where adhesion promoting proteins are present (Wilson CJ *et al* 2005). Digital hydrophobic-hydrophilic surface contrasts provide guidance for cell registration, with surface wettability strongly influencing cell adhesion (Wilson CJ *et al* 2005). For example, small proteins have a higher affinity for hydrophobic surfaces (Sigal GB *et al* 1998) where they become disordered and denatured. Albumin, a cell repellent protein, shows stronger adhesion on hydrophobic than hydrophilic surfaces (Kidoaki S and Matsuda T, 1999, Sethuraman A *et al* 2004). The difference in protein orientation and secondary structures on hydrophobic and hydrophilic surfaces has also been the focus of some studies. Vibrational spectroscopy has been used to demonstrate

that albumin is randomly oriented on hydrophobic surfaces (Kim J and Somorjai GA, 2003) with secondary structure exhibiting lower levels of organization (Roach P *et al* 2005). On the other hand, cell adhesion promoting proteins have been shown to assemble in a bio-active way onto hydrophilic surfaces (Curtis SG *et al* 1984). Antibody recognition techniques were successfully used to demonstrate that fibronectin (cell adhesion protein) adsorbed onto hydrophilic polystyrene surfaces remains conformationally active (Underwood PA *et al* 1993). However, wettability is not the only parameter at play for cell patterning. For example, PEG, a well established cell adhesion resistant surface coating, is hydrophilic and yet resists protein absorption. Nevertheless, the integrity of protein orientation and secondary structures are essential for cellular recognition and attachment and could be responsible for directing cell patterning.

In an attempt to investigate the differences in cell adhesion and cell repellent protein configuration on hydrophobic and hydrophilic surfaces, infra-red (IR) ellipsometry measurements were undertaken at the Department of Interface Spectroscopy (ISAS, Berlin). Human serum albumin (HSA) and collagen I (adhesion protein) was deposited on hydrophobic and hydrophilic surfaces and the variation between amide bands I and II were recorded at 37ºC. The experiment with collagen was inconclusive. Due to technical issues, the solution containing the proteins had to be heated outside the IR elipsometry apparatus, which meant heating the solution up to 42ºC so as to be able to measure at 37ºC once inside the chamber. Although this poses no problem for HSA, collagen I denatures at 37ºC (Leikina E *et al* 2002) and could not be analyzed accordingly. In addition, collagen has multiple levels of structural ordering and usually requires preparation in acid solutions which would not accurately mimic the events occurring during plasma stencilling patterning. Therefore the collagen results were omitted from this study. On the other hand, HSA results showed that there was a change in the spectra from hydrophilic to hydrophobic surfaces. The Amide II band (between 1510 and 1580 cm^{-1}) had a higher amplitude than the amide I band (between 1600 and 1700 cm^{-1}) on the hydrophobic surface (Figure 2.3.5(left)), whereas on the hydrophilic surface, both amide bands I and II were of

similar amplitude (Figure 2.3.5(right)). The Amide II band is associated with N-H bending vibrations and C-N stretching vibrations and can relate to conformational shifts of the protein structure (Lunin VV *et al* 2008). IR spectroscopy can provide insights into the effects of surface wettability for protein conformational shifts although the exact mechanism behind this phenomenon remains unclear. Further detailed investigations using a battery of complementary surface analysis, biochemical and cell experiments would be required to gain further insights. This significant endeavour could have tremendous impact in many application areas such as implants, cosmetics, self-cleaning materials, cell biology research, pharmaceuticals and many more. From the results presented herein, adhesion proteins present in the FCS are likely to self assemble in a bioactive state on hydrophilic areas only, therefore mediating cell adhesion and patterning.
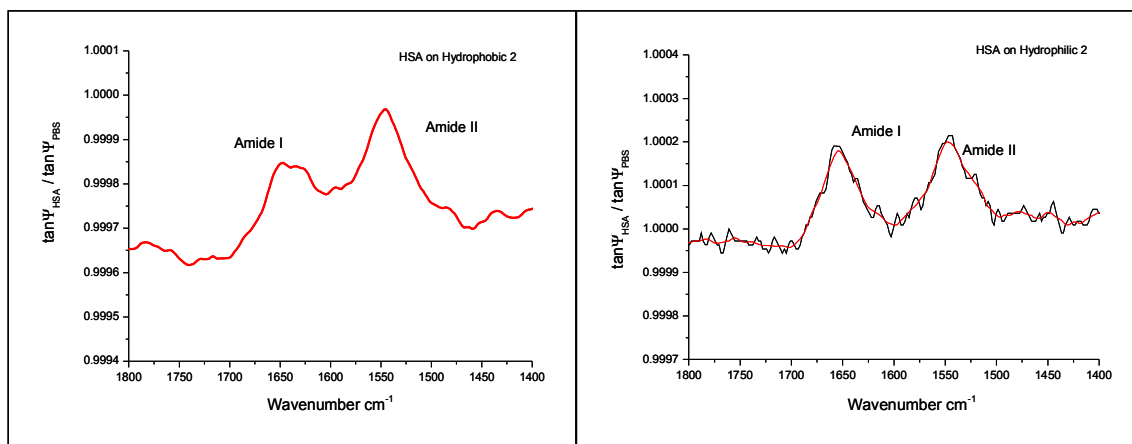
Figure 2.3.5: IR ellipsometry measurements for HSA amide I and II peaks on hydrophobic (left) and hydrophilic (right) surfaces at 37°C after 30 minutes of incubation.

2.3.5 Plasma stencilling for patterning cells of various origins

Plasma stencilling was also undertaken to pattern 9 other mammalian cell lines from different tissue origins on PDMS and methylated glass substrates. Human breast cancer cells (MCF7, figure 2.3.6(a)), human neuroblastoma cells (SH-SY5Y, figure 2.3.6(b)), human keratinocytes (HaCaT, figure 2.3.6(c)), poorly adherent human embryonic kidney cells (HEK293, figure 2.3.6(d)), human

epithelial cells (SW620, NCM460 and HT29), human fibroblasts (142BR), and murine macrophages (J774.2) were all successfully patterned by plasma stencilling. Cells were cultured for periods in excess of 10 days with the patterns remaining stable (with periodic media exchange every 3-4 days). SEM imaging was used to demonstrate the compactness of cellular assembly on the plasma activated tracks, which is typical of the *in vivo* tissue state. Figure 2.3.7 shows this close cellular packing but also demonstrates the cell repellent nature of hydrophobic PDMS, with the SW480 cells unable to adhere to the hydrophobic PDMS border between plasma activated and untreated regions. Also, pattern broadening is observed at the intersection of the hydrophilic tracks. This can be attributed to double ECM secretion from the cells at the corners of the pattern that could be masking the PDMS and allowing pattern broadening.
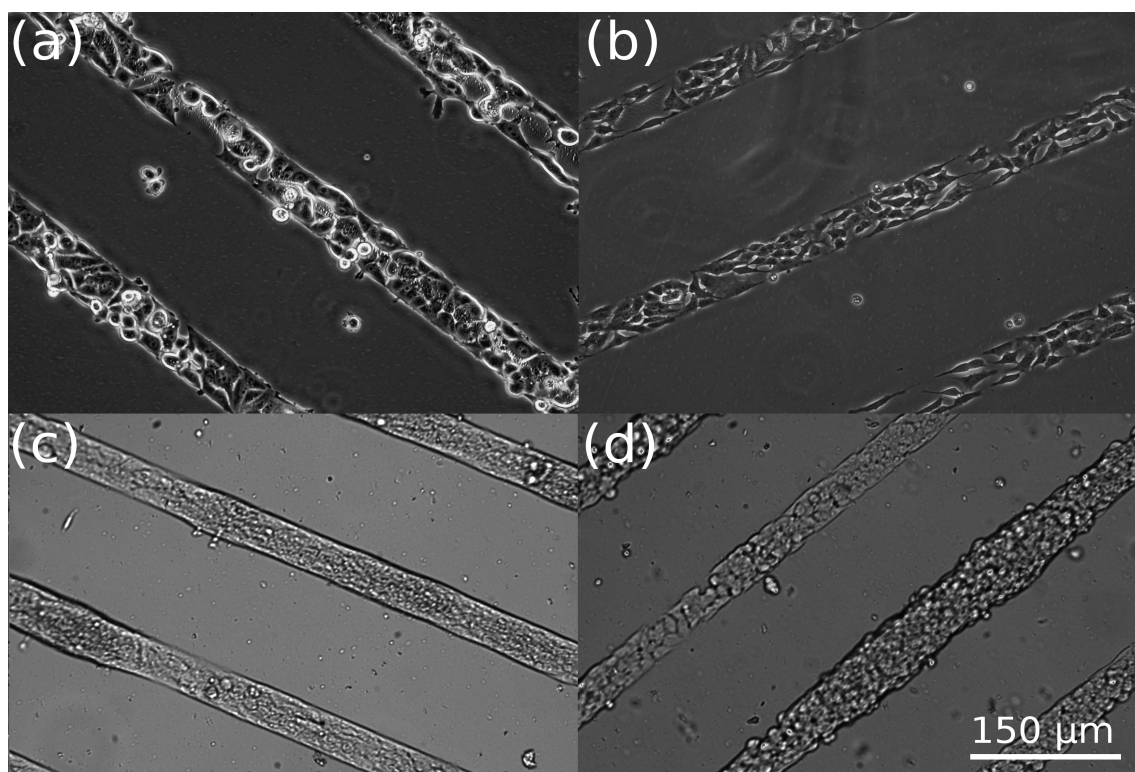
Figure 2.3.6: Plasma stencilling on PDMS at 48 h of incubation. MCF 7 (a), SH-SY5Y (b), HaCaT (c) and HEK 293 (d) cells successfully patterned within the 50 µm plasma activated tracks.
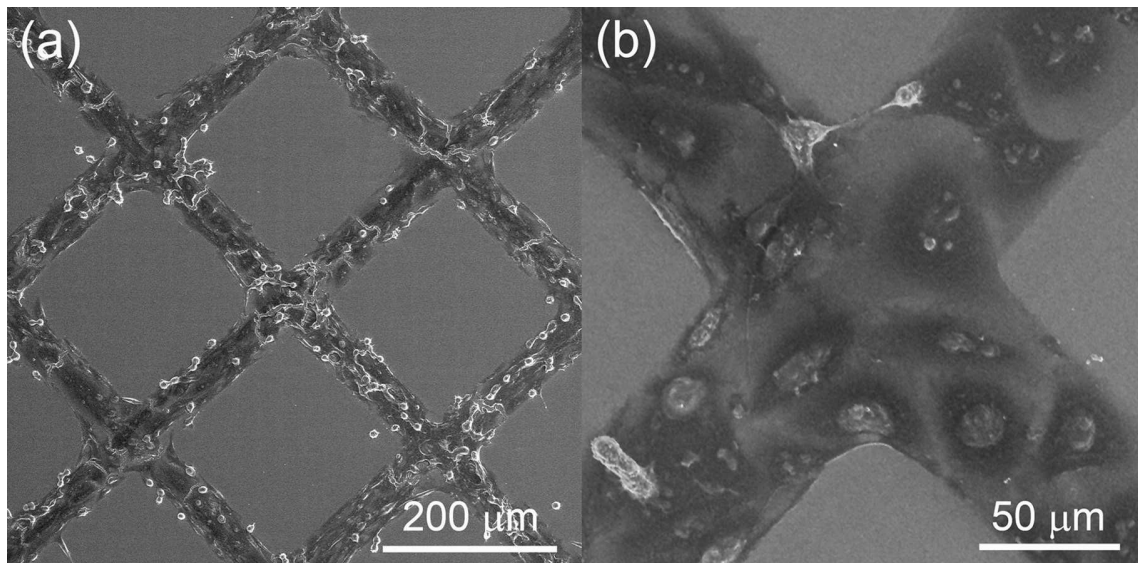
Figure 2.3.7: Imaging by SEM shows confinement of the SW480 epithelial cells to plasma activated regions of a glass surface (a). Tight cellular packing, akin to the *in vivo* tissue state, confined to the plasma activated tracks (b).

2.3.6 Mathematical characterization of cellular patterns

To evaluate the effectiveness of cell patterning by plasma stencilling, we introduced equations (see section 2.2.6). The pattern efficiency was determined by measuring the number of cells growing on the activated regions compared with the number of cells growing on an equal-sized, non-activated region of the same substrate. The pattern filling refers to the percentage area occupied by the cells in relation to the total activated area and is needed to fully evaluate cellular behaviour on the plasma activated tracks over time. This is because 100% cell patterning efficiency can be obtained with one cell if the cell is adhering to the plasma activated region. Measuring filling efficiencies adds valuable information for pattern coverage and complements the patterning efficiency for a complete assessment of cellular patterns. Table 2.3.3 shows the dynamic behavior of SW480 cells during a 10 days cultivation period on 20 μm and 50 μm wide plasma activated tracks.

Table 2.3.3: SW480 epithelial cell pattern and cell size characterisation during culture for 10 days.

Sample		mean patterning efficiency	mean filling efficiency	mean cell size
24 hours	(20 µm)	93.0 ± 3.0%	61.0 ± 1.0%	146 ± 11 µm^2
3 days	(20 µm)	96.9 ± 0.0%	80.0 ± 1.4%	158 ± 1 µm^2
8 days	(20 µm)	96.7% (*n*=1)	93.0% (*n*=1)	127 µm^2
10 days	(20 µm)	96.9% (*n*=1)	97.0% (*n*=1)	126 µm^2
24 hours	(50 µm)	97.9 ± 0.8%	92.5 ± 1.9%	186 ± 1 µm^2
2 days	(50 µm)	99.1 ± 1.5%	95.9 ± 1.1%	169 ± 9 µm^2
3 days	(50 µm)	97.7 ± 1.5%	97.2 ± 1.3%	187 ± 6 µm^2
6 days	(50 µm)	94.5 ± 1.6%	100.0 ± 0.0%	195 ± 6 µm^2
10 days	(50 µm)	98.2 ± 0.0%	100.0 ± 0.0%	247 ± 4 µm^2

Patterning efficiency is greater than 93% at any given time for both track sizes, indicating that untreated PDMS can resist cell adhesion for prolonged periods of time under cell culture conditions. The filling efficiency, the ability of cells to colonize the activated region, increased over time for both track sizes, which is an indication of cell division and growth. With 50 µm wide tracks, 100 % filling efficiency was obtained after 6 days whereas it took 10 days for the 20 µm wide tracks to be almost completely colonized (97%). These results show that smaller features are harder to occupy and take longer to fill than larger area. This can be expected as it will be harder for a cell to randomly find a smaller region than a big one and will take longer to migrate to that region. Also, and as demonstrated in various studies (Singhvi R *et al* 1994, Chen CS *et al* 1997 and 1998), smaller features can induce apoptosis or affect cell division rates, and this could explain the slower filling rates observed on the 20 µm wide tracks. Nevertheless, the results demonstrate that selective surface modification by plasma stencilling offers a highly effective route for cell patterning. In addition, the development of such a mathematical characterisation for cell patterning could be used as a

standard method to evaluate the effectiveness of other cell patterning techniques.

2.3.7 Summary of cell behaviour on plasma activated patterns

The behaviour of cells from different tissue origins on the patterns or even the effect of different pattern geometries on the rate of cellular colonization could prove useful for the generation of new implant materials but also for a better understanding of spatially organised cell cultures. The variation in cellular behaviour on different size patterns was evident even with such simple linear geometries. Figure 2.3.8 shows SW480 cells on 50 μm and 20 μm wide tracks. Following cell delineation for counting with ImageJ (NIH) (shown in section 2.2.6, figure 2.2.6), the differences in cell size and morphology were striking. Table 2.3.3 shows that on the 50 μm wide tracks, cell footprint sizes increased from 186 μm at 24 h to 246 μm following 10 days of cultivation, which is similar to normal cell culture behaviour. In comparison, cell footprint sizes only increased to 126 μm at day 10 on the 20 μm wide tracks, which is almost half the footprint area from the cells on 50 μm wide tracks. Cells patterned on the 20 μm wide tracks are likely to be more confined as the track width is at the single cell size scale and is too small for a cell to adhere and grow normally. As cellular division occur and the filling efficiency increases the cells become tightly packed and elongated, a trait that is not seen on the 50 μm wide tracks (figure 2.3.8). This indicates that cell division and growth rates as well as morphology are impacted when cells are patterned on a single cell sized pattern (20 μm wide tracks or smaller). Therefore, pattern dimensions can impact cell size and morphology, and this has particular implications for single cell patterning.
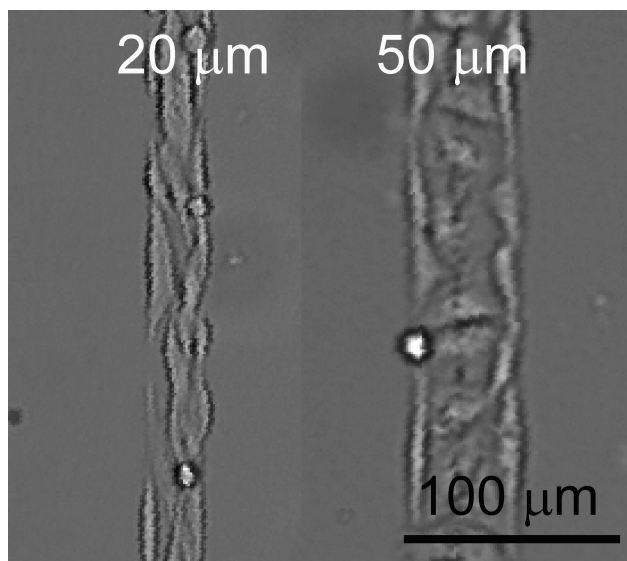
Figure 2.3.8: SW480 cells patterned by plasma stencilling on 20 and 50-μm-wide plasma activated tracks (substrate is PDMS).

2.3.7 Patterning arrays

For the generation of cellular arrays, a different type of stencil had to be constructed. A 120-μm-thin polyimide sheet was micromilled to obtain a 4 x 4 matrix of 200 μm diameters holes and was used to selectively plasma activate PDMS substrates (figure 2.3.9(a)). Cells were seeded directly following plasma activation and were incubated overnight. An array of isolated cell islands, each ~200 μm in diameter, was successfully patterned and is shown in figure 2.3.9(b). Following 48 hours of culture, patterning efficiency was 97.4 ± 2.3% and filling efficiency was 99.3 ± 0.7% (*n*=7, SW480 cells). These results suggest that plasma patterning using different stencils and geometry is also highly effective and reproducible with high pattern and filling efficiencies. Other stencil materials could also be used to generate arrays, such as Parylene C (Wright D *et al* 2008) and PDMS (Whitesides GM *et al* 2001). The production of stencils with miniature (<200 μm) through holes for applications such as single cell or sub-cellular array patterning, is problematic as it is difficult to prepare stable stencils that are suitably thin. Without thin stencils the aspect ratio is necessarily large and introduces major difficulties for precision fabrication.
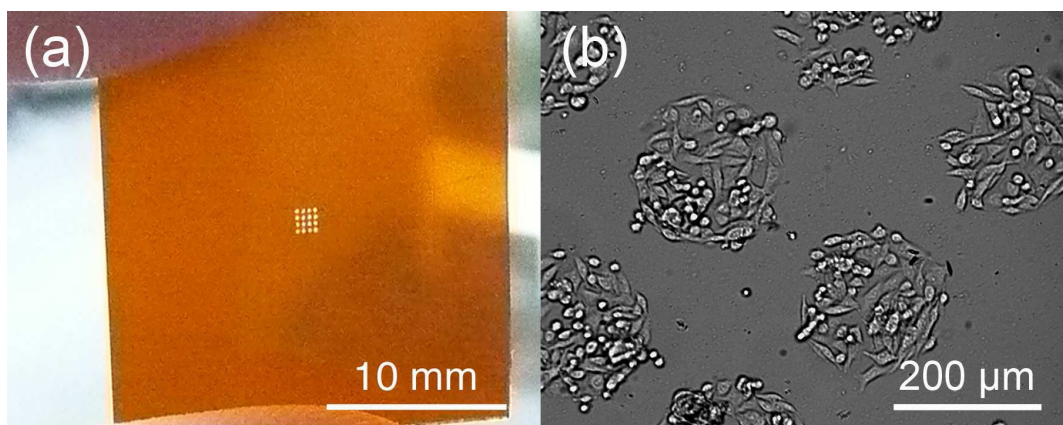
Figure 2.3.9: Polyimide stencil with a 4 x 4 array of 200 µm diameter through holes produced by micromilling (a) and a cellular array on the plasma stencilled PDMS substrate (b).

To provide a solution for patterning smaller arrays at high aspect ratios, we have developed a parallel dielectric barrier discharge (DBD) prototype. It has been previously shown that DBD devices are able to produce a single microplasma (West J *et al* 2007, Chai J *et al* 2005). For example, scanning microplasma can produce ~400 µm wide activation tracks (Tan HML *et al* 2007) and microelectrode-based electrochemical oxidation has been previously used to produce single 300-µm-diameter cell adhesion islands (Kaji H *et al* 2006). For the construction of a parallel DBD device and for the ignition of multiple microplasmas, we have assembled 7 tungsten microelectrodes inside a 7-fold glass microcapillary coupled to a Tesla generator (figure 2.3.10(a)). Operating at 35 kHz and 5-7 kV, 7 independent microplasmas of similar intensities were observed (figure 2.3.10(b)), with the PDMS substrate and glass capillaries aligned to the counter electrode and acting as the dielectric. During the stencil fabrication process, each electrode was recessed inside each glass micro capillary to produce an air volume of ~8 nL when in contact with the substrate. This air gap was used to fuel the plasma. Cellular islands were obtained with as little as 10 s of treatment, followed by immediate cell seeding and overnight incubation (figure 2.3.10(c)). Cell adhesion was also observed outside the array

indicating that plasma activation is not restricted within the stencil. In order to eliminate this excess plasma activation shielding of the stencil is required. Shielding the glass capillary with shrink tubing did not effectively restrict the plasma within the stencil nor did adding a layer of PDMS around the glass capillary.
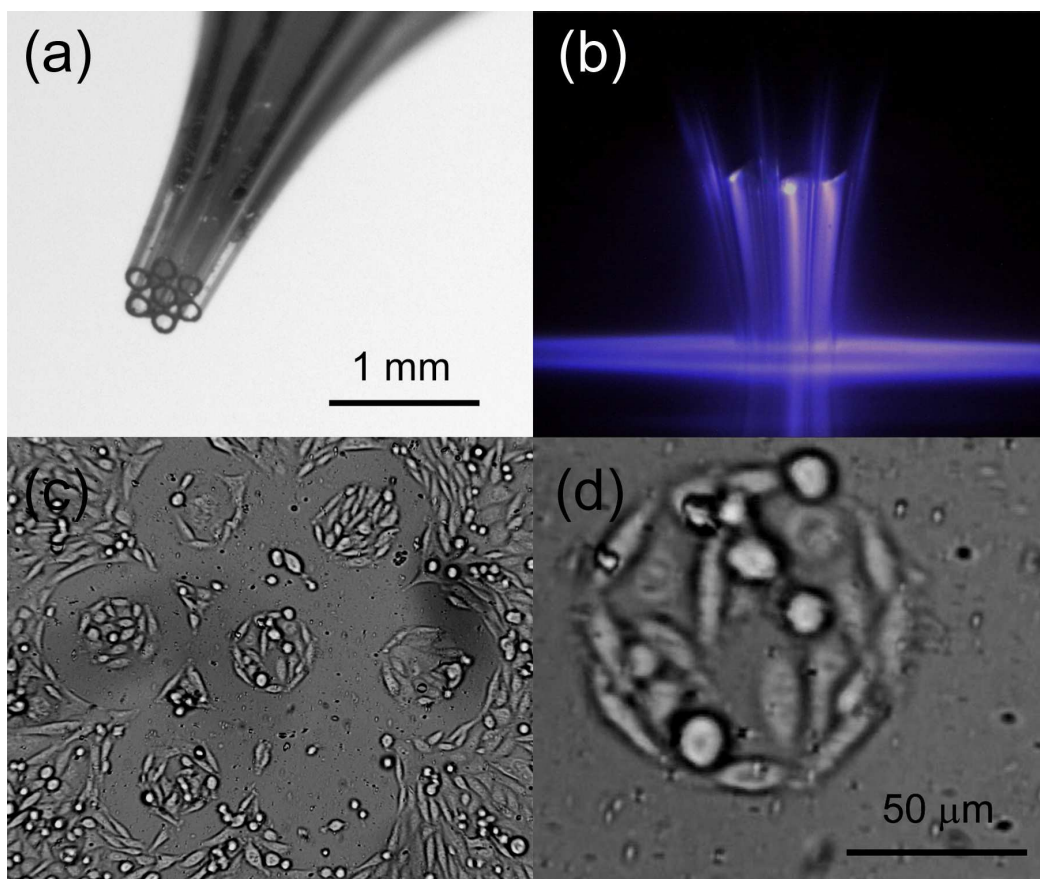
Figure 2.3.10: A 7-fold glass microcapillary DBD stencil system (a). High energy DBD operation producing parallel microplasmas (b). Actuation with a 6.5 kV, 35 kHz signal for 10 s generated a cellular array (c) with clearly demarked individual islands (d).

A smaller counter electrode matching the diameter of the 7-fold capillary glass stencil was also used in an attempt to focus the plasma albeit unsuccessfully. These issues highlight the fact that producing arrays by plasma stencilling is challenging. Nevertheless, a cellular array with ≤100 µm diameter cellular islands

was obtained (figure 2.3.10(d)), with the activated area matching the inside diameter of the capillaries. Interestingly, commercially available plasma displays operate with similar principles as the described DBD systems and this technology could be re-engineered for high resolution patterning over large areas. For example, plasma discharges between anode and cathode under atmospheric pressure have a diameter limitation of 24 μm^2 in a helium environment and 6 μm^2 in an argon environment (Franzke J, 2009) which is suitable for the production of single cell arrays.

2.3.8 Packaging

The ability to enclose cellular patterns inside a microfluidic chamber brings many advantages. Perfusion systems can easily be adapted to provide continuous exchange of nutrients and metabolic products to the culture, mimicking an *in vivo* microenvironment. In addition, microfluidics can be used for the spatial delivery of compounds with a high degree of precision by hydrodynamic focusing. For example, different streams of fluids have been directed to different regions of a single bovine capillary endothelial (BCE) cell, therefore offering a route for the delivery of various reagents to defined parts of a cell (Takayama S *et al* 2003). The delivery of substances to subcellular regions of a cell is a powerful tool to investigate local effects of signaling pathways on receptor clustering for example, but also allows the non-exposed regions of the cell to act as a control. Similarly, such a system could be employed to deliver multiple compounds at various concentrations to cells patterned in arrays for high throughput bioassays such as drug testing. Hydrodynamic focusing is also a great approach to perform extremely fast mixing of reagents. Knight JB *et al* (1998) reported a continuous-flow mixer incorporating a hydrodynamic focusing geometry with mixing times of less than 10 μs and sample consumption rates of nanolitres per second. In addition, microfluidics can be used to generate concentration gradients for the study of chemotaxis. Diao J *et al* (2006) have used microfluidic principles to

create chemical gradients and loaded *Escherichia coli* strain RP437 by hydrodynamic focusing to study chemotactic migration.

PDMS is the most popular material for microfluidic chip fabrication (Beebe DJ *et al 2002*) and is also the preferred substrate for plasma stencilling. Cell patterns on PDMS can therefore be packaged inside a PDMS microfluidic chamber by plasma bonding. Indeed, the same plasma treatment can be used to produce cell patterns and for bonding the microfluidic chamber. It has been shown that plasma activation of PDMS produces silanol groups as a result of oxidation which enable PDMS-PDMS bonding with MPa bond strengths (Chen HY *et al* 2008). PDMS-glass bonding following plasma treatments is also possible due to spontaneous dehydration following oxidation (Chaudhury MK and Whitesides GM, 1992). In both cases, the elimination of protein deposition steps prior to cell patterning is a key advantage. This permits a straight forward plasma bonding step to include cell patterns inside the microfluidic chamber without the danger of damaging the integrity of proteins that would otherwise be present. To demonstrate the simplicity of this approach, we have packaged SW480 patterned cells inside a static microfluidic chamber for four days without media exchange (figure 2.3.11). The ability to easily combine the spatial control of cells with the spatial delivery of compounds clearly provides many capabilities for applications ranging from fundamental cell biology to high throughput bioassays.
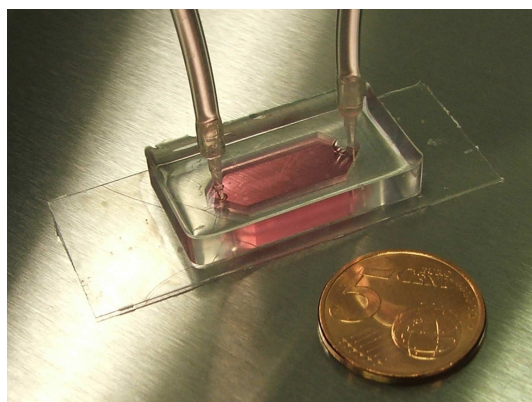
Figure 2.3.11: PDMS microfluidic system incorporating patterned cells. Plasma stencilling was used for both cell patterning and to enable bonding between both PDMS layers.

2.4 Conclusions and outlook

In this chapter, plasma stencilling techniques for the straight forward patterning of 10 mammalian cell lines on hydrophobic and cell repellent poly(dimethylsiloxane) (PDMS), methylated glass and bacterial grade polystyrene surfaces are presented. Cell lines from various tissue origins were successfully patterned for lengthy cultivation periods (>10 days) and without the need for additional surface modification steps. A Tesla generator or a dielectric barrier discharge (DBD) system (operating at atmospheric pressure and without gas supplies) in combination with microengineered stencils were used to selectively transform the surface to a hydrophilic state for cell patterning. Plasma treatments resulted in surface oxidation which selectively rendered the surfaces hydrophilic and wettable on an otherwise hydrophobic and cell repellent surface. Parallel or orthogonal tracks were achieved by using a PDMS microfluidic stencil to controllably route the plasma with the same dimensions as the microchannel, cellular arrays were generated using either a polyimide stencil with micromachined through holes or, for smaller cellular arrays, a novel microcapillary-based DBD system. Simple equations were also introduced to characterize the efficiency of patterning and the pattern occupany, and could be used as a standard approach for evaluating and comparing the efficacy of patterning techniques. Finally, with the plasma activation process enabling PDMS-PDMS bonding, the inclusion of cellular patterns inside a microfluidic chamber was also demonstrated. In summary, these simple, rapid, inexpensive, reproducible, effective and potentially universal cell line patterning techniques are ideally suited for adoption by the biology community.

3

Thin Film PDMS for Cell Patterning
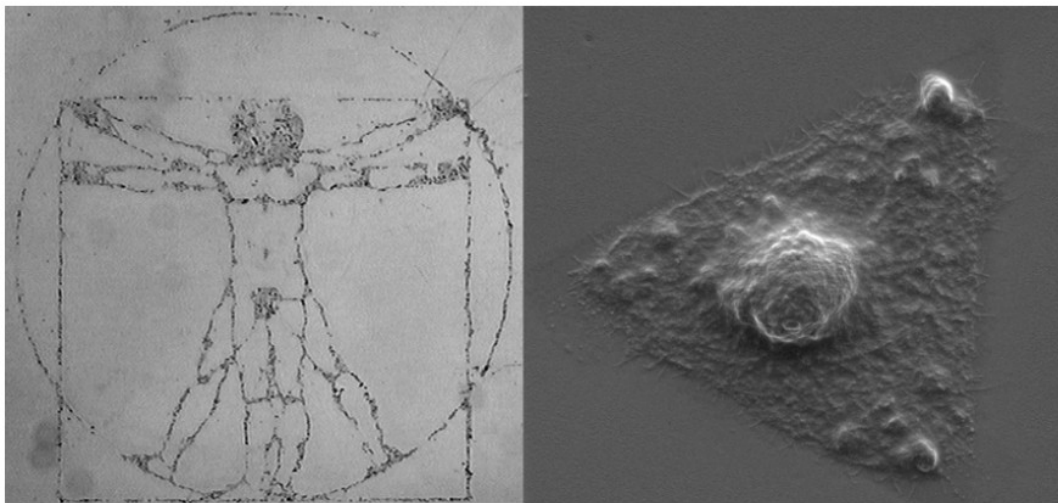
<u>The work in this Chapter was published in part as:</u>

'Microarrays for the scalable production of metabolically-relevant tumour spheroids: A tool for modulating chemosensitivity traits'.
Hardelauf H, **Frimat JP**, Stewart JD, Schormann W, Chiang YY, Lampen P, Franzke J, Hengstler JG, Cadenas C, Kunz-Schughart LA and West J;. *Lab on a chip,* DOI:10.1039/C0LC00089B.

<u>Part of the work in this Chapter won Best Poster Award at Nano-Bio-Tech 2008 and 2009 as:</u>

'*Directed Organization of cellular patterns*'.
Frimat JP, Mariani MM, Kettler R, Jacob P, Franzke J and West J. The 12th Annual European Conference on Micro and Nanoscale Technologies for the Biosciences, Montreux, Switzerland, November 2008; And

'Micropatterning Approach for the Massively Parallel Production of uniform Tumour Spheroids'.
Menne H, **Frimat JP**, Cadenas C, Franzke J and West J. The 13th Annual European Conference on Micro and Nanoscale Technologies for the Biosciences, Montreux, Switzerland, November 2009.

3.1 Introduction

In the previous chapter, hydrophobic surfaces were selectively oxidized to generate hydrophilic patterns for cell adhesion. In particular, PDMS was found to be cell repellent when hydrophobic, and this feature was used to constrain cell patterns. However, the inability of producing individual subcellular (<10 µm) scaled plasmas in a parallel fashion over large areas translated into a lack of pattern design freedom and scalability. Therefore, to enable single cell size array production over large areas and in a reproducible manner, absolute freedom of pattern design is required which could not be achieved by the plasma stencilling methods.

In this chapter, and based on the knowledge gained from the previous chapter, hydrophilic tissue culture grade substrates have been selectively transformed to generate hydrophobic PDMS patterns to confine cell adhesion. A variety of techniques using PDMS to generate hydrophilic–hydrophobic contrasting surfaces for cell patterning have been reported (Patrito N *et al* 2007, De Silva MN *et al* 2005 and 2007, Rhee SW *et al* 2005). For example, the deposition of thin metal films on PDMS through a mask and in the presence of a gaseous plasma creates hydrophilic patterns following removal of the thin metal

film (Patrito N *et al* 2007). Unfortunately, this method involves complex chemistry and requires complicated and costly equipment. In addition, precision spraying has been used to deposit laminin on PDMS and even PDMS on glass to create patterns for cell adhesion (De Silva MN *et al* 2005). However, this serial write method does not offer subcellular resolution and freedom of design is limited. In this study, thin perforated films of hydrophobic PDMS were deposited by microcontact printing (µCP) onto standard cell culture surfaces to produce micropatterns for cell adhesion. This novel approach, termed thin film PDMS µCP can reproducibly generate sub-cellular scaled patterns as well as patterning larger areas, with absolute freedom of design on tissue culture grade substrates such as glass or polystyrene. It operates on the same principles as standard protein µCP, where instead of proteins, liquid PDMS is transferred from the stamp onto the surface and subsequently cured to generate a stable thin film micropattern. This allows patterns of hydrophobic-hydrophilic contrast to be created with a high level of reproducibility. Unlike standard protein µCP where the reproducibility of protein patterns with uniform quality remains challenging, PDMS prints can be easily identified by conventional microscopy to ensure reproducibility between different printed chips from different batches but also to ensure the quality of the pattern prior to cell patterning.

An alternative technique, termed PDMS micro-embossing (µE), was also developed where liquid PDMS was deposited onto a standard cell culture surface and embossed on a hot plate using a stamp to create through holes reaching the substrates hydrophilic surface. Upon removal of the stamp, the hydrophobic thin film PDMS is perforated, allowing the cells to access the exposed hydrophilic tissue culture surface and adhere.

The developments of these techniques have produced fast, cheap, reproducible and highly effective methods for cell patterning. With available microstructured stamps, the process itself requires no complex instrumentation nor complicated surface modification steps. The simplicity of these methods makes them ideally suited for adoption by the biology community. They can serve as tools to standardize cell biology and present simple analytical, quantitative,

reproducible and high throughput data acquisition capabilities to develop novel analytical platforms for cell biology. To demonstrate such possibilities, the PDMS µCP method was used to produce an array for the scalable production of uniform human tumour spheroids for cancer research studies. The PDMS µCP method was also used to develop a novel neurotoxicology platform which will be discussed in chapter four.

3.2. Materials and methods

3.2.1 Thin film patterning

A microcontact printing (µCP) approach was used for thin film PDMS patterning. The PDMS stamps were prepared using a prepolymer mixed with curing agent at a ratio of 10:1 (wt/wt) and then thoroughly degassed using a vacuum desiccator. A microstructured SU-8 master was fabricated by standard methods and used to mould the PDMS (Sylgard® 184, Dow Corning) stamps at 70ºC for 30 minutes. Prior to PDMS patterning the stamps were sterilized using 70% ethanol. A thin film of liquid PDMS was used to ink the stamps. An uncured PDMS pre-polymer and curing agent mixture (1:5, w/w) was dissolved in chloroform (1:10, w/w) to produce liquid PDMS, and a 500 µL volume was applied to a glass substrate and spin-coated at 6000 rpm for 30 s. The chloroform evaporated to leave a uniform film of PDMS. Inking the PDMS stamp with liquid PDMS was achieved by simple conformal contact of the stamp with the thin film for ≤10 s. The inked stamp was then used to print liquid PDMS on glass or tissue culture grade polystyrene substrates. Thermal curing at 70°C for 10 min was used to produce a stable thin film PDMS pattern with the perforations exposing areas of the underlying glass substrate. This procedure is illustrated in figure 3.2.1. For higher resolution patterning, excess liquid PDMS was first removed by contact printing for ≤10 s on a sacrificial glass slide, followed by a second print, again for ≤10 s, on the cell culture substrate. Secondary prints were used throughout this study.

As an alternative to the µCP method, an embossing technique was also developed termed PDMS micro-embossing (µE). Thin film PDMS was deposited, as described above, by spin coating onto a cell culture substrate. The substrate was then placed on a hot plate at 70ºC, and the PDMS stamp was pressed (~0.15 N mm^{-2}) against the substrate for 1 minute before removal. This was followed by a further 10 minutes of thermal curing. The simple embossing procedure is illustrated in figure 3.2.2. The surface free energy of 5 replicate PDMS prints was evaluated by contact angle measurements of a 1 µL sessile water droplet, and the topography of the patterned thin films was characterized by white light interferometry (NewView 5000 Microscope, Zygo).
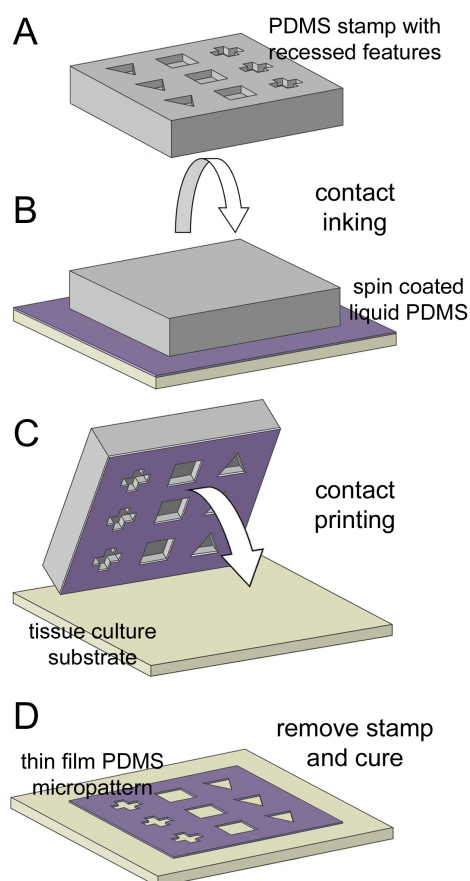
Figure 3.2.1: Schematic of thin film PDMS patterning by microcontact printing (µCP).
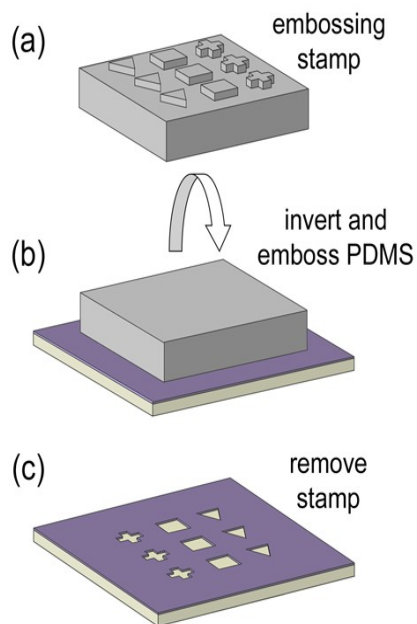
Figure 3.2.2: Schematic of thin film PDMS patterning by micro-embossing (µE).

3.2.2 Cell culture

Cell lines were purchased from DSMZ (Germany) or from ECACC (UK), and all cell culture media and consumables were purchased from Sarstedt AG & Co. (Germany) or PAA Laboratories GmbH (Germany). The 10 human cell lines used in this study were epithelial cells of colon origin (SW480, SW620, NCM460 and HT29), breast carcinoma cells (MCF-7 and BT474), lung carcinoma cells (NCI-H1792), keratinocytes (HaCaT), neuroblastoma cells (SH-SY5Y), and poorly adherent human embryonic kidney cells (HEK293), as well as primary mouse hepatocytes and neurons. All cells were cultured under standard conditions according to supplier recommendations. Typically, Dulbecco's modified Eagle medium (DMEM) supplemented with 10% (v/v) foetal bovine serum, 1% (v/v) Glutamax and 1% (v/v) penicillin and streptomycin was used. Cells were harvested using trypsin once 80-90% confluency was attained. Patterning involved seeding cells in a 1 mL suspension containing 2×10^5 cells and incubated for 12-24 hours at 37°C with 5% CO_2. The suspension was then removed, replaced with fresh media and incubated for up to 15 days, with 3-4

day periodic exchange of the media. An inverted microscope (IX71, Olympus) or an environmental SEM (Quanta 200F, FEI) was used to image the cell patterns.

3.2.3 Spheroid culture

For the mass production of spheroids, PDMS prints were prepared with a spot diameter of 150 µm and spaced by 400 µm to 2000 µm to form a hexagonal array of equidistant adhesion sites. Human HT-29 colon carcinoma cells were seeded on these patterns in a 1 mL suspension containing 2 x 10^5 cells and incubated for 72 hours at 37 °C in a 6% CO_2 atmosphere. The suspension was then removed and replaced by fresh media with 3-4 day periodic exchange. An inverted microscope (IX71, Olympus) equipped with a digital camera (XC30, Olympus) was used to image the developing spheroids and Cell[A] image analysis software was used for measuring the diameter of the spheroids.

3.2.4 Spheroid fixation

Spheroid fixation was required for taking high resolution images by SEM (Quantam200F, FEI, operating at 90 Pa.). SEM imaging required fixation: The arrays were incubated twice in 1 x PBS for 5 minutes and then fixed for 24 hours in SAV 4% neutral buffered formaldehyde (Liquid Production, Germany), followed by a final 1 x PBS wash for 5 minutes and air drying for a further 24 hours. The spheroid arrays were coated with gold for electron imaging.

3.2.5 Spheroid shape characterization

The spheroids were harvested manually and inserted in a 50-60°C warm 2% (w/v) agarose solution inside a Petri dish. Following embedding of the spheroids inside the agarose, the Petri dish was rapidly cooled to fix the spheroids. Small cubes (1mm³) of agarose, each containing a spheroid, were cut from the agarose block using a razor blade. All three axes from the spheroid were imaged by microscopy (IX71, Olympus).

3.3 Results and discussion

3.3.1 Characterization of PDMS microcontact printing (µCP) patterns

Thin film PDMS deposition by PDMS µCP onto cell culture substrates is simple and inexpensive, reproducibly producing patterns for cell adhesion. Following µCP, the thin PDMS film remained characteristically hydrophobic, with a contact angle of 107.4 ± 1.5°. This is consistent with wetting properties of PDMS prepared by standard methods and also suggest that the chloroform does not affect the surface properties of the PDMS. White light interferometry (WLI) measurements showed that the PDMS thin film thickness of the second print was on average 40 nm high. However, topographical analysis also revealed that the border between the PDMS and exposed substrate was higher, with a height maxima of about 120 nm (see figure 3.3.1).
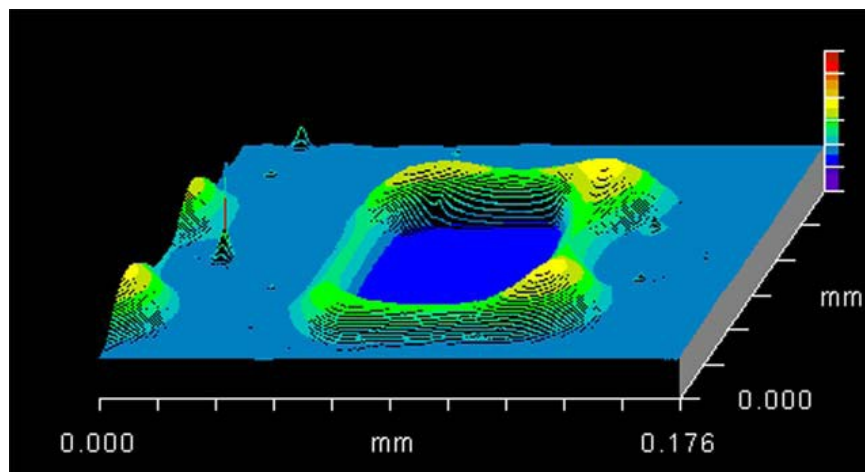
Figure 3.3.1: White light interferometry (WLI) analysis of a square pocket produced by PDMS µCP. The thin film has an average height of 40 nm with height maxima of 120 nm surrounding the exposed cell adhesion area.

These raised regions surrounding the open areas could be caused from the adsorption by capillary flow (Suh KY *et al* 2001) of the liquid PDMS into the stamp recessed features during inking. During printing, this excess liquid PDMS is transferred onto the substrate, and following curing, produce these 'sand bag'

features on the surface. It is important to note that although there is a variation in the thin film height, the overall thickness remains much lower than the height of an adherent cell and can be considered to be 2-D in nature.

3.3.2 Precision of patterning by thin film PDMS microcontact printing (µCP)

Following thin PDMS film deposition by µCP, the fidelity of pattern transfer was analyzed by measuring the difference in sizes between recessed features of the stamp and exposed areas on the surface. The 'sand bag' features, resulting from excess PDMS being transferred during printing, can impact the fidelity of the prints. In addition, due to the PDMS being in a liquid state during printing, PDMS spreading prior to thermal curing can occur resulting in shrinkage of the patterns.

To investigate the effect of this problem and whether feature dimensions or spacing (density of pattern) can impact pattern dimension fidelity, a printed array of islands with diameters ranging from 25-70 µm and spacing ranging from 40-140 µm was analyzed. The different pattern density from the combinatorial stamp can also be recorded as a ratio between PDMS printed and non-printed areas, as shown in table 3.3.1.

Table 3.3.1: The different pattern densities ratios for the combinatorial array. A value of 1 means there is no PDMS on the slide while a value of 0 means that the slide is completely covered by PDMS.

Diameter (µm)→ Distance (µm)↓	25	30	40	50	70
40	0.15	0.2	0.29	0.39	0.58
50	0.11	0.15	0.22	0.29	0.45
70	0.07	0.09	0.14	0.19	0.29
100	0.04	0.05	0.08	0.11	0.18
140	0.02	0.03	0.05	0.07	0.11

In this case PDMS pattern density ratios varied from 0.02 (25 µm diameter spaced by 140 µm) to 0.58 (70 µm diameter spaced by 40 µm), with the majority of ratios falling between 0.02 and 0.2. Figure 3.3.2 shows that there were no direct relationships between pattern density or dimensions and loss of fidelity for PDMS µCP (black squares). For all dimensions and spacing, the PDMS printed thin films showed pattern shrinkage, with the printed features having on average a loss of 4.1± 1.9 µm in diameter when compared to the stamp.
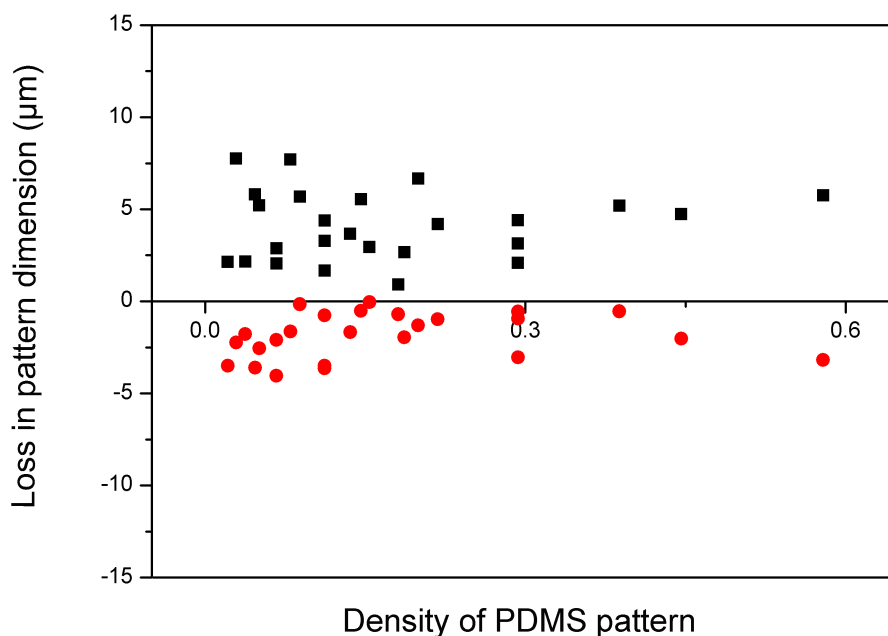
Figure 3.3.2: Loss of pattern dimension (in µm) in relation to pattern density for both PDMS microcontact printing (µCP) (black squares) and micro-embossing (µE) (red circles).

As discussed previously, the use of third or fourth prints (instead of second, see section 3.2.1) can be useful to reduce the loss in pattern fidelity. An example of a fourth print is shown in figure 3.3.3 where a channel width of 3.73 ± 0.35 µm could be obtained (using a stamp with a feature size of 5 µm). WLI analysis

recorded a PDMS height of 4.61 ± 0.639 nm for the fourth prints. Therefore higher resolution capability can be obtained by using third or fourth prints although thinner PDMS films may have reduced stability under cell culture conditions. This is because thinner films can be punctured when exposed to media and cells leading to pattern loss. Another possibility to reduce the loss in resolution would be to spin coat less PDMS ink or higher rpm values and therefore have less adsorption inside the recessed features of the stamp. Notwithstanding these issues, an example of a PDMS µCP array of square adhesion islands is shown in figure 3.3.4(a) with the loss being reproducible across each pattern and sufficiently suitable for patterning single cells (figure 3.3.4b), for printing precision patterns over large areas (figure 3.3.4c) or even to constrain single cells inside various geometries such as a triangle (figure 3.3.4d).
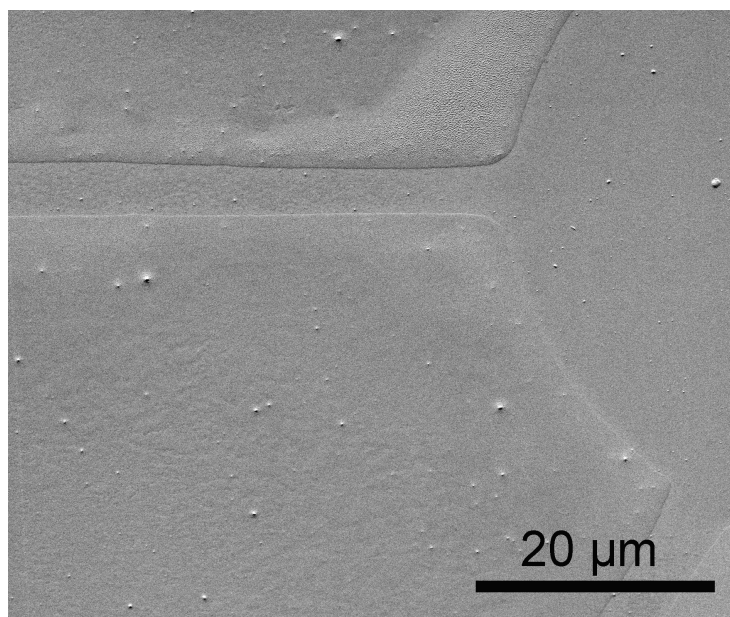
Figure 3.3.3: The use of subsequent prints reduces pattern resolution loss. A fourth consecutive print showing a PDMS channel width of 3.73± 0.35 µm from a 5 µm wide template.
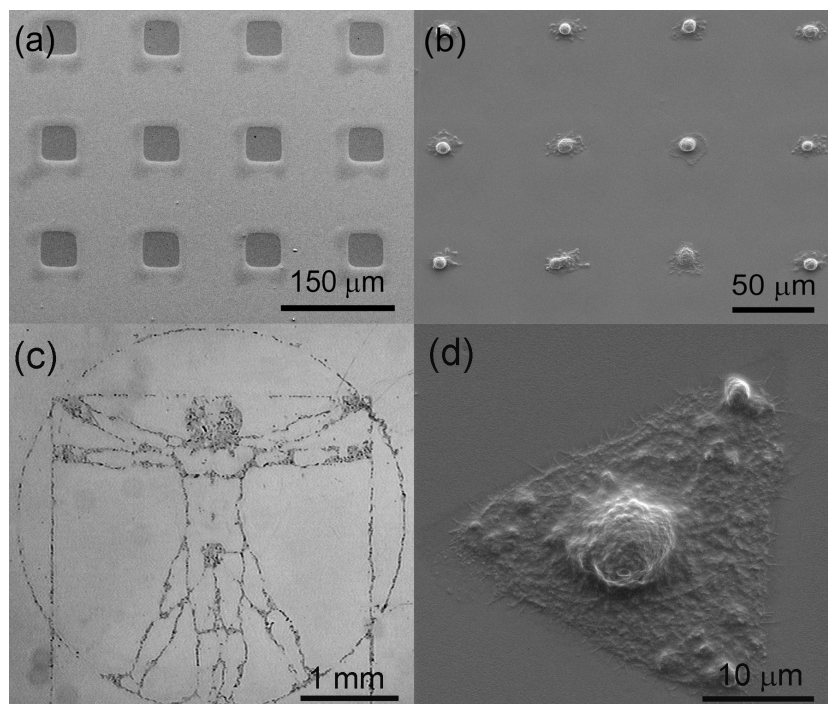
Figure 3.3.4: Thin film PDMS patterned by µCP, with darker regions representing the underlying cell culture surface (a). SW480 single cell array (b), SW480 cells patterned on a large scale as demonstrated with a reproduction of Da Vinci's Vitruvian Man (c) and a triangular pattern for the geometric control of a single SW480 cell (d).

It is important to note that standard protein µCP offers a higher pattern resolution capability than PDMS µCP. But PDMS µCP is a much more reliable technique for cell patterning, reproducibly producing micropatterns over large areas. In addition, the PDMS stamps can be quickly washed with hexane (1-2 min) to remove the liquid PDMS from the surface and used again following N_2 drying. Similarly to protein µCP, the stamps have shown good cell patterning quality following 10 successive prints, demonstrating that the stamps are reusable. Finally, the PDMS printed surfaces can be stored at room temperature for at least 10 days while retaining good cell patterning quality.

3.3.3 Characterization of PDMS micro-embossing (μE) patterns

Analogous to the above mentioned PDMS μCP method, and in an attempt to achieve higher cell patterning resolution, PDMS micro-embossing (μE) was developed. This technique involves the embossing of thin PDMS films onto cell culture substrates to create cell adhesive regions. The embossing was done using the stamps designed for PDMS μCP but with the difference that the stamp had protruding features for embossing instead of recessed features for printing. In this approach, the same substrate is used for liquid PDMS spin coating and cell patterning, with an average final film thickness of ~250 nm. A force of ~0.15 N mm^{-2} was applied onto the stamp for embossing and to remove the liquid PDMS from under the protruding features. The embossing was performed manually on a 70°C hot plate for 1 minute so as to cure the liquid PDMS in between the protruding features. These emboss the micropattern which remains following removal of the PDMS stamp. Similarly to PDMS μCP, the sandbagging effect was also present, with height maxima of 420 nm at the border between PDMS and the exposed surface. Again, capillary effects (Suh KY *et al* 2001) may influence the way the liquid PDMS behaves at the interface between microstructure and surface, resulting in these sand bags features. It is also possible that the liquid PDMS that is pressed under the stamps protruding features is accumulating inside the intervening areas of the microstructures, allowing excess liquid PDMS to be present at the borders following embossing and stamp removal.

3.3.4 Precision of patterning by thin film PDMS micro-embossing (μE)

Following thin film PDMS micro-embossing (μE), pattern fidelity was analyzed by measuring the differences in sizes between protruding features on the stamp and embossed features on the surface. The 'sand bag' features, resulting from excess PDMS being pressed during embossing, can impact the fidelity of the prints. To assess any loss in pattern resolution by PDMS μE and whether feature dimensions or spacing (density of pattern) can impact pattern fidelity, the combinatorial array experiment used for PDMS μCP was also undertaken for

PDMS µE. Islands with diameters ranging from 25-70 µm and spacing ranging from 40-140 µm (see table 3.3.1) were embossed and measured for loss in pattern resolution. Similarly to PDMS µCP, PDMS µE resolution was not affected by feature size or pattern density, as shown in figure 3.3.2. Unlike PDMS µCP, regardless of pattern feature sizes and densities, embossed patterns were 2.1 ± 1.7 µm larger than the stamp features. The increase in pattern size could be caused by the deformation and widening of the PDMS protruding microstructures during the embossing process.

Nevertheless, the higher precision of the PDMS µE technique was used to generate higher resolution patterning features. A thin PDMS film was embossed to produce cross-shaped patterns for single SW480 cell patterning. As shown in figure 3.3.5(a), these generate patterns suitable for single SW480 cells to adhere but also to grow in the shape of the embossed features.

However, the major problem with PDMS µE is that the liquid PDMS under the protruding microstructures of the stamp is not always completely removed following µE. As shown in figure 3.3.5(b), PDMS residue can be found inside the islands (lighter grey regions) although partial PDMS exclusion is also shown (darker grey regions). One possibility to reduce this drawback is to spin-coat a thinner PDMS film so as to facilitate the removal of the excess PDMS during embossing. It is also worth noting that there appears to be a directional character to the tear in the resulting embossed PDMS which is also shown in figure 3.3.5(b) (see arrows). This directional removal of PDMS is likely to be a result of the manual removal of the stamp and could be overcome by using automated equipment with vertically aligned parallel contacting of the stamp and substrate. Another drawback of the thin film PDMS µE method is that the protruding microstructures from the PDMS stamp can be transferred onto the substrate upon removal of the stamp. An example of the production of these microscale 3-D structures is shown in figure 3.3.6, where a stamp with protruding triangle, square and cross features was used. This drawback can be explained by the lack of thermal control and timing as well as low precision during the manual removal of the stamp. On the other hand, the production of PDMS microscale 3-D

structures on a thin PDMS underlayer could be desirable for applications where the substrate can be made cell adherent but not the microstructures. It is also important to note that the production of these microstructures is at random and not all the protruding features from the stamp are transferred (as shown in figure 3.3.6).
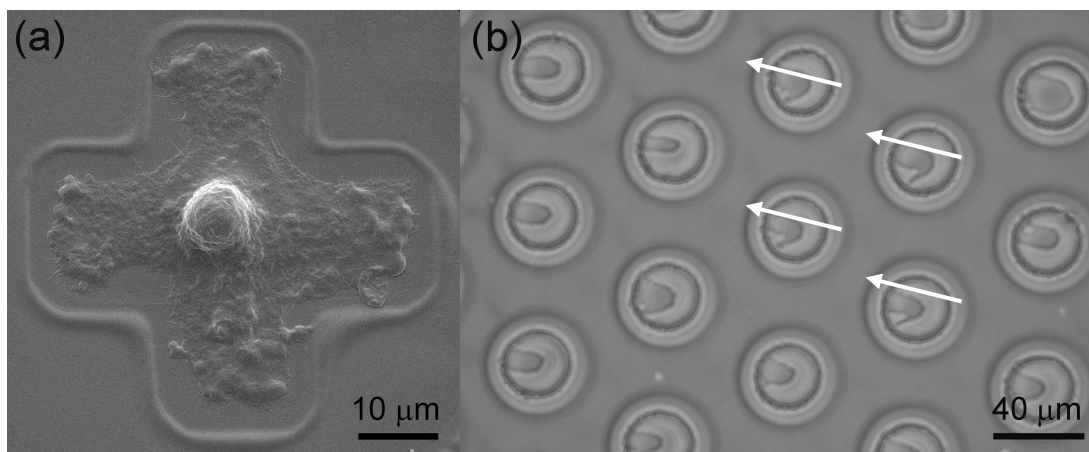
Figure 3.3.5: SW480 epithelial cell in a cross-shaped geometry patterned by PDMS µE (a). Embossed thin film PDMS in a hexagonal array, with PDMS left inside the pockets following µE (b). Directional tear following removal of the stamp is indicated by the white arrows (b).
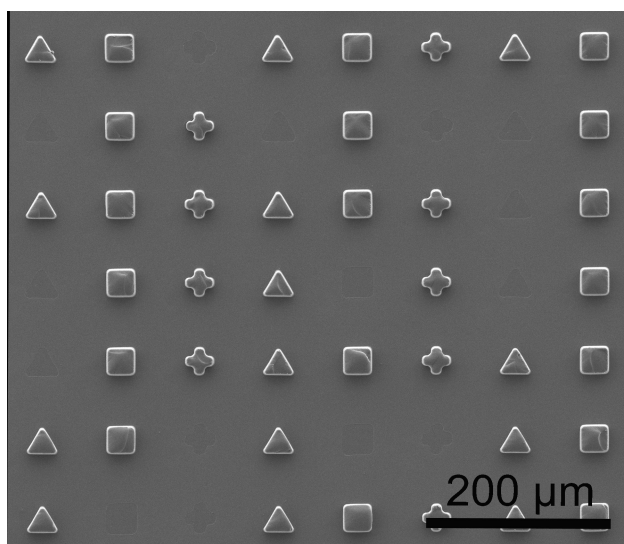
Figure 3.3.6: Transfer of protruding PDMS features from the stamp onto the surface following µE and thermal curing. In this case a stamp with protruding triangle, square and cross features was used.

Therefore, thin film PDMS µE requires greater technical accuracy to reproducibly generate micropatterns for cell adhesion, an issue that could be tackled with automated equipment to assist with precision, weight, time and temperature control. In addition, the use of a non-elastomeric stamp (solid or metallic) could also improve the patterning precision of PDMS thin film µE by reducing the deformation of the protruding features observed when using a PDMS stamp. But the risk with using non-elastomeric stamps is that pattern transfer reproducibility could be affected, especially across larger areas.

3.3.5 Cell patterning by PDMS microcontact printing (µCP)

Similar to the plasma stencilling approach, direct protein patterning was not necessary to successfully pattern cells by PDMS µCP and µE. Instead, proteins already present in the cell culture media passively assemble onto the exposed hydrophilic and cell adhesive regions of the tissue culture polystyrene or glass surfaces. The exact mechanisms for cell patterning without the need for directly patterning proteins are not completely understood with the knowledge to date discussed in chapter two, section 2.3.4. Importantly, the use of tissue culture grade polystyrene or glass surfaces as the patterning substrate provides identical physico- and biochemical surfaces to those found in standard tissue culture flasks ensuring that the cellular pattern is the only experimental variable. PDMS µCP is extremely fast and inexpensive, with PDMS thin film deposition taking 1 minute, curing 10 min and seeding cells 30 seconds. In this way, mass production of patterned substrates can easily be undertaken for large scale experiments at a very low cost.

To demonstrate the widespread applicability of the technique, 10 human cell lines from various human tissue origins have been patterned by PDMS µCP. Epithelial cells of colon origin (SW620 cells, NCM460 cells, SW480 cells (figure 3.3.7(a)) and HT29 cells (figure 3.3.7(b)), keratinocytes (HaCaT cells), epithelial-like breast cancer cells (MCF-7 and BT474 cells), lung carcinoma cells (NCI-H1792 cells), neuroblastoma cells (SH-SY5Y cells (figure 3.3.7(c)) and poorly adherent human embryonic kidney cells (HEK293). PDMS µCP also offers

absolute freedom of design over large areas, as exemplified by the chapter content figure, where Da Vinci's Vitruvian Man (500 µm x 500 µm) was replicated (16-fold) with SW480 cells over a 2 cm x 2 cm surface area. In addition, primary mouse hepatocytes and neurons were also successfully patterned by PDMS µCP. These were achieved by printing the thin film PDMS onto collagen or poly-L-lysine coated glass surfaces. These surface coatings are routinely used to culture these primary cells, although the additional layer and associated material roughness and thickness heterogeneity leads to reduced pattern transfer fidelity and decreased film adhesion which impacts pattern stability.
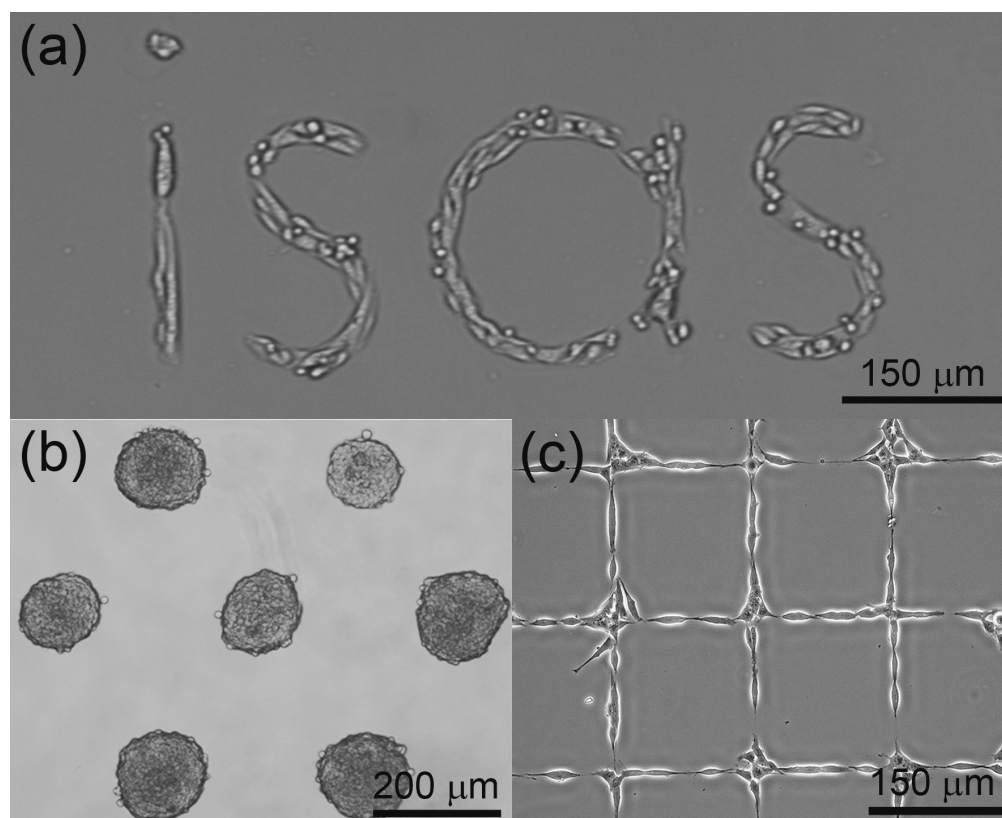
Figure 3.3.7: SW480 cells patterned as the ISAS logo (a). HT29 cells patterned in a hexagonal array (b) and SH-SY5Y neuroblastoma cells patterned as a network (c).

3.3.6 Application: Mass production of tumour spheroids

I supported the following research which was undertaken by **Heike Hardelauf** *(née Menne) of the Miniaturisation Group at ISAS.*

Tumour *in vitro* models for the development of anti-cancer therapies or for the investigation of critical events involved in the onset of cancer traditionally rely on monolayer cell cultures. The disadvantage of such a model is that it does not correctly mimic the tissue architecture, cell-cell and cell-matrix interactions or mass transfer barriers found in naturally occurring tumours, resulting in poor predictive value and failure to identify new therapies. It has been previously reported that the multicellular tumour spheroid model compared with the monolayer model has a more representative cellular architecture with authentic cell-cell interactions and the establishment of mass transfer gradients and associated metabolic profiles and ultimately pathophysiological states (Hirschhaeuser H *et al* 2010) which is a better mimic of the *in vivo* tumour microenvironment.

Various methods currently exist for the production of the multicellular tumour spheroid model. All of these techniques rely on the ability of the cells to form dense tissue aggregates when cell-cell interactions are promoted by inhibiting cell-surface interactions. For example, the use of spinner flasks, gyratory shakers or rotating wall vessels (Ingram M *et al* 1997, Friedrich J *et al* 2007) to continuously agitate the cell suspension can be used for the large scale production of heterogeneously-sized spheroids. Alternatively, and for smaller scale production, the use of cell resistant surfaces has also been reported to induce cellular aggregation and spheroid formation. Concave and cell resistant surfaces such as those found in microtitre plate wells coated with agarose, (Friedrich J *et al* 2009), poly-hydroxyethyl methacrylate (poly-HEMA) (Ivascu A and Kubbies M, 2006), or a droplet's air–liquid interface (Sutherland RM 1988, Kelm JM and Fussenegger M, 2004, Timmins NE and Nielsen LK, 2007) have all been used to initiate the self-assembly of cells into tissue aggregates for the production of spheroids. These methods, termed agarose overlay or hanging

drop method, are able to produce homogeneously-sized spheroids because the cellular aggregation process for each spheroid is compartmentalized (i.e.: one per well). However, these methods have limited scope for mass production as they involve tedious and manually intensive operations. Widespread adoption of this spheroid model in routine cancer research would therefore require new automated methods for the scalable production of tumour spheroids (Hirschhaeuser F *et al* 2010).

Highly parallelized microwell formats have also been previously used for the mass production of spheroids (>1000) during stationary culture. The construction of the microwell array can be achieved by using anisotropically etched silicon (Ungrin MD *et al* 2008) or microstructured SU-8 moulds (Nakazawa K *et al* 2006, Park J *et al* 2007 and Gallego-Perez D *et al* 2010). Another material used for spheroid production is poly(ethylene glycol) (PEG), a material which inhibits protein adsorption and consequently cell adhesion. PEG can either be embossed to harbor spheroid growth (Karp JM *et al* 2007), or thiolated and coated onto platinum-coated PMMA microwells (Sakai Y *et al* 2007). Interestingly, µCP islands of collagen (Fukuda J *et al* 2006, Mori R *et al* 2008) or Arg-Gly-Asp peptide (Inaba R *et al* 2009) inside microwells can be used to centre cellular aggregation and spheroid growth. It has also been shown that adhesion patterns alone can direct the centre of spheroid assembly, and was demonstrated using PEG brushes (Otsuka H *et al* 2004), PEG micropatterned hydrogels (Yoshimoto K *et al* 2009, Kojima R *et al* 2009), or using collagen/PEG micropatterned chips (Tamura T *et al* 2008, Wang W *et al* 2009).

3.3.7 Mass production of spheroids by thin film PDMS microcontact printing (µCP)

A critical observation was made when patterning HT29 cells by thin film PDMS µCP. Following 2 days incubation, HT29 cell aggregates were forming on the exposed tissue culture substrate and following 10 days, spherical-shaped aggregates were observed (figure 3.3.7(b)). Hexagonal arrays with a pitch of 450 µm and spot diameter of 150 µm were patterned by PDMS µCP. Figure 3.3.8

shows spheroid formation over a period of 10 days where initial cells settled within the 150 µm diameter islands at 24h followed by the formation of a monolayer at day 2, a hemisphere at day 4 and a full spheroid by day 10 (235 µm (SD ± 12 µm)). A spheroid growth curve was also recorded where spheroid diameter was plotted against time (figure 3.3.9), demonstrating that the growth of spheroids gradually increases until day 12 and then reaches a plateau. Due to the high level of reproducibility for PDMS µCP and the ability to pattern large areas, highly parallel production of uniform tumour spheroids was achieved and is shown in figure 3.3.10(a). Each patterned glass slide contains 1675 adhesive spots with an average HT29 cell pattern occupancy of 97.3%. Mass production can be achieved by inserting the patterned glass slides inside a 6 well plate (figure 3.3.10(b)), generating a total of 10,050 adhesion sites from which an average of 9779 spheroids were formed (97.3%). It is important to note that patterning HT29 cells on hexagonal array prepared by PDMS µCP efficiently generated high pattern occupancy levels across the whole surface and showed excellent chip-to-chip and batch-to-batch reproducibility (>95%). In addition, harvesting efficiency was on average 99.0% high, with 9678 out of 9779 uniformly-sized spheroids being harvested. The ability to massively produce spheroids in parallel by PDMS µCP has the advantage of minimizing the required incubator space for the generation of high throughput experimentation. Moreover, the use of a 'mother dish' for the mass production of spheroids has the further advantage of reducing pipetting operations, speeding up the process significantly. Both the hanging drop and the agarose overlay method require individual pipetting steps for the production of every single spheroid whereas the PDMS µCP methods only requires a single pipette step to automate the production of 1675 spheroids. In addition, because the spheroids are attached to the surface, media exchange can be performed without the risk of losing spheroids.
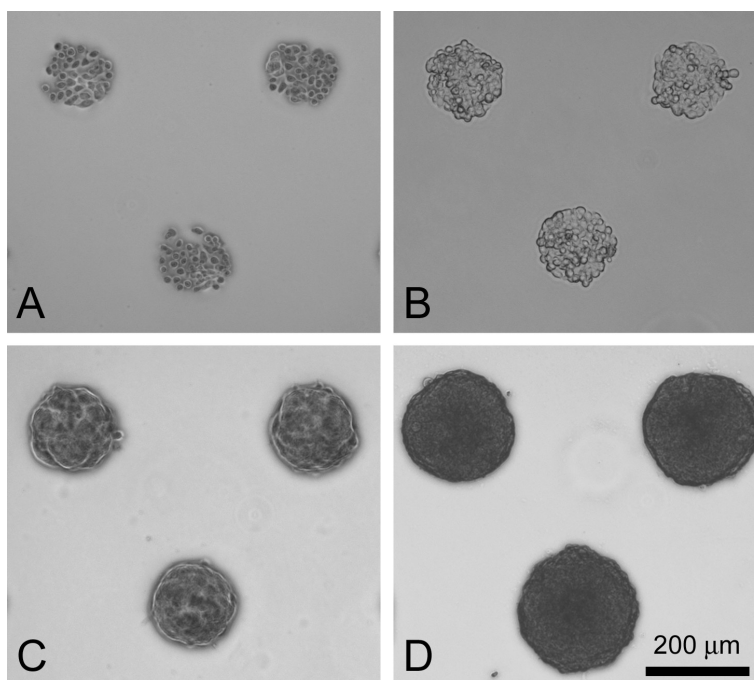
Figure 3.3.8: Human HT29 colon carcinoma spheroid growth on arrays with a 450 μm pitch: Collections of cells adhered to the exposed areas of the glass substrate within the first day (A), monolayers were formed on day 2 (B), hemispheres were formed by day 4 (C) and fully developed spheroids with a diameter of 235 μm (SD ± 12 μm) were formed by day 10 (D).
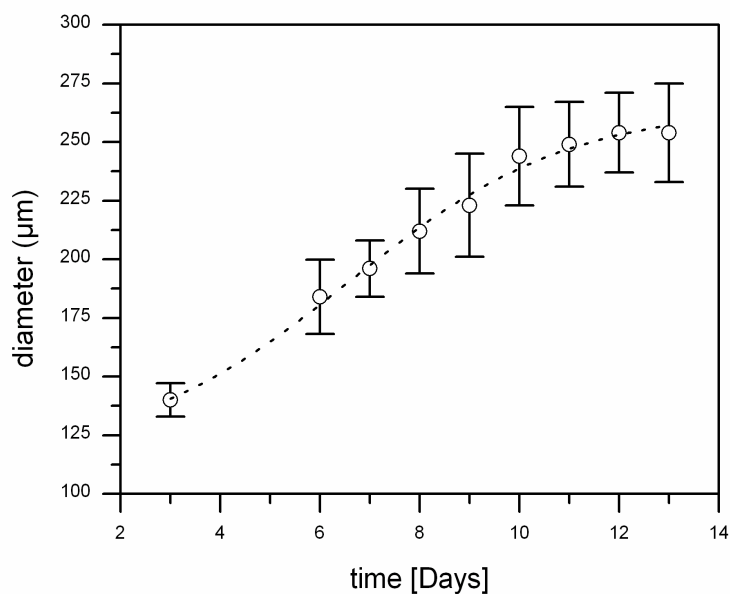
Figure 3.3.9: Spheroid diameter monitored over a period of 12 days on arrays with a 450 μm pitch and a 150 μm spot diameter.
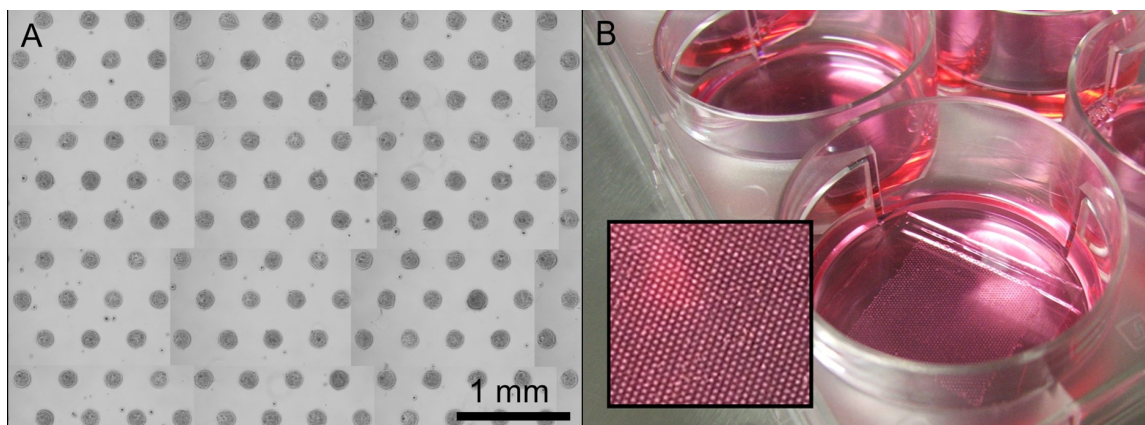
Figure 3.3.10: Mass production of tumour spheroids on an array with a pitch of 450 μm. Image compilation of a 0.55 cm^2 region of an array containing 137 uniformly-sized spheroids following 5 days cultivation (a). Mass production of ~10,000 uniform spheroids inside a 6 well plate (b).

Array-based cultivation of BT474 cells and NCI-H1792 cells for spheroid production was also successful as shown in figure 3.3.11, indicating that arrayed-based spheroid production can be achieved with other spheroid-forming cell types.
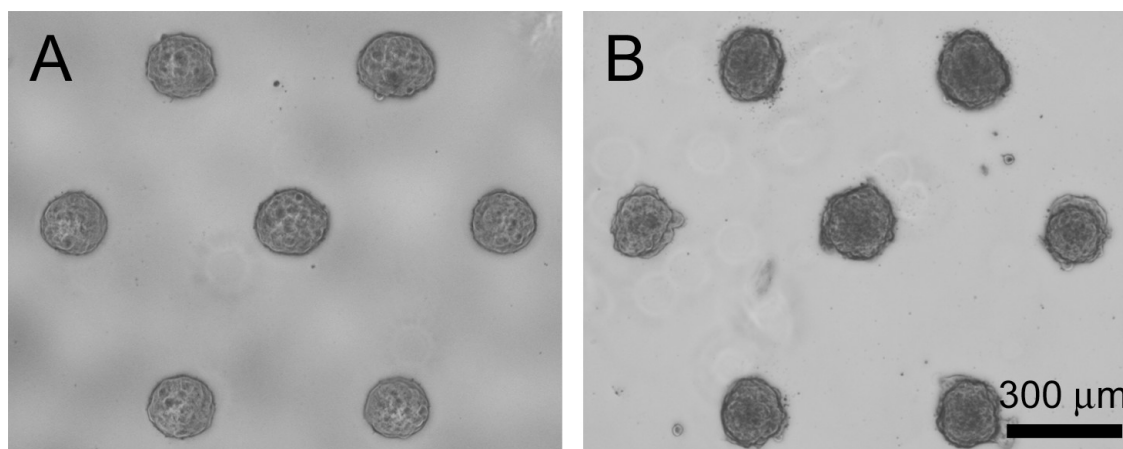
Figure 3.3.11: Demonstration of spheroid production by thin film PDMS μCP with other cell types. Array-based culture of BT474 cells at day 3 (A) and NCI-H1792 cells at day 7 (B).

3.3.8 Spheroid shape characterization

To accurately mimic the *in vivo* tissue-like state of tumours, spheroids must be spherical in shape and possess a truly 3 dimensional architecture. SEM imaging of the HT29 spheroids showed that the spheroids have indeed a 3-D spherical morphology as shown in figure 3.3.12(a) and (b). However, in order to produce 3-axis imaging and perform circularity measurements, spheroids were harvested and embedded in an agarose hydrogel and analyzed from all 3 axes. As demonstrated by figure 3.3.12(c), the tissue aggregates were truly spherical in morphology: $x = 91\%$; $y = 93\%$; and $z = 94\%$.
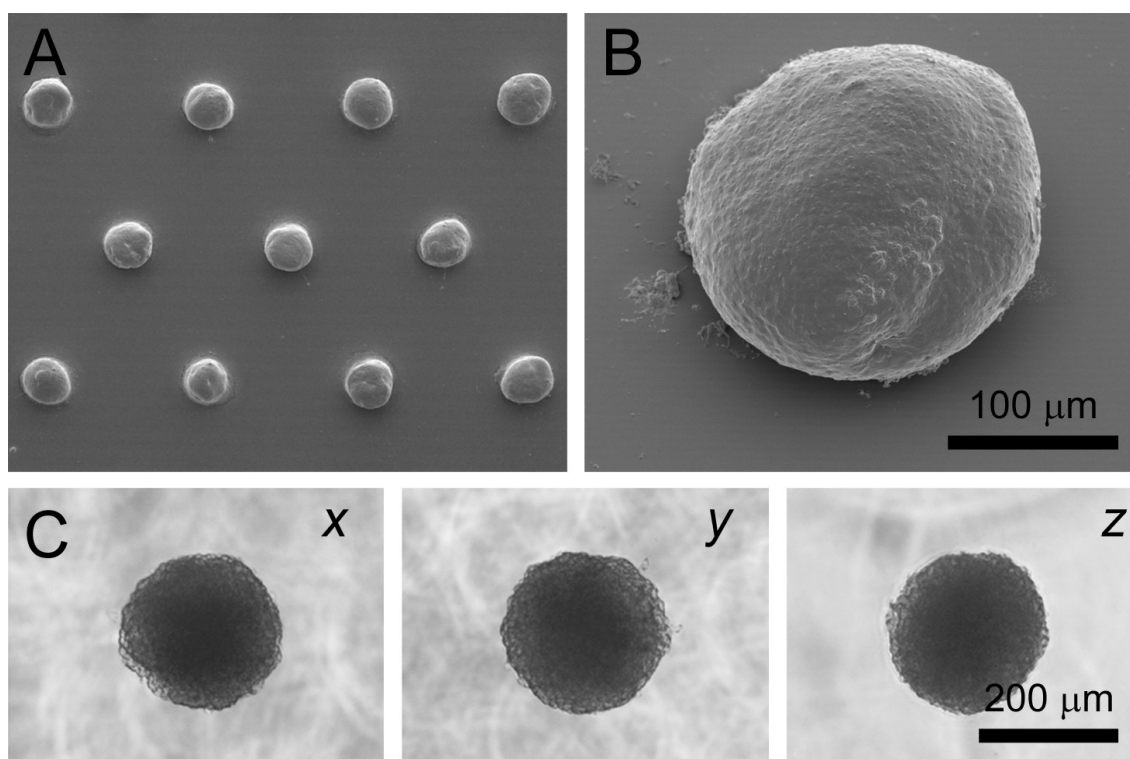
Figure 3.3.12: Spheroids cultivated on the array adopt a highly spherical morphology. SEM imaging of a formaldehyde-fixed array of uniformly-shaped spheroids (A) and an individual adherent spheroid (B). Agarose embedding was used for 3–axis imaging (C) and circularity measurements ($x = 91\%$; $y = 93\%$; $z = 94\%$).

The spherical morphology of the HT29 cell aggregates is a pre-requisite for tissue models *in vitro* and provide the spheroids with symmetrical radial internal mass transfer gradients. Tissue density was also measured using sedimentation rate analysis and showed that the spheroids were typically dense (~1040 kg m^{-3}), a value that closely resembles *in vivo* tissue densities.

3.3.9 Array Packaging

Similarly to the plasma stencilling methods, inclusion of cellular patterns inside microfluidic devices is also straight forward. The use of PDMS as the material for printing or embossing brings the option to allow easy bonding with a PDMS microfluidic chamber or device. PDMS can be simultaneously printed on the side of the patterns to provide a bonding interface with the chamber. Issues included the need to shield the pattern area during plasma activation. The reason being that the free oligomers present in thin PDMS films (5-40 nm in height) are polymerized or oxidized during plasma activation and prevent the hydrophobic recovery. Instead of microfluidic devices, it is also possible to include patterns inside microtiter plates by a variety of methods including plasma-bonding (Chen HY *et al* 2008), using an additional PDMS coating on the microtitre plate as thermal curing adhesive or by using the PDMS as a compression seal. Such formats can be used for the development of parallel and automated high throughput assays. This is of particular relevance to screen and assess novel anti-cancer drugs based on the spheroid model. On a more global view, the ability to combine the spatial control of cells within microlitre chambers enables the development of new multiplexing experiments. This quantitative and reproducible data acquisition tool can have a great impact for commercial applications as well as for gaining valuable information for cell biology research.

3.4 Conclusions and outlook

In this chapter, two patterning techniques involving thin film PDMS deposits were developed based on the cell repellency character of PDMS. Higher pattern resolution was achieved by PDMS micro-embossing (µE) but PDMS microcontact printing (µCP) offers much higher reproducibility in patterning making it the preferred technique for cell patterning. Patterns could be successfully generated with absolute freedom of design over long cultivation periods (>14 days), from large scale to single cell scale and without the need for directly patterning proteins. This streamlined and inexpensive approach is also rapid, and 10 human cell lines were successfully patterned by PDMS µCP. Mouse primary neurons and hepatocytes were also patterned by PDMS µCP onto poly-*L*-lysine or collagen coated substrates. In addition, the stamps used for PDMS thin film deposition were re-usable and the exposed areas for cell adhesion were identical to standard tissue culture surfaces. Thin film PDMS µCP was successfully used to pattern HT29 cells (as well as BT474 cells and NCI-H1792 cells) for the parallel and mass production of 3D spheroids, with high reproducibility and excellent control of the uniformity of spheroid size. Large spheroids which were genuinely spherical and densely aggregated (equivalent to *in vivo* tissues) could be produced by this approach.

The PDMS micropatterning techniques are cheap, simple and efficiently producing patterns over large areas. Just like standard protein µCP, thin film PDMS µCP offers absolute freedom of design but unlike standard protein µCP, thin film PDMS µCP also offers the added benefit of being highly reproducible. These features make the thin film PDMS µCP method accessible and desirable to biologists and microengineers alike. There is potential for this technique to be applied to widespread as well as specialized applications and has value for both academic and industrial research. The development of novel cost effective bio assays in cell biology can be anticipated using thin film PDMS µCP and the next chapter will discuss the use of thin film PDMS µCP for the development of a new neuronal network analytical display.

4

Neuronal Microarrays for Neurotoxicity Screening

<u>This work was published in part as:</u>

'*The network formation assay: a spatially standardized neurite outgrowth analytical display for neurotoxicity screening*'.

Frimat JP, Sisnaiske J, Subbiah S, Menne H, Godoy P, Lampen P, Leist M, Franzke J, Hengstler JG, van Thriel C and West J. *Lab on a Chip 2010, Volume 10:701-706*.

*The work presented was highlighted in the media, including the RSC's Chemical Technology, the New York Times and the MIT Technology Review.

<u>A German and an international patent were successfully filed as:</u>

'Verfahren zur Messung des Neuritenwachstums' ('A Standardized Neurite Outgrowth Assay');
West J, **Frimat JP**, Sisnaiske J, Hengstler JG and van Thriel C.
DE 10 2009 021 876.9, EP 09 012 960.2 and PCT/EP2010/002811. May, 2010

Promotion of scientific work in road safety relevant topics (Award);

"Screening for neurotoxicity of volatile organic compounds in vehicles",

Frimat JP, Sisnaiske J, van Thriel C, Hengstler JG and West J. Deutscher Verkehrssicherheitssrat (DVR), Germany 2009-2010:

The work herein was presented in part in oral presentations as:

'The Network Formation Assay: Rapid in vitro neurotoxicity screening'.

Frimat JP, Hardelauf H and West J*, *in Proceedings of NanoBioTech2010,* Montreux, Switzerland*,* 15-17 November, 2010. And;

'Spatially standardized cell biology'.

Frimat JP, Menne H, Chiang YY and West J*, *in Proceedings of the 2010 Royal Society of Chemistry Analytical Research Forum*, Loughborough, UK, 26–28 July 2010.

The work presented in this chapter was also presented in part on posters as:

'A neuronal network display for neurotoxicity screening'.

Frimat JP, Sisnaiske J, Hardelauf H, Subbiah S, Leist L, Lampen P, Franzke J, Hengstler JG, van Thriel C and West J*, *in Proceedings of µTAS 2010, The 14th International Conference on Miniaturized Systems for Chemistry and Life Sciences*, Groningen, Netherlands*,* 3-7 October, 2010, pp1628–1630. And;

'Spatially standardized cell biology'.

Frimat JP, Menne H and West J, *in Proceedings of Micro- and Nanofluidics for Cell Biology*, Leiden, The Netherlands*,* 18-22 January, 2010. And;

'A network formation assay using micropatterned neuronal nodes'.

Frimat JP, Sisnaiske J, Menne H, Franzke J, Hengstler JG, van Thriel C and West J. The 13th Annual European Conference on Micro and Nanoscale Technologies for the Biosciences, Montreux, Switzerland, November 2009.

.

4.1 Introduction

Following the successful development in the last chapter of the PDMS patterning and demonstration for the mass production of uniformly-sized tumour spheroids, this chapter details another microarray-based application. The application involves the patterning of neurons for the screening of neurotoxic compounds. Global policies, notably Europe's REACH legislation (Registration, Evaluation and Authorization of Chemicals) and the United States Environmental Protection Agency directives, have been put forward to provide comprehensive toxicity data for over 100,000 substances over the next decade. Yet it is estimated that over 30,000 compounds have not been adequately tested nor appropriately evaluated. Standard assays in toxicity testing typically involve the use of *in vivo* rodent models which are time consuming, resource intensive and arguably unethical as many animals are required to screen large numbers of chemicals. There is presently great emphasis on the use of simplified *in vitro* cell culture experiments for high-throughput screening applications. These could be used to reduce animal experiments in the current chemical safety assessment procedures (Lein P *et al* 2005, Coecke S *et al* 2007, Radio NM *et al* 2008, Leist M *et al* 2008). However, neurotoxicology was identified as the one major area where the correlation between the *in vitro* data and the data from the acute oral (i.e; *in vivo*) toxicity test was spoiled. Therefore the development and validation of new *in vitro* cell-based neurotoxicity assays is required in order to provide better predictive value as well as to decrease the use of animal testing (Lein P *et al* 2005, Radio NM *et al* 2008) and meet the demands of widespread neurotoxic compound screening. In addition, novel analysis platform must fit within the traditional mode of thinking so that new results can act as reference standards and be directly comparable with existing methods and be easily accepted within the neurotoxicology community (i.e. a disruptive technology is unwanted). In order to successfully introduce a new *in vitro* assay, attention must also be focused on the production of an *in vitro* model that accurately mimics the critical cellular events of neurodevelopment events found *in vivo*. Functional neurons morphological

characteristics include axonal and dendritic outgrowths (collectively termed neurites in the field of neurotoxicology) which are essential for neuronal interconnectivity and neuronal network formation. These distinct phenotypic characteristics of differentiated neurons are hallmark neurodevelopment end-point indicators and neurite outgrowths are typically the subject of measurements in the traditional neurite outgrowth assay. Traditionally, the neurite outgrowth assay uses sparsely seeded neuron cultures in order to isolate individual neurons and aid the identification, visualization and measurements of neurite outgrowths. For example, the assay can measure the number of neurites per cells (Radio NM and Mundy WR, 2008) or the neurite length or the branching complexity (Vutskits L *et al* 2006). The obvious disadvantage with these methods is that they are extremely manually intensive and time consuming. This is because each individual neuron cells must be manually identified, localized, imaged and the chaotic outgrowth neurite length measured. Therefore, high content screening platforms with automated image capture and analysis have been developed to acquire neurite outgrowth related data more efficiently (Liu D *et al* 2007). These platforms require neuron fixation and antibody staining to aid feature recognition and various groups have reported that these results have an equivalent accuracy to manual tracing (Radio NM *et al* 2008, Ramm P *et al* 2003). The disadvantage with these platforms is that fixation makes the assay terminal and dynamic information, the development of neurite outgrowths over time, cannot be recorded. Despite these progresses, methods for the simple and rapid quantification of the neurotoxic effects of test substances are still needed.

As stated previously, microtechnologies can be used to meet many of the criteria needed for the development of modern bioanalytical platforms. In neurobiology, microfluidic channels and various interconnected compartment geometries have been used to study axon guidance (Francisco H *et al* 2007) and neuronal regeneration processes (Taylor AM *et al* 2003 and 2005, Kim YT *et al* 2009). Spatiotemporal investigations of electrophysiological function have also been carried out on microelectrode arrays (Thomas CA *et al* 1972, Keefer EW *et al* 2001, Tscherter A *et al* 2001, van Vliet E *et al* 2007, Ban J *et al* 2007). In

addition, microelectrode arrays can be coupled with microfluidics for the monitoring of neuronal network activity (Suzuki I *et al* 2005, Ravula SK *et al* 2006, Morin F *et al* 2006). Spatial control of neurons via cell patterning methods (MrKsich M *et al* 1997, Kane RS *et al* 1999, Folch A and Toner M, 2000, Whitesides GM *et al* 2001) have also been used to couple neurons with electrodes for the measurements of potential propagation within an engineered network. These have been measured at precise locations within the engineered architecture (Romanova EV *et al* 2004, Mourzina Y *et al* 2006) and also along single axons (Patolsky F *et al* 2006).

The ability to spatially control neuron positioning for probing action potential propagation has been investigated for over 20 years (Kleinfeld D *et al* 1988), with the early work involving photolithographic silane patterning methods for neuron positioning (Kleinfeld D *et al* 1988, Healy KE *et al* 1994, Corey JM *et al* 1996). Other advances in microtechnology capabilities have led to the development of microcontact printing methodologies that enable cell patterning by printing cell adhesion molecules (Singhvi R *et al* 1994, Ruiz A *et al* 2008). Building on these developments, there is great scope to apply neuropatterning techniques to address widespread and routine challenges in neurobiology (and the life sciences in general)

In this study the value of cell patterning for neurotoxicity testing is demonstrated. A neuronal microarray was produced by thin film PDMS printing and used as a simple neurite interconnection display for the ultrafast and sensitive dose dependent measurement of acrylamide neurotoxicity. This novel approach was termed the network formation assay (NFA).

4.2 Concept

Neurite outgrowths serve as hallmark neurodevelopmental end-point indicators which can be correlated, using biokinetic models, with *in vivo* observations (Forsby A and Blaauboer B, 2007) and thereby provide predictive value for screening the neurotoxicity effects of test substances where the molecular targets and modes of action are unknown (Lein P *et al* 2005 and 2007, Radio NM *et al* 2008). Traditionally, neurite outgrowth assays involve the use of sparsely seeded cell cultures (for illustration see figure 4.2.1(A)), with the resource intensive task of identifying single neurons and measuring their outgrowths. The presented NFA combines the benefits of the neurite outgrowth assay with cell micropatterning to provide a spatially standardized analytical platform. A uniformly spaced hexagonal array of adhesion nodes is used to pattern neurons. Neurite outgrowths interconnect the cellular nodes and result in the development of a neuronal network (for illustration see figure 4.2.1(B)). Critically, the array system standardizes the neurite outgrowth length, thereby eliminating length measurements. The distance is also designed to satisfy standard neurite classification criteria which require a length equal to or greater than one or more cell body diameters (Morooka T and Nishida E 1998, Adlerz L *et al* 2003, Das KP *et al* 2004). The use of analysis coordinates and a common outgrowth length both significantly streamline the identification and measurement effort for high throughput neurotoxicology screening.
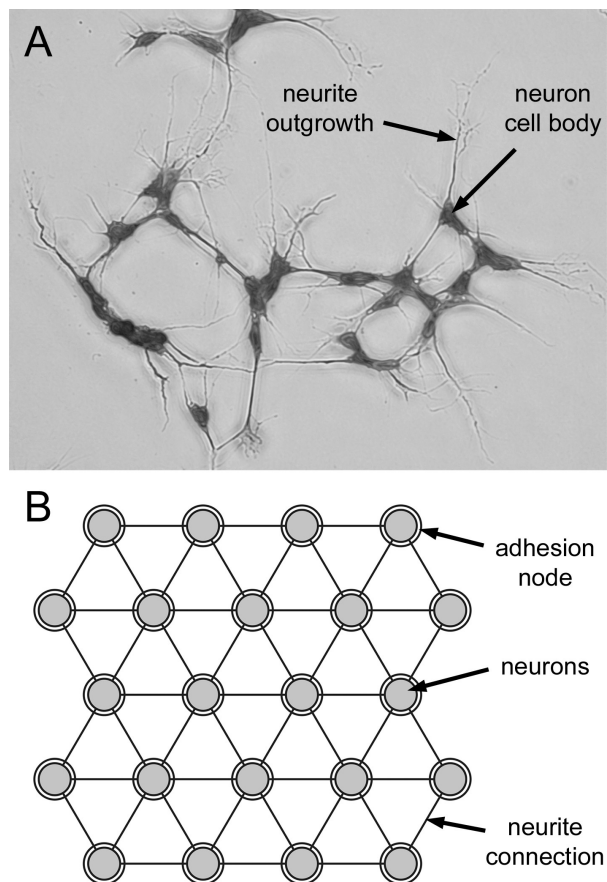
Figure 4.2.1: Differentiated SH-SY5Y neurons cultured on standard tissue culture substrates have an irregular distribution and elaborate complex and 'chaotic' neurite outgrowths (A). Cells were fixed and stained with Giemsa to aid visualization. Illustration of the network formation assay end-point where hexagonally patterned neurons are interconnected by neurite outgrowths (B).

4.3 Materials and methods

4.3.1 Thin film PDMS microcontact printing (µCP)

In this study we have used thin film PDMS (µCP) on tissue culture substrates. PDMS (Sylgard® 184, Dow Corning) stamps were fabricated by moulding a microstructured SU-8 master with a degassed mixture of pre-polymer and curing

agent (10:1, w/w) at 70°C for 30 min. Production of the PDMS patterns was performed as previously described in section 3.2.1, figure 3.2.1. To demonstrate the widespread applicability of thin film PDMS printing, various cell types were patterned on combinatorial arrays comprising adhesion islands with different dimensions and geometries. Neurotoxicity experiments used a hexagonal micropattern to provide a uniformly spaced array of 367 cell adhesion nodes. Each node had a diameter of 70 µm and was separated from neighbouring nodes by 100 µm (figure 4.3.1). Narrow adhesion bridges between nodes were not included in the design. The absence of this feature allows unconstrained neurite outgrowth and also standardizes the neurite interconnection length by restricting the neurons to the adhesion nodes. The entire 20 x 20 mm pattern contained a 5 x 5 matrix of individual arrays, harboring a total of 9175 adhesive nodes.
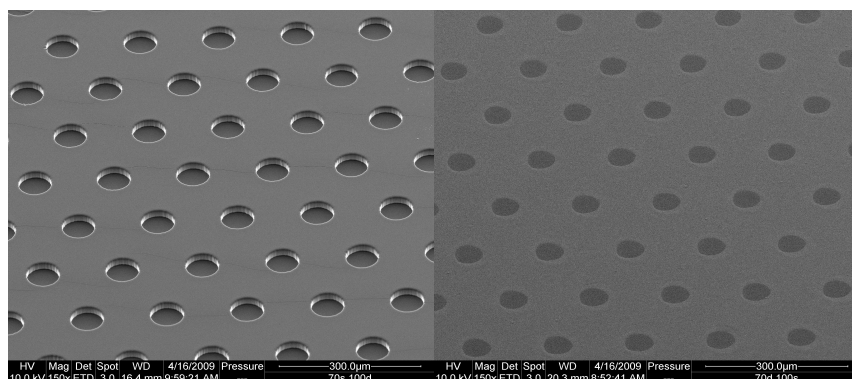
Figure 4.3.1: SEM image of a PDMS stamp (left) and resulting thin film PDMS print (right).

4.3.2 Cell culture and imaging

In the neurotoxicity experiments, human SH-SY5Y neuroblastoma cells (DSMZ, Germany) were used. Cells were differentiated using 10 µM trans retinoic acid (Sigma) for 3 days and then harvested for seeding on the arrays. An inverted microscope (IX71, Olympus) or an environmental SEM (Quanta 200F, FEI) was used to image the cell patterns. The blue fluorescent nuclear dye 4',6-diamidino-2-phenylindole dihydrochloride (DAPI FluoroPure grade, Invitrogen) was used to

ascertain the number of cells occupying individual nodes at 24 h after patterning. Cells were first fixed in 4% glutaraldehyde for 15 min, then washed twice for 5 min in 1x phosphate buffered saline (1x PBS), followed by stepwise alcohol dehydration. Briefly samples were equilibrated in 1x PBS, immersed in deionized H_2O with 30 nM DAPI for 1 min, followed by multiple 1x PBS rinses and finally dried in preparation for fluorescent microscopy.

4.3.3 Neurotoxicity and cytotoxicity testing

To demonstrate the NFA, the arrayed cells were exposed to acrylamide which is a reference neurotoxic compound. Thin film PDMS patterns were prepared on glass substrates (1 x 26 x 26 mm) and transferred to Petri dishes (Ø 55 mm) for cell seeding. Following cell patterning a quality control procedure was undertaken. Only arrays with pattern occupancies in excess of 75% were used for subsequent neurotoxicity measurements. The differentiated SHSY5Y neuron arrays were then cultured for 3 days in 7 mL of serum-containing media (10%) along with acrylamide at final concentrations ranging from 0–5 mM. Experiments were undertaken in triplicate, with array occupancy and neurite interconnection measurements taken daily. Array occupancy was defined as the percentage of the 367 cell adhesion nodes that contain one or more cells. The NFA involved a streamlined analysis approach, measuring the number of neurites connecting immediately neighbouring neuronal nodes and not connections to more distant nodes. Difficulties discerning multiple connections between the same neuronal node neighbours were also obviated by classifying these together as a single connection. To reduce the impact of sample–sample pattern occupancy variations values are converted to neurite interconnections per occupied neuronal node. To document the process cell arrays and neurite interconnections were imaged using an inverted microscope (IX71, Olympus). Cytotoxicity was measured using the CellTiter-Blue® Cell Viability Assay (Promega): a 100 mL volume of media containing 5 x 10^4 pre-differentiated SH-SY5Y cells was added per well of a 96 well plate. Cells were cultured in serum-containing media along with acrylamide at concentrations ranging from 0–500 mM for 24 h. Following

exposure, a 20 µL volume of the CellTiter-Blue® resazurin reagent was added to the culture media and incubated for 4 h at 37°C for conversion by viable cells into the fluorescent compound resorufin. Fluorimetry involved excitation at 540 nm and emission detection at 595 nm.

4.3.4 Pathway controls

Inhibitors of MAPK and PI-3K signaling pathways were used as positive controls for the NFA. Pathway control experiments involving the use of PD98059 (Sigma) to inhibit MEK1/2 signaling and LY29002 (Sigma) to inhibit PI-3K signaling were undertaken to evaluate the ability of the NFA to detect pathway specific mechanisms of neurite outgrowth inhibition. Pre-differentiated and patterned SH-SY5Y cells were exposed to the inhibitors at 5, 15.8 and 50 µM concentrations with network formation analysis at 24 h. To confirm pathway specific inhibition Western blot analysis was also undertaken: Each well of a 6 well plate was seeded with 5 x 10^5 predifferentiated SH-SY5Y cells and exposed to the inhibitors at 5, 15.8 and 50 mM concentrations for 1 h, followed by harvesting and homogenization on ice in RIPA buffer (150 mM NaCl, 50 mM Tris–HCl, 1 mM EDTA, 1 mM NaF, 1 mM Na_3VO_4, 1 mM phenylmethylsulfonyl fluoride, 0.1% SDS, 1% NP-40 and 1% sodium deoxycholate, pH 7.4 with 0.5% (v/v) protease inhibitor cocktail (Sigma)). After centrifugation at 15,000 g for 30 min at 4°C the protein concentration was measured using the bicinchoninic acid (BCA) Protein Assay Kit (Pierce). Aliquots containing 50 mg of protein were separated on a 10% SDS polyacrylamide gel and transferred to a polyvinylidene difluoride membrane (Perkin-Elmer). The membrane was blocked in TBS-T (Tris-buffered saline with 0.1% (v/v) Tween-20) containing 5% (w/v) bovine serum albumin fraction V and incubated overnight with primary antibodies (1:1000 rabbit anti-ERK1/2; 1:1000 rabbit antiphospho- ERK1/2; 1:1000 rabbit anti-Akt, 1:1000 rabbit anti-phospho-Akt and 1:1000 rabbit anti-α-tubulin). After washing in TBS-T, blots were incubated for 1 h with a secondary antibody (1:1000 anti-rabbit IgG) conjugated to horseradish peroxidase. All antibodies were obtained from Cell Signaling Technology, Inc. The antibody-labeled bands were detected by

incubating the membrane with Western Lightning Chemiluminescence Reagent Plus (Perkin-Elmer), followed by imaging using a chemiluminescence documentation system (ChemiLux CSX-1400M, INTAS). The integrated density of the labeled bands was analyzed using ImageJ (NIH).

4.3.5 Network probability simulation

A simulation based on probability theory was developed to predict the impact of pattern occupancy on the probability of network formation. The simulation was undertaken using MATLAB®, and first involved defining the scale (in this case 367 adhesion nodes) and boundaries of the hexagonal array. The network comprised patterned neurons (i.e. occupied nodes) and interconnecting neurites which were encoded as numerical identities. In the initial condition, the array is completely occupied (i.e. all nodes contain neurons) and all possible connections between neighbouring nodes exist. A single node positioned within the array can share a maximum of 6 connections with neighbouring nodes (nodes at the array boundary can share a maximum of 3 or 4 connections). A uniform probability distribution function was then used to vacate a single node, and associated connections, followed by logging the number of remaining connections across the array. This process, with equal node selection probability, is iterated until the entire array is empty. To obtain results with statistical confidence the pattern depletion process (from 100% to 0%) was repetitively cycled 10,000 times.

4.4 Results and discussion

4.4.1 SH-SY5Y neuron-like cell patterning

In the previous chapters, digital hydrophilic–hydrophobic surfaces were used for cell patterning (Frimat JP *et al* 2009). In this chapter, the thin film PDMS µCP method was used to pattern SH-SY5Y neuron-like cells for the development of a

spatially standardized neurite outgrowth analytical display for neurotoxicity testing.

The human SH-SY5Y neuroblastoma cell line was used in this study as it has neurodevelopmental end-points similar to those found in the *in vivo* state of humans. The addition of retinoic acid to the culture induces the SH-SY5Y neuroblastoma cells to differentiate into neurons. The differentiation process promotes an increase in neurite outgrowth and the formation of functional synapses (Adem A *et al* 1987, Påhlman S *et al* 1990). In addition, it has been reported that retinoic acid differentiaton decreases the level of cellular proliferation while promoting cell adhesion (Påhlman S *et al* 1984), which are key advantages for cell patterning. The PDMS µCP method was successfully used to pattern the differentiated neuron-like SH-SY5Y cells. A SEM image of the thin perforated PDMS film with a hexagonal array of adhesion nodes produced by PDMS µCP is shown in figure 4.4.1(A). The hexagonal arrangement was chosen as it provides equidistant spots and ensures that all connections are of the same length and spatially uniform. As described previously, the PDMS thin films were deposited on glass substrates, providing identical physico- and biochemical surface adhesion properties as the one found in commercially available standard tissue culture surfaces. The darker exposed regions of the hexagonal pattern are therefore pristine glass which is hydrophilic, promoting cell adhesion and cell patterning, as demonstrated in Figure 4.4.1(B) with differentiated SH-SY5Y cells patterned on the hexagonal array. The ability to pattern neuron cells by the PDMS µCP method confirms previous reports that have demonstrated that neuron cells do not adhere on hydrophobic PDMS (Frimat JP *et al* 2009, De Silva MN *et al* 2004 and 2006, Reyes DR *et al* 2004, Millet LJ *et al* 2007). As mentioned in the last chapter, no further surface modification steps were necessary to successfully generate cellular patterns. The neuronal array patterns were generated following overnight incubation of the neurons in media containing serum (as described in chapter 2, section 3.2.2) with neurons growing only on the exposed hydrophilic regions of the underlying untreated glass substrate.
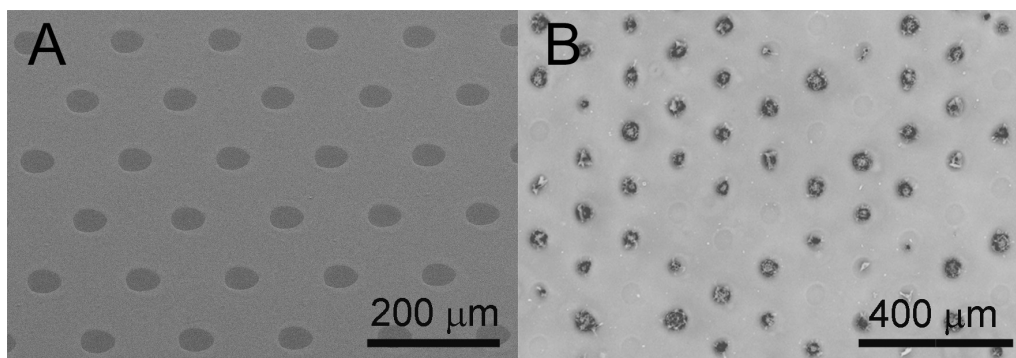
Figure 4.4.1: Planar PDMS print imaged by angled SEM. The hexagonal array contains 70 µm diameter adhesion nodes separated from neighbouring nodes by 100 µm (A). Large area image of differentiated SH-SY5Y neurons patterned with an occupancy of 83% (B).

The correct assembly of bio-active extracellular matrix proteins only on the hydrophilic regions is the most probable mechanism promoting cell adhesion and cell patterning (Underwood PA *et al* 1993, Kim J and Somorjai GA, 2003, Roach P *et al* 2005). For a more detailed overview regarding the role of serum proteins in cell patterning, see section 2.3.4. The use of hydrophobic PDMS-coated areas therefore inhibits cell adhesion and allows cellular patterns to be maintained over lengthy cultivation periods (e.g. 2 weeks).

4.4.2 Optimisation of neuron array dimensions

In order to successfully develop the NFA, a suitable distance between the nodes needs to be identified so as to provide adequate neuronal interconnection lengths between neighbouring nodes. Following a combinatorial experiment where the separation distance between the nodes increased from 40 µm to 140 µm, a distance of 100 µm was chosen. This allowed the nodes to be interconnected by neurites and not by the cells themselves, as observed when using shorter separation distances. The use of a 100 µm separation distance allows a single glass slide (25x25 mm) to contain 25 arrays each with 367 adhesion nodes, providing a total of 9175 nodes. Pattern occupancy by the differentiated SH-SY5Y cells across the array was reproducibly above 70%, and

also showed reproducible occupancy levels on all the arrays from the same batch as well as from different batches, as shown in figure 4.4.2.
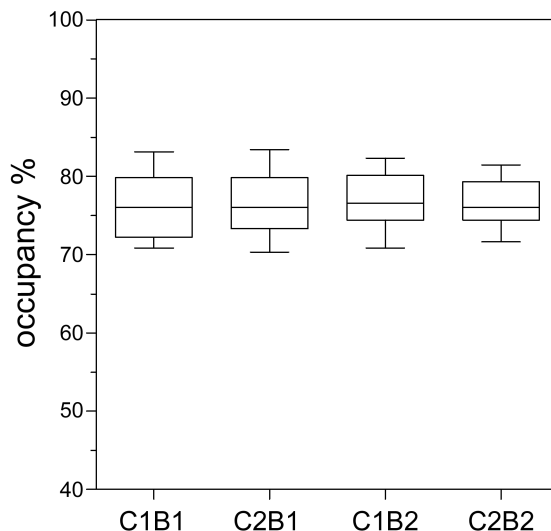
Figure 4.4.2: Box and whiskers plot showing the reproducibility of the pattern occupancy across the 25 arrays for pairs of chips (C1 and C2) and for two different batches (B1 and B2).

During the NFA experiments, the mean pattern occupancy within the arrays from four separate experiments varied from 77.6% (SD ± 3.7%) to 84.4% (SD ± 2.1%), again indicating excellent reproducibility. Unlike other cell lines, higher pattern occupancy could not be obtained following the initial day of patterning (e.g. HT29 cells, section 3.3.7). This could be explained by the natural behaviour of these neuron cells to cluster together. As a result, the neurons tend to cluster together within preoccupied nodes instead of colonizing nearby empty nodes. It is important to note that only arrays with a >75% occupancy were used and this was achieved by a rapid visual screening of the whole slide to identify the best arrays. A box and whiskers plot of the pattern occupancies is shown in figure 4.4.3(a). A combinatorial experiment was also undertaken to identify a suitable node diameter, with diameter sizes ranging from 25 μm to 100 μm. Importantly, single SH-SY5Y differentiated cells (25 μm node diameter with spacing above 30 μm) were not able to interconnect as well as isolated populations of differentiated SH-SY5Y cells (70 μm node diameter with spacing above 30 μm). This

observation may relate to the fact that this type of neuron like cell line requires specific cellular signaling provided by neighboroughing cells to trigger neurite outgrowth and cannot interconnect as such when isolated as single cells. Nevertheless, a node diameter of 70 µm was chosen so as to be sufficiently large to harbor a small population of neurons and to allow neurite outgrowth interconnections to form.

Following 24 hours of patterning, nuclei-DAPI staining was performed to count the number of cells occupying each 70 µm wide nodes. The combined frequency distribution data of a triplicate 367-node experiment is plotted in figure 4.4.3(b) and shows that there was an average of 7 cells per node.
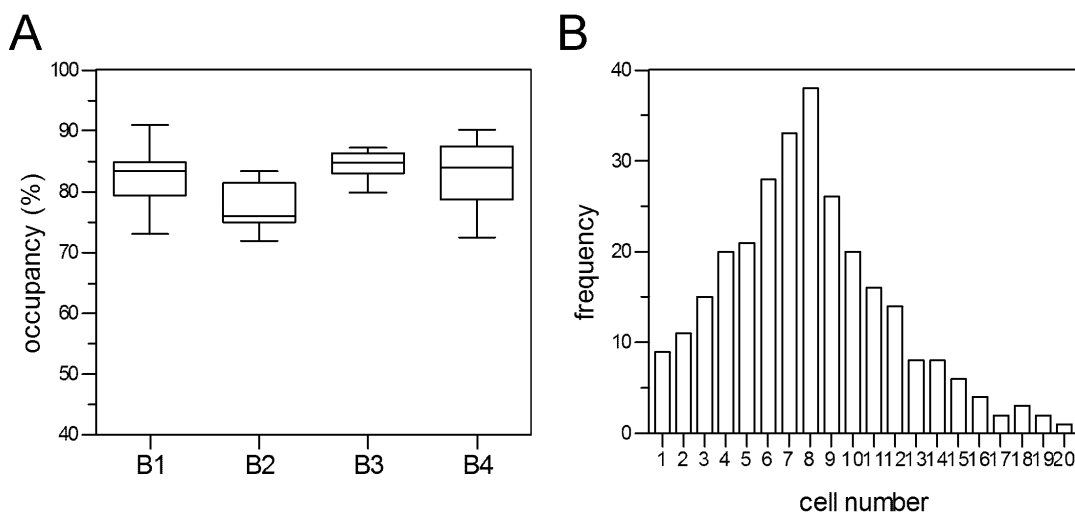
Figure 4.4.3: Box and whiskers plot of the batch to batch (B1-4) pattern occupancy variation after 24 hours of cultivation (A). Frequency distribution of the number of cells per adhesion node across an entire array (*n* = 3, B). Cell number was inferred from DAPI-stained nuclei counts.

As demonstrated above, reproducible patterning of differentiated SH-SY5Y cells was achieved and the parameters for the hexagonal array were identified as 70 µm diameter nodes separated by 100 µm. The 100 µm distances between the nodes also satisfies the neurite classification criteria. Neurite outgrowths are defined as having a length equal to or greater than one or more times the cell body diameter. A typical neuron cell diameter is between 10 and 25 µm (Morooka

T and Nishida E 1998, Adlerz L *et al* 2003, Das KP *et al* 2004) and therefore the 100 µm distance provides optimal conditions for the NFA and a neurite interconnection analysis platform.

4.4.3 Neuronal network formation

The formation of interconnections between the neuronal nodes is the main focus of the assay with the hexagonal array configuration providing equal distance between nodes and therefore equal neurite outgrowth lengths. The development of such a neuronal network over a period of 3 days is shown in figure 4.4.4(a-c). The arrows indicate the neurite interconnections which are formed following the initial day of patterning (figure 4.4.4(a)). As the period of incubation continues over the following 48 hours an increase in neurite interconnections is observed (figure 4.4.4, arrows in b-c). During the 3 day period, the number of neurite interconnections per node across the array increased from 99.8 (SD ± 3.3) to 303.3 (SD ± 17.6), with the data plotted as interconnections per node in figure 4.4.4(d). The pattern occupancy also increased from 84.9 (SD ± 0.9%) to 94.1 (SD ± 1.4%) by the third day. This shows that cell division and proliferation is still present, and time lapse microscopy also suggested that neurons can be translocated to vacant nodes by 'pulling' themselves along neurite outgrowths (http://www.ifado.de/en/researchapplications/research groups/neurotox/network-plasticity/index.html). Other reports of array-based neuronal migration events have been previously documented (Ruiz A *et al* 2008). It is interesting to note however that although the PDMS acts as an effective neuron repellent material, the neurite outgrowths are able to cross the PDMS barrier and interconnect with adjacent nodes. Chemical gradients could be at play to direct the growth cones of neurites towards each other. Observations made on live networks also suggest that once the neurite interconections are formed, they are not in contact with the PDMS but are instead suspended.
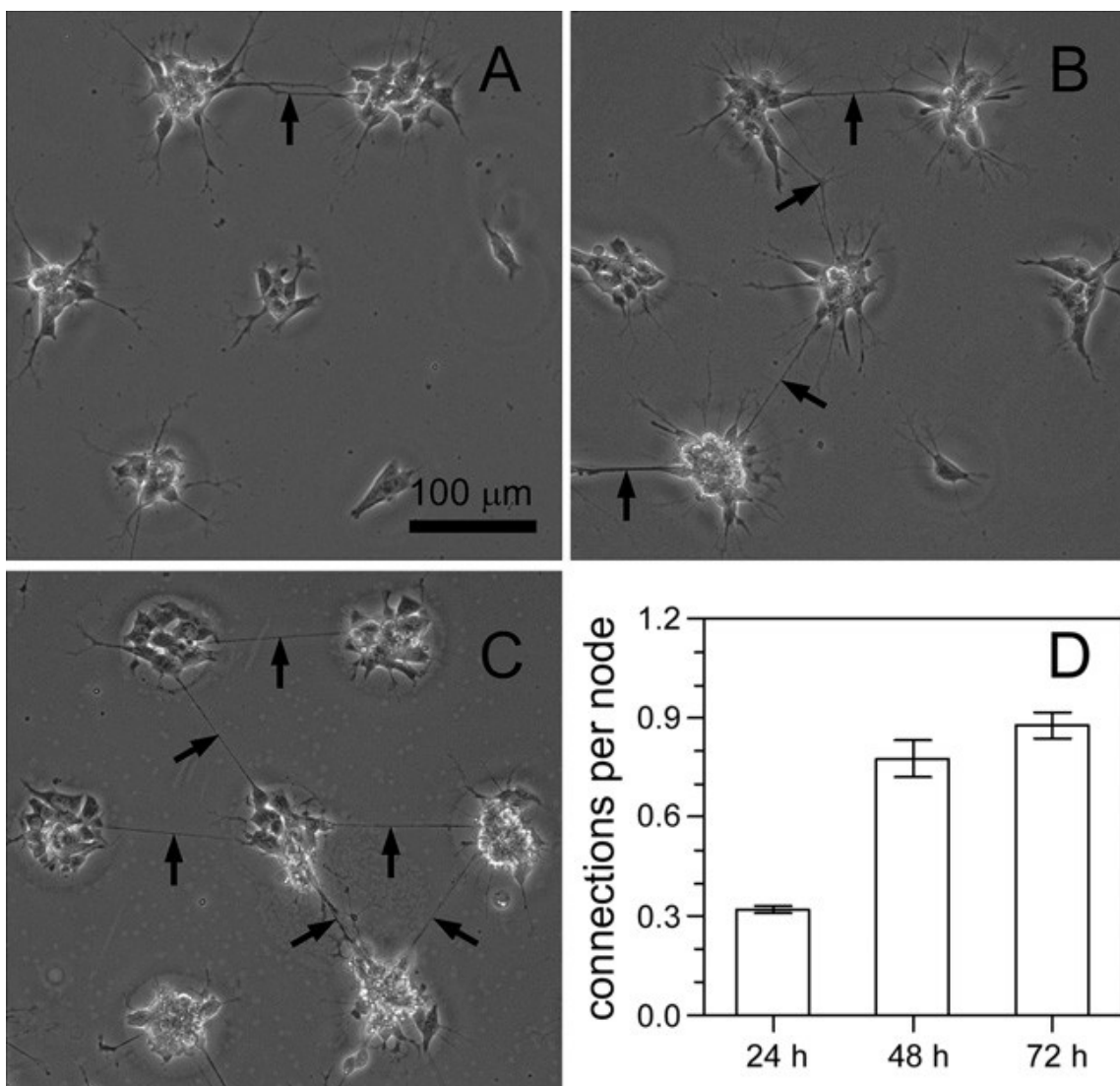
Figure 4.4.4: Microscopy time course panel of neuronal network development at 24 h (A), 48 h (B) and 72 h (C). Connecting neurites are indicated with black arrows. During the 3 day period, the mean number of connections per occupied node increased from 0.32 to 0.88 (D).

4.4.4 Neurotoxicity testing

Typically, the standard neurite outgrowth assay is based on sparsely seeded neurons that are isolated so as to aid the visualization and identification of neurite outgrowths. The NFA provides adhesion nodes that are separated by 100 μm, thus standardizing the interconnecting neurite length. As mentioned previously, the 100 μm distances is compatible with neurite classification criteria.

In addition, neurite interconnection measurements could have a higher indication of functionality than neurite outgrowth alone as neuronal connectivity is required for key behavioural functions such as memory and learning. The main advantage of the NFA is that it eliminates the need for measuring individual neurite outgrowth lengths, as the interconnections all have the same length when interconnected. The neurons are registered within a hexagonal array which eliminates the need for locating the neurons as well. The combination between the standardization of neurite length and cell patterning enable the straight forward visualization of the neuronal network for ultrafast screening purposes. Unlike other neurite outgrowth assays (Liu D *et al* 2007), the NFA is easy to visualise and does not require fixing and staining to identify neurite outgrowths which also brings the opportunity to continuously monitor the network for temporal studies.

To validate the NFA and to demonstrate its capability, a dose response experiment using the neurotoxin acrylamide was undertaken with differentiated SH-SY5Y neurons at passage 12 and passage 10. The CellTiter-Blue® Cell Viability Assay was undertaken in parallel to compare cell viability with neuron interconnection after 24 hours of exposure to acrylamide. The result from both the NFA and the CellTiter-Blue® Cell Viability Assay are plotted in figure 4.4.5. The NFA generated a sigmoidal dose response curve over two orders of magnitude which was 7.55-fold more sensitive than the viability assay. It is important to note that whilst the CellTiter-Blue® Cell Viability Assay is measuring gross cytotoxic effects, the NFA is measuring specific neurotoxic effects on neurite outgrowth and neurite interconnectivity. While the viability assay registered a 50% inhibition concentration (IC_{50}) at 5.1 mM (95% CI 4.2–6.1), the NFA showed a 20% reduction in network formation (NI_{20}) at 0.26 mM (95% CI 0.12–0.46) when compared with controls. The NFA experiment was repeated with SH-SY5Y cells at passage 10, producing a NI_{20} value of 0.28 mM (95% CI 0.17–0.38, figure 4.4.5), demonstrating a high level of reproducibility with narrow 95% confidence intervals. Although degeneration is different neurotoxicological mechanism, previous reports by Nordin-Andersson and colleagues have also

demonstrated that acrylamide concentrations of 0.25 and 0.21 mM can cause up to 20% neurite degeneration (ND$_{20}$) in SH-SY5Y cells (Nordin-Andersson M *et al* 1998 and 2003).
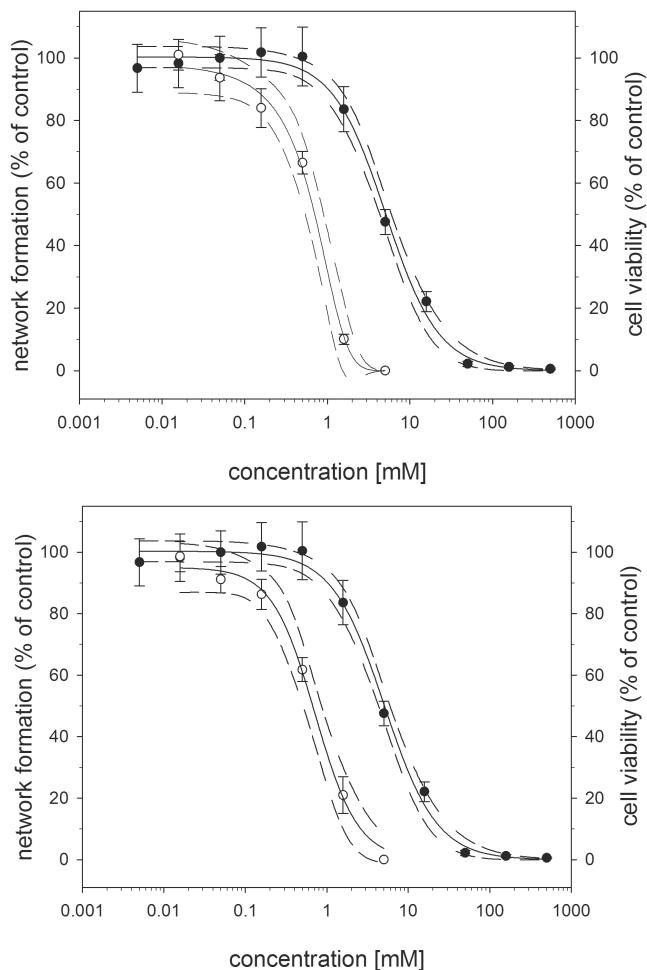
Figure 4.4.5: Sigmoidal acrylamide dose response curves from the NFA (open circles) and the CellTiter-Blue® Cell Viability Assay (black circles). Data was obtained following 24 hours of exposure to acrylamide using cells at passage 12 (a) and 10 (b). The network format assay was reproducible. In these separate experiments the resulting NI$_{20}$ value was 0.26 mM (a) and 0.28 mM (b). Data points with standard deviation are plotted along with non-linear regression curves for the mean (continuous line) and the 95% confidence intervals (dashed lines).

The NFA could also be used to measure network degeneration instead of network formation. Here the network would be allowed to develop for a given

period of time following which a toxic compound would be introduced. The number of connections could then be monitored and degeneration measured. It is important to note that neurite degeneration is a different neurotoxicological process from neurite outgrowth and it is likely that degeneration processes require higher concentrations or longer exposure times. However the similarity in the NFA NI_{20} and the Nordin-Andersson *et al* ND_{20} indicate that a there must be another force at play. Indeed, the use of 10% FCS in our experiments is likely to confer some level of resistance to the neurons which could explain why our NI_{20} value is as high as the ND_{20} value found by Nordin-Andersson and colleagues (which differentiated the neurons in non-serum-containing medium containing N2 supplements). Several studies have highlighted the protective character of FCS as well as other growth factors and the cell protection is believed to be achieved by activation of the p42/44 MAPK signaling pathway (Sandau KB *et al* 1999). In addition, the ND_{20} value found by Nordin-Andersson and colleagues was measured following 72h of exposure whereas the NFA NI_{20} was measured after 24h of exposure. This suggests that following 24h of exposure, the ND_{20} value measured would be inferior to 20%, complementing the idea that degeneration processes require longer exposure times.

Due to the simplicity of the analytical read out with the NFA, data acquisition is extremely fast as only the interconnections require counting. It takes on average 3 hours to manually record the dose response analysis for 367 nodes with 7 different drug concentrations in triplicate (7707 nodes). In contrast, the traditional protocol for manual assessment of neurite length is a labour intensive task, requiring on average 10 hours to record neurite outgrowth activity from 200 cells only (Radio NM *et al* 2008). The NFA is not only reproducible and extremely fast but in addition, the cell patterning angle brings in the option to have neurite interconnections at pre-defined coordinates which is highly desirable for automated image capture and processing. Furthermore, as the analytical end-points are not terminal in the NFA as the data acquisition does not require cell fixation and staining, periodic or even continuous monitoring of the network formation dynamics is possible.

In this study, the NFA was used to monitor neuronal arrays over a period of 3 days following exposure to different concentrations of acrylamide (from 0 to 5 mM). The phenomenon of neuronal network recovery was observed on arrays exposed to ≤0.5 mM acrylamide by day 3. This was determined by recording the amount of interconnections within the neuronal arrays treated with ≤0.5 mM acrylamide and comparing them with untreated arrays at day 3. This suggests that early stages of analysis are required for sensitive neurotoxic testing using the NFA. On the other hand, high acrylamide concentrations of 1.58 and 5 mM were cytotoxic, with cell death causing pattern occupancy depletion by 48 hours of exposure. The notion that pattern occupancy could be used as a surrogate cytotoxicity measure was also analyzed and the results are plotted in figure 4.4.6.
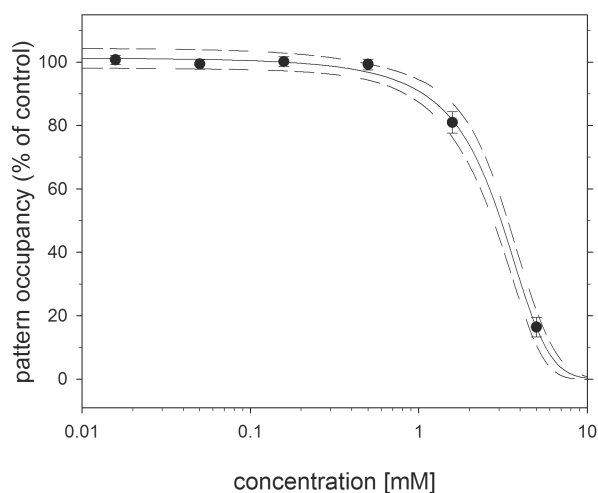
Figure 4.4.6: Acrylamide concentration plotted against pattern occupancy. Data was obtained following 48 hours of exposure to acrylamide. Data points with standard deviation are plotted along with non-linear regression curves for the mean (continuous line) and the 95% confidence intervals (dashed lines).

The data demonstrates that when acrylamide concentration is plotted against pattern occupancy, an IC_{50} of 3.1 mM is obtained, similar to the 5.1 mM value obtained using the CellTiter-Blue® Cell Viability Assay. Therefore, using the NFA, cytotoxic effects can be easily discerned from neurotoxic effects within the same experiment (and thus cells) by comparing pattern occupancy with number

of interconnections. This simple feature is also representative of the NFA detecting a higher level of neuron functionality than the viability assay. The combination of both connectivity and occupancy data generated by the NFA can be used to distinguish between cytotoxic effects and neurite outgrowth inhibition effects. These results clearly demonstrate that there is an acrylamide concentration window (between 0.26 mM and 3.1 mM, see figure 4.4.5 and 4.4.6) where the neurons may still be viable but are sufficiently intoxicated by acrylamide that their ability to produce neurites and connect is impaired.

4.4.5 Pathway inhibitors

Intact cellular signaling via the mitogen-activated protein kinase (MAPK, ERK1/2) and the phospoinositide-3-kinase (PI-3K, Akt/PKB) pathways has been shown to be critical for neurite formation and outgrowths (Nishimura T *et al* 2008). In an attempt to demonstrate the NFA can detect the targeted inhibition of pathways required for neurite formation and outgrowth, inhibitors of both pathways (PD98059, an inhibitor of MAP kinase signaling and LY29002, an inhibitor of the PI-3K pathway) were used at concentrations ranging from 5 and 50 µM to assess their impact on network formation. The level of protein phosphorylation (ERK1/2 for the MAPK pathway and Akt for the PI-3K) was compared with total protein and α-tubilin controls by densitometry analysis of Western blot bands. As shown in figure 4.4.7 A-D, phosphorylated protein levels demonstrate that PD98059 exposure resulted in a concentration dependent decrease in ERK1/2 phosphorylation and LY29002 also caused a concentration dependent decrease in Akt phosphorylation. To complete the demonstration, figure 4.4.7 E-F shows that in the same concentration range, neurite outgrowth (as measured using the NFA) was dose dependently inhibited by both PD98059 and LY29002. The high levels of pattern occupancy (shown by the black bars in figure 4.4.7 E and F) indicate that cytotoxicity was not induced by the presence of PD98059 or LY29002 at the above mentioned concentrations. From these results, the inhibition of PD98059 (50 µM) and LY29002 (15.8 µM) impaired the onset of neurite development while cell viability remained unaffected which make these

two candidates suitable NFA pathway controls. Taken together, these results show that the NFA end-point measurement is pathway dependent and that functional MAPK as well as PI-3K pathways are critical for network formation.
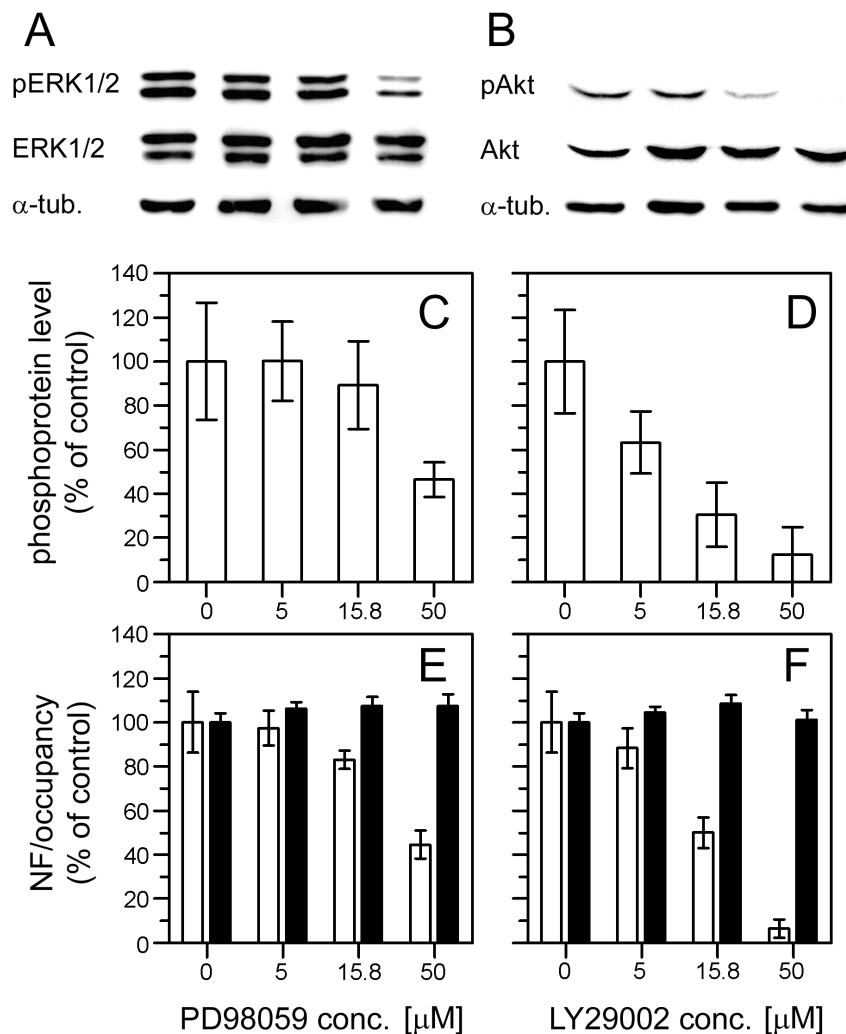
Figure 4.4.7: Western blot image of the phospho-ERK1/2 (MAPK) dose response to PD98059 along with total ERK1/2 and α-tubulin controls (A). Western blot image of the phospho-Akt (PI-3K) dose response to LY29002 along with total Akt and α-tubulin controls (B). Densitometry analysis of the phospho-ERK1/2 dose response to PD98059 (C) and the phospho-Akt dose response to LY29002 (D). NFA results (NF, white bars) of the dose response to PD98059 (E) and LY29002 (F). Occupancy, a cytotoxicity indicator, is also presented (black bars).

4.4.6 Network probability simulation

Pattern occupancy has a great impact on the probability of neurite outgrowths connecting to neighbouring neuronal nodes. The assay measures connections between directly neighbouring nodes and does not consider connections between further nodes meaning that the absence of neighbours translates into no connections being formed. As expected, lower pattern occupancy results in a lower probability of forming interconnections which has important implications when data generated by different arrays (with different pattern occupancies) are compared. In order to correct the pattern occupancy variations within the experiments, neurite connection numbers were recorded as connections per occupied node. This allows a linear relationship to be drawn between pattern occupancy and network formation probability but does not take into consideration the proximity effect of neurons forming neurite connections only with directly neighbouring nodes. This problem was addressed by developing a network probability simulation. The probability theory-based simulation facilitates data normalization and helps to evaluate pattern occupancy distributions from 0 to 100%. In turn, this allows the impact of pattern occupancy on network formation probability to be predicted. Results from a 10,000 cycle simulation are presented in figure 4.4.8. The repeated simulation showed errors levels below 1% of the standard deviation, producing an exponential plot for the pattern occupancy against network formation probability. To experimentally confirm the simulation prediction, lower cell dilutions were seeded on the arrays to obtain an estimate of network formation across a large range of pattern occupancy values (28–85%). These are plotted in figure 4.4.8 as the number of connections per node (at 24 hours, black circles). The data clearly validate the predictions generated by the simulation, also suggesting that the neurons randomly occupy the arrays. It is important to note that the variation in the probability of network formation was most impacted at higher levels of pattern occupancies. As demonstrated in figure 4.4.8, an array with 70% occupancy has less than half as many connections as an array with 100% occupancy. Therefore, the simulation is of particular benefit for data normalization in events where the variation in pattern occupancy from chip to chip is high.
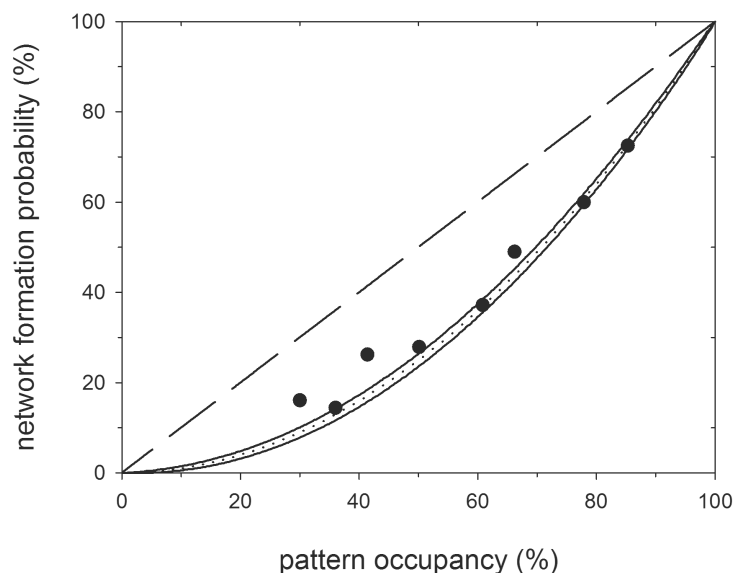
Figure 4.4.8: Simulation of occupancy versus network formation probability with experimental results overlaid for verification. The 10,000 cycle simulation mean (dotted line) is plotted with the 95% confidence intervals (continuous lines). The connection per occupied node prediction (dashed line) is plotted along with experimental data points (black circles) taken at 24 hours. The array is not fully occupied after 24 hours, requiring data normalization based on the values obtained with 85% pattern occupancy.

4.5 Conclusions and outlook

In this chapter, the NFA is introduced as a spatially standardized analytical display for high throughput neurotoxicity screening. The simple and widely applicable thin film PDMS µCP technique was used to pattern human neurons within a hexagonal array. Patterning offers a route to assign assay coordinates for automation but most importantly it standardizes the neurite outgrowth lengths. Over a period of 3 days, neurite interconnections spontaneously assemble within

the PDMS network, a dynamic process that can easily be monitored without the need for fixation or staining. It is worth noting that traditional neurotoxicity assessment relies on neurite outgrowth measurements as end-point indicators whereas the NFA measures interconnectivity (the basis of memory and learning) which provides a higher potential functional indicator than outgrowth alone.

In the presence of neurotoxic substances which affect neurite outgrowth the extent of network formation is inhibited. The NFA allows quantitative measurements of neuronal interconnections to be compared for the identification of neurotoxic compound concentrations. The NFA was validated using acrylamide, a known neurotoxin, which dose-dependently inhibited neuronal network formation resulting in a NI_{20} value of 0.26 mM, consistent with literature values. Specific inhibition of the MAPK and PI-3K signalling pathways, which are necessary for neurite outgrowth, can serve as valuable assay controls. Similar to acrylamide, these were also shown to exhibit a dose-dependent response, inhibiting the network formation capability while also dose dependently reducing protein phosphorylation. In addition, pattern occupancy levels can serve as indicators of cytotoxic concentrations. The results obtained demonstrate that a 7.55-fold lower value was measured for neurotoxicity compared to cytotoxicity, indicating that neurotoxicity can be distinguished from gross cytotoxicity within the same experiment and thus cells.

Straightforward developments are required for the widespread adoption of the assay to progress the neurotoxic hazard assessment effort as well as impact the field of neurodevelopmental biology. The NFA analytical display can easily be modified or improved. The evaluation of growth supplements, differentiation cues and passage history (Bużańska L *et al* 2009) should be undertaken as should other cell models. For high throughput (HTP) screening, the array can be included within a standard microtitre plate format (Azioune A *et al* 2009).

Further developments should focus on the use of primary neurons cells as the *in vitro* goal standard for the NFA. These cells have an *in vivo* like morphological, biochemical and electrophysiological characteristics than the SH-SY5Y cell line. This gold standard could be used to validate the predictive value

of routine cell lines, including the SH-SY5Ys. Preliminary experiments for patterning primary neurons have been successful. An example of a primary neuron network is presented in figure 4.5.1, with the neurons freshly harvested from a mouse embryo and patterned on the hexagonal array for 7 days (using a poly-L-lysine pre-coated glass slide and with 3.7-μm-wide interconnecting tracks). Also of interest is the standardization of the assay with the use of non-transformed and self-renewing human neural stem cells (Radio NM *et al* 2008). However, for widespread adoption, the NFA will have to be validated and to conform to assay standards defined by the neurotoxicology community and guidelines established by the regulatory authorities.

The NFA format can be useful in many areas of neurobiology. The assay can examine conditions for neurite outgrowth inhibition as described herein. But in addition, the NFA could be used to test substances that promote neurite outgrowth. Similarly, the NFA can be used for either dynamic network degeneration or regeneration experiments. A substance can be tested for its ability to disrupt an existing neuronal network or for its ability to restore or promote neuron network formation. These advancements will help towards understanding the processes required for the restoration of damaged brain tissues or spinal cord injuries to the prevention of brain debilitating conditions such as Parkinsons disease. The NFA could also benefit the field of pharmaceuticals where each new drug discovered needs to be assessed and proven not to disrupt the nervous system. In addition, toxicity associated with recreational substances such as LSD, cocaine or even alcohol and caffeine, could be further investigated and modes of action better understood with the NFA. Conveniently and as mentioned previously, information relating to the dynamics of network formation can be recorded with the NFA as cell fixation is not required for neurite identification. This could allow investigations into areas of developmental neurobiology experiments to be undertaken where network plasticity (which is involved in memory formation and learning) could be investigated.
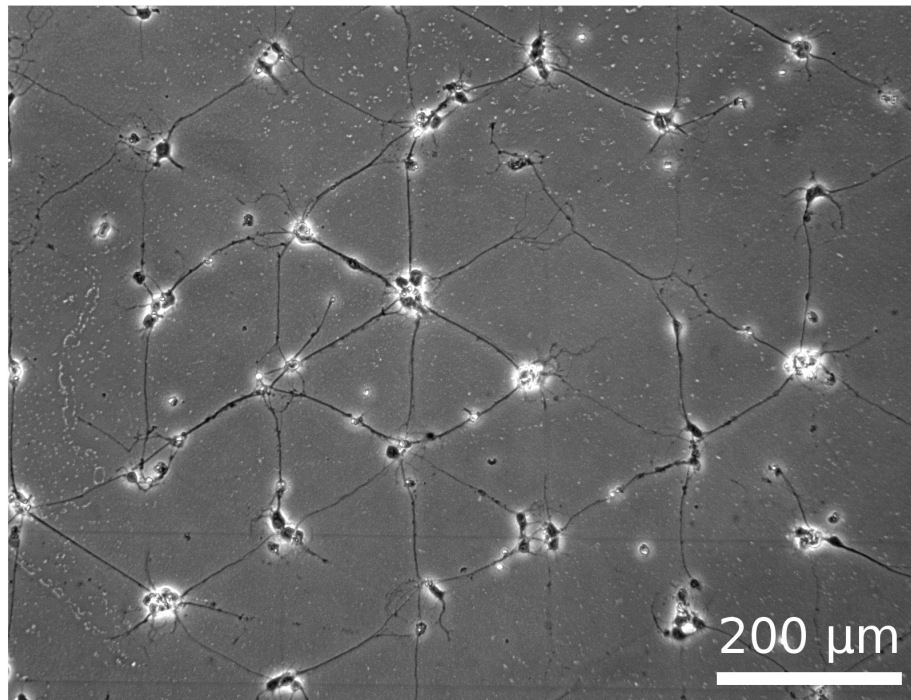
Figure 4.5.1: Neuronal network composed of primary neurons freshly harvested from a mouse embryo.

5

Microfluidic Arrays with Cellular Valving for Single Cell Pairing Experiments

<u>The work presented in this chapter was also presented in part on posters as:</u>

'Microfluidic arrays with cellular valving for contacting single cell co-cultures'.

Frimat JP, Chiang YY and West J, *in Proceedings of NanoBioTech2010,* Montreux, Switzerland*, 15-17 November, 2010. And;

'Intimate couples: Single cell co-culture using digital microfluidics'.

Frimat JP, Franzke J and West J. The 13th Annual European Conference on Micro and Nanoscale Technologies for the Biosciences, Montreux, Switzerland, November 2009.

5.1 Introduction

In this chapter, a highly parallel microfluidic approach for contacting single cell pairs is presented. The approach combines a differential fluidic resistance trapping method with a novel cellular valving principle for homotypic and heterotypic single cell co-culturing. Cell-cell interactions are a major topic of research as these interactions dictate the behaviour of mammalian cells and are responsible for tissue organization, structure and function. Different modes of communication exist between cells. The most direct mode of communication is termed juxtacrine signaling and requires physical contact between 2 cells to allow the exchange of material and information. Cancer (Burdick MM *et al* 2001), immune cell activation (Singer A and Hoydes RJ *et al* 1983), stem cell differentiation (Dang SM, *et al* 2004), tissue regeneration (Maas-Szabowski N *et al* 2003) and embryogenesis (Armstrong N *et al* 1993) can all be triggered through various contact modes of communication between cells. There is widespread interest in distinguishing single cell responses from those of the ensembled population and new tools which can both highly parallelise experiments and enable the precise position of cell pairs are required.

As mentioned previously, microfabrication can produce systems with cellular and sub-cellular length scale features for the study of co-cultures. Heterotypic co-cultures can be produced by either exploiting the differential

adherence of different cell types or by partial masking of the surface for the first cell type to adhere followed by removal of the mask for patterning the second cell type. Examples of early co-culture studies include photolithographic-based collagen patterning to achieve a heterotypic co-culture (Bhatia SN *et al* 1997) or selectively masking surfaces using microfluidic poly(dimethylsiloxane) (PDMS) stencils (Folch A and Toner M, 1998) or Parylene C stencils (Wright D *et al* 2007) to generate heterotypic cellular interfaces. Other techniques that have been used in the context of heterotypic co-culture studies include using electrochemically active surfaces to modulate ligand presentation (Yousaf MN *et al* 2001) or using photoresponsive polymer films (Kikuchi K *et al* 2009) for sequential patterning. A more recent approach was to not only selectively treat the surface but also the cells. Here surface-tethered DNA sequences can be made complementary to DNA sequences presented on the cells surfaces by metabolic labelling and cells can be patterned as adjacent co-cultures by hybridization (Douglas ES *et al* 2007). Alternatively, co-cultures can be established on two interdigitated silicon plates which exploit the crystal plane for perfect alignment and the establishment of the heterotypic cellular interface (Hui EE and Bhatia SN, 2007).

Microfluidics can also be used to great effect for cell positioning and single cell handling. Typically, cells travel along a fluidic path of least resistance and end up being trapped or mechanically anchored onto sub-celluar-sized apertures where analysis can take place (Yang M *et al* 2002) or even high efficiency electroporation (Khine M *et al* 2005 and Valero A *et al* 2008). Depending on the design, usually this approach leads to sequential trapping of single cells onto a row of microfluidic exits. When the single cell traps are mirrored across the width of a narrow microchannel, contacting heterotypic co-culture of spherical cells can be achieved. Using this approach, Lee PJ *et al* (2005) have demonstrated molecular transfer between the cytosolic compartments of 2 cells. Higher density arrays can also be achieved using fluidic streamlines where it is possible to position many cells into 2-layer (Di Carlo D *et al* 2006a and 2006b) or sieve-like (Faley SL *et al* 2008 and 2009) microstructured traps. Recently, cell pairing and fusion was achieved by Skelly AM and co-workers (2009). Here a clever

microfluidic device was designed for single cell trapping and fusion where a second cell type could be included in the occupied traps by a reverse parking method.

The microfluidic arraying systems discussed above all rely on differential fluidic resistances principles to transport cells into each trap. Once the cells are loaded by the fluidic streamline into the traps, the streamline is diverted and additional cells cannot be trapped. Following these principles further, Tan and Takeuchi designed a linear particle trap array allowing sequential cell arraying by connecting every trap with a superimposed serpentine bypass microchannel. (Tan WH and Takeuchi S 2007). Parallel arrays of trap structures and the efficient use of bypass channels have also been useful for tracking yeast (Rowat AC *et al* 2009) and human cell lineages (Kobel S *et al* 2010). Finally, a dynamic microarray device for paired bead-based analysis was developed containing a mirrored meander-shaped dynamic microfluidic design for the observation of interactions between paired beads (Teshima T *et al* 2010).

In this chapter a cellular valving principle is introduced for the first time. In combination with the Tan and Takeuchi microfluidic architecture, a highly efficient and reliable single cell coupling microfluidic based device is demonstrated.

5.2 Concept

The cellular valving concept is based on exploiting the difference in morphological states between cells in suspension and cells attached to a surface. Cells in suspension have a general spherical morphology whereas cells attached to a surface adopt a more flattened morphology. Therefore placing a viable cell at an exit within a microfluidic circuit can be used as a valve, as initial positioning will close the exit and subsequent cell attachment will lead to the cell flattening and the exit reopening. Within a differential fluidic resistance circuit, this principle can be used to couple single cells. The Tan and Takeuchi serpentine

microfluidic arraying system design was modified to include mirrored traps interfaced by sub-cellular-sized apertures with the linear path along the series of apertures. Illustrated in figure 5.2.1, the serpentine flow path has a higher fluidic resistance than the linear path ($R_2 > R_1$) (see figure 5.2.1(A)), producing a higher linear flow rate Q_1 than the serpentine flow rate Q_2:

$$Q_1/Q_2 = \left(\frac{C_2(\alpha_2)}{C_1(\alpha_1)}\right) \cdot \left(\frac{L_2}{L_1}\right) \cdot \left(\frac{W_2 + H}{W_1 + H}\right)^2 \cdot \left(\frac{W_1}{W_2}\right)^3 > 1$$

where W_1 is the aperture width, W_2 is the channel width, L_1 is the aperture length, L_2 is the length of each U-bend channel segment, and $C(\alpha)$ are constants defined by the aspect ratio ($0 < \alpha < 1$) and derived from the Darcy friction factor and the Reynolds number. The aperture $C_1(\alpha_1)$ value is 78.8 and the microchannel $C_2(\alpha_2)$ value is 57.9 (Tan WH and Takeuchi S 2007). The following sequence can be used for single cell coupling: A first cell is transported within the linear flow and trapped at the first aperture. The cell blocks the linear path, increasing the local fluidic resistance ($R_{1'} > R_{2'}$) and diverting the streamlines (and the subsequent cells) into the serpentine pathway for trapping at the second aperture ($R_{2''} > R_{1''}$, see figure 5.2.1(B)). The process enables the serial arraying of single cells. The cells adhere and flatten, acting as a valve in the open state to restore the $R_2 > R_1$ condition (see figure 5.2.1(C)). The flow is reversed and contains a second cell type for the serial arraying, as before, of single cells within the empty traps (see figure 5.2.1(D)). The two cell types are in close proximity and can contact one another through the aperture connecting the mirrored traps. In this manner both heterotypic and homotypic single cell co-cultures can be established, with the array format providing the means to couple hundreds of single cell pairs for high throughput screening and the observation of rare events.
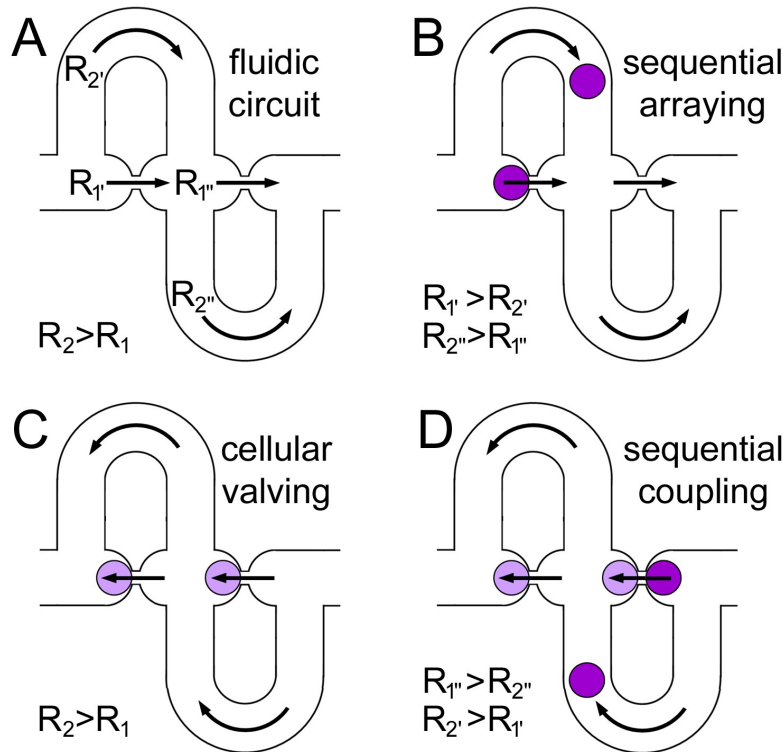
Figure 5.2.1: The cellular valving principle for single cell coupling. The linear path, through the apertures between the mirrored cell pockets has a lower fluidic resistance R_1 than the serpentine path R_2 (A). Loading of a spherical single cell (purple) reverses the fluidic resistance ratio, acting to divert subsequent cells ($R_{1'} > R_{2'}$) for sequential ($R_{2''} > R_{1''}$) single cell arraying (B). Viable cells adhere and flatten (lilac), restoring $R_2 > R_1$ (C). Flow reversal is used for introducing a second spherical single cell type and sequential single cell coupling ($R_{1''} > R_{2''}; R_{2'} > R_{1'}$, D).

5.3 Materials and methods

5.3.1 Microfluidic circuit design

The dimensions of the microfluidic circuit are defined by the dimensions of the cell types under investigation. Human SW480 epithelial cells (Ø 14.6 µm, SD ± 3.0), MCF-7 epithelial-like breast cancer cells (Ø 17.9 µm, SD ± 1.5) and HT29

colon carcinoma cells (Ø 14.7 µm, SD ± 1.1) were used in this study. To singularly accommodate these cells, traps with diameters (and typical trap/cell diameter ratios) of 15 µm (x1.0), 22 µm (x1.5), 30 µm (x2.0) and 37 µm (x2.5) were designed. The serpentine channel design had a width of 40 µm, with U-bend segment lengths of 300, 500, 700 and 900 µm to provide different flow ratios (0.6 to 1.8). The aperture design was 5 µm in length and 6 µm in width. Channel bifurcations were used to define 8 parallel analysis channels each containing 25 trap pairs (totaling 200 per device).

5.3.2 PDMS microfluidic chip preparation

PDMS microfluidic circuits were prepared by moulding a 28-µm-high SU-8 master fabricated by standard photolithography methods. The PDMS (Sylgard® 184, Dow Corning) prepolymer was mixed with the curing agent at a ratio of 10:1 (w/w) and thoroughly degassed. PDMS was poured onto the SU-8 master and cured at 80°C for 20 minutes. The resulting PDMS microstructures were documented by SEM imaging (Quanta 200F (FEI)) and are shown in figure 5.3.1. Ordinarily inlet and outlet openings are produced by puncturing, resulting in large numbers of particle contaminants which present the risk of blocking the fluidic circuit. Instead, we used a frame to align 700-µm-diameter vertical pins for moulding the inlet and outlet features. The pins were also used to position Luer ports (Scandinavian Biomedical Microdevices ApS, Denmark) for their inclusion within the microfluidic device during thermal curing (figure 5.3.2). The inlet-outlet moulding frame has 2 operating features. When closed, the Luer ports are raised above the SU-8 master to allow PDMS casting and when open, the Luer ports slide down the metallic rods into the PDMS. Once cured, a syringe needle was used to ensure that the fluidic inlets and outlets are open, followed by a N_2 flow wash.
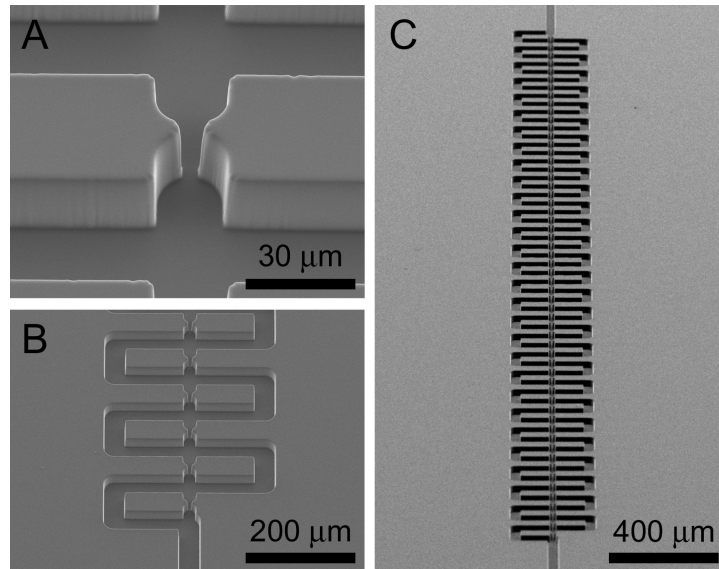
Figure 5.3.1: Microfluidic single cell co-culture array system fabricated by PDMS replica moulding. SEM image of a mirrored pair of single cell traps (A), a series of 6 trap pairs (B) and an entire microfluidic circuit (C).
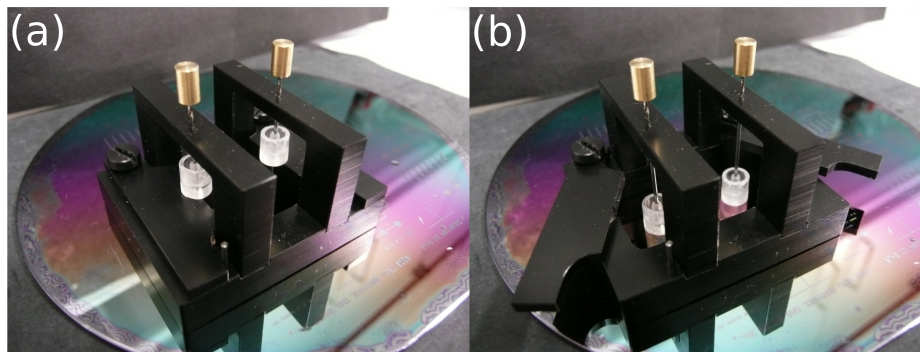
Figure 5.3.2: Microfluidic inlet-outlet moulding frame. The 'close' position allows PDMS to be poured inside the frame (a) and the 'open' position allows the flat-based Luer ports to be incorporated within the PDMS during curing (b).

5.3.3 Device packaging

To seal the device, thin (<400 µm) and flat PDMS-glass bilayer substrates were prepared by pressing a small volume of PDMS deposit between a glass coverslip and a polystyrene surface, with curing for 10 minutes at 80°C. Again the PDMS was sterilised with 70% ethanol followed by deionised water and N_2 dried. Device

assembly was achieved by plasma bonding. An oxygen plasma treatment (40 seconds at 1 mBar in an O_2 filled chamber) (Plasma chamber from Diener electronics GmbH) was used to activate both surfaces for PDMS–PDMS bonding. Immediately after bonding, media was loaded to preserve the hydrophilic state of the plasma-activated PDMS (Delamarche E *et al* 1998) and support the adhesion of cells (Frimat JP *et al* 2009 and 2010). Alternatively, bonded devices were left overnight for the diffusive return of oligomers, thereby restoring the hydrophobic state of the PDMS surface (Kim J *et al* 2000), followed by atmospheric pressure air plasma stencilling with a Tesla generator operating with 30 kV at 2 MHz (Frimat JP *et al* 2009, see chapter two). The plasma is routed along the linear path of least resistance, oxidising the PDMS surface to produce a hydrophilic path which supports cell adhesion, while the surrounding PDMS remains biologically inert to confine cell adhesion to the trap regions. Flows were driven by a syringe pump (PHD 2000, Harvard Apparatus) interfaced to the Luer ports via Tygon™ tubing (ID 1.3 mm). For slow continuous flows, 1 mL pipette tips were inserted into the Luer ports for the hydrostatic pressure-driven delivery of media and cells.

5.3.4 Particle loading

A syringe and syringe pump (HARVARD) were connected to the device via the flat-based interconnecting Luer ports. Polystyrene particles (G. Kisker GbR, Germany) of 20 μm in diameter were loaded at 500 μm s^{-1} inside the circuit to test trapping efficiencies. Both hydrophilic and hydrophobic circuits were tested. The particles (200,000 particles per mL) were loaded in a 1 x PBS solution containing 0.1% SDS.

5.3.5 Cell culture and imaging

Human SW480 epithelial, HT29 colon carcinoma and MCF-7 epithelial-like breast cancer cells were purchased from DSMZ (Germany). Cells were cultured in Dulbecco's modified Eagle medium (DMEM) supplemented with 10% (v/v) foetal bovine serum (or 10% (v/v) foetal bovine serum gold (PAA Germany) for the

HT29 cell line), 1% (v/v) Glutamax and 1% (v/v) penicillin and streptomycin (Sarstedt AG & Co., Germany). Cells were harvested using 0.25% (w/v) trypsin once 80% confluency was attained. Alternatively cells were harvested and gently disaggregated using accutase (PAA Germany), a protease and collagenolytic mixture that retains the structural and functional integrity of the cells' surface proteins. The cells were introduced to the microfluidic system and continuously perfused with media by gravity feed during incubation at 37°C in a 6% CO_2 atmosphere. The single cell coupling protocol involved loading cells at ~50 µm/s for 30 minutes, followed by incubation for 6 hours for cell adhesion and flattening. The pipette tips were then exchanged and the gravity-driven flow was reversed for loading the second cell type. Single cell co-cultures were incubated with continuous media perfusion at ~5 µm/s for periods of up to 5 days. Single cell cultures and co-cultures were imaged using an inverted microscope (IX71, Olympus, Germany).

Fluorescent immunostaining targeting connexin 43 (Cx43) was used to observe the connexon gap junctions formed between cell partners within the microfluidic system. Before cell fixation, the entire chip was flushed with 1 x PBS at 37°C for 10 minutes at ~50 µm/s. For cell fixation, SAV neutral buffered 4% formaldehyde (Liquid Production, Germany) was introduced inside the chip for 1h at room temperature followed by another 1 x PBS flush for 20 minutes at ~50 µm/s and a stepwise alcohol dehydration with final equilibration in 1 x PBS. To block non-specific binding, a 5% milk/1 x PBS solution was used at room temperature and incubated on chip for 1 hour. The 5% milk/1 x PBS was filtered through a 200 nm filter 3 times to ensure no aggregates were present. Again the chip was washed with 1 x PBS for 20 minutes at ~50 µm/s. The primary antibody (rat anti-Cx43, Novus Biologicals, 1:100 in 0.1% BSA/1xPBS/0.1% Tween 20) was introduced and incubated at room temperature for 2.5 hours followed by flushing with 1 x PBS for 30 minutes at ~50 µm/s. Mouse secondary antibodies labeled with Cy5 (Novus Biologicals, 1:100 in 0.1% BSA/1x PBS/0.1% Tween 20) were then delivered and incubated for 2 hours at room temperature followed by a 1 x PBS flush for 30 minutes at ~50 µm/s and drying overnight (in the dark).

Immunostained connexin junctions were documented by fluorescent microscopy with emission detection at 670 nm.

There are, however, numerous issues related to 'on chip' immunostaining. Typically, blocking steps involving high levels of BSA (wt 0.3%) are necessary as well as multiple washing steps and lengthy incubation times. Due to the low flow velocity that is critical to conserve cellular integrity, washing time and channel blockage can become lengthy. Regarding the channel blockage issues during washing and staining, every solution added to the device was filtered three times through a 200 nm pore filter to remove a maximum of unwanted debris. Instead of blocking the non-specific binding elements with high levels of BSA, a filtered 5% milk/1 x PBS solution containing 0.1% Tween 20 was used to further reduced any non specific bindings. One advantage of using hydrostatic driven feed in the form of pipette tips is that not only is it cheap but the system is self regulated and many devices can be stored inside the incubator during these lengthy washing steps therefore ensuring better cell viability. Including microfluidic chips with syringe pumps inside an incubator is more problematic. Interestingly, when using such low velocities and thus low pressures, device bonding may not even be necessary and device sealing could be achieved by conformal contact. This would bring the advantage of being able to remove the PDMS device lid and transfer the cells from buffer to buffer with ease, eliminating the above mentioned issues.

5.3.6 Shear stress simulation

The CFD flow module of SolidWorks (Dassault Systèmes SolidWorks Corp., MA, USA) was used to simulate the shear stress conditions that the cells experience during microfluidic culture. The highest shear forces are exerted on flat, adherent cells at the microstructured aperture during the loading of the second cell type and during co-culture with media perfusion. The simulation considered the microfluidic dimensions listed above, with a trap diameter of 30 µm and a U-bend channel length of 700 µm. A single adherent cell was modeled with an umbonate

morphology, having a diameter of 25 µm and rising from zero height at the perimeter to the dome's centre height of 3 µm. For modeling single cell couples, umbonate pairs were connected via a 5 µm long and wide structure. The laminar flow state was described by solving the Navier Stokes equations, using the properties of water and the no-slip condition. For the cell loading simulation the inlet velocity was set to 50 µm/s, and for the co-culture perfusion simulation the inlet velocity was set to 5 µm/s. In both cases, an atmospheric pressure (101 kPa) condition was assigned to the outlet of the device. A mesh comprising 800,000 uniformly-sized rectangular elements was applied with shear stress computations requiring ~7 hours.

5.4 Results and discussion

5.4.1 Single particle arraying

Prior to using live mammalian cells, the Tan and Takeuchi principle was tested using polystyrene microparticles. Preliminary experiments successfully replicated the Tan and Takeuchi principle and homogeneously-sized polystyrene particles with a 20-µm-diameter were arrayed by the differential fluidic resistance paths as shown in figure 5.4.1(a). However issues were found due to the polystyrene particles sticking to each other and to the PDMS, blocking the microchannels. To improve the trapping rate of microparticles, the solution containing the particles was modified to contain 0.1% SDS. Here, successful trapping was obtained with above 80% of traps occupied establishing the system as suitable for single cell arraying.

5.4.2 Single cell arraying

The potential of single cell analysis is currently being restricted by the poor efficiency of microfluidic single cell trapping efficiencies. In most cases, single cell trapping efficiency is around 10-20% (Faley SL et al 2008, Wlodkowic D et al

2009) and at best between 70 and 80 % (Matsunaga T *et al* 2008, Rowat AC *et al* 2009). To date, optimization of single cell devices have produced single cell trapping efficiencies of up to 97% (Kobel S *et al* 2010). In our study, using the differential fluidic resistance system mammalian cells were reliably and efficiently arrayed (~99%) regardless of the heterogeneity of the cell's diameters (figure 5.4.1 (b and c)).
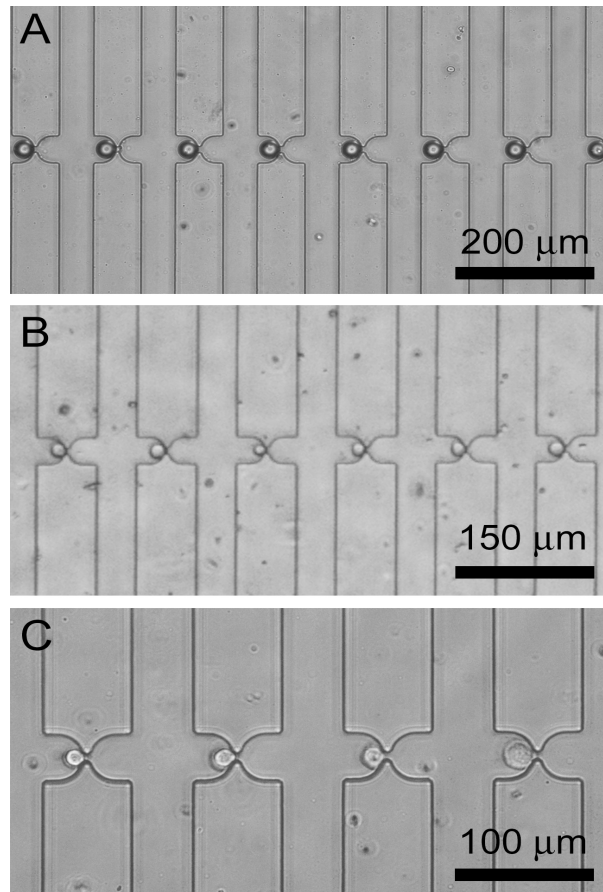
Figure 5.4.1: The differential fluidic resistance circuit was used for the efficient arraying of monodisperse 20-µm-diameter particles (A) and a variety of cells, including HT29 human colon carcinoma cells (Ø ≈ 14 µm, B) and MCF-7 epithelial-like breast cancer cells (Ø ≈ 18 µm, C). For these demonstrations, a flow ratio of 1.4 was used with a trap diameter of 30 µm.

Mammalian cells are characteristically different in size even within the same cell line population. For example, HT29 colon carcinoma cells had an average diameter of 14.7 µm and standard deviation of ± 1.1, MCF-7 epithelial-like breast cancer cells had an average diameter of 17.9 µm, (SD ± 1.5) and SW480 epithelial cells had an average diameter of 14.6 µm, (SD ± 3.0). Furthermore, suspended mammalian cells are not structurally comparable to microparticles. The plasticity of cellular membranes allows cells to slightly deform which could explain better trapping efficiencies. However, preliminary experiments using SW480 cells indicated that 29.5% (SD ± 8.6) of the pockets were occupied by multiple cells instead of singles. Two main problems were identified; firstly the SW480 cell size heterogeneity (SD ± 3.0 which is equivalent to 20%) could mean that smaller cells are not able to divert the fluidic path and consequently additional cells can get trapped (see figure 5.4.3a (inset)). Secondly and most significantly, the cells were not fully disaggregated following the trypsin treatment meaning that the cell suspension contained single cells as well as aggregates of 2 to 5 cells. These can then be trapped resulting in multiple cell trapping. To address this issue, the use of accutase instead of trypsin, a highly effective tissue dissociation cocktail, was showed to disaggregate cells more efficiently than trypsin and significantly (*p < 0.001) increased the level of single cell trapping from 69.5% (SD ± 8.6) to 80.6% (SD ± 4.3). In addition, the use of accutase instead of trypsin allows the cell's surface proteins to be better preserved which is desirable when studying communication events between cells.

Loading the particles and cells inside the microfluidic device was initially performed at relatively high velocities (≥1 mm/s) using a syringe pump. In order to avoid damaging the cells, lower velocities were used. It was reported that trapping cells within these microfluidic circuits is velocity independent (Tan WH and Takeuchi S 2007) and therefore cell trapping can be performed using slower velocities. To achieve velocities at the scale of microns per second, the syringe pump was replaced with a hydrostatic-driven feed. This was constructed by using pipette tips that were fitted into the Luer ports of the microfluidic device where the difference in the height of the media allows the flow velocity to be controlled. The

highest shear stress caused by the fluidic restrictions is found at the trap interface. In order to estimate the shear stresses experienced by the cells at the aperture between the two traps, a simulation study using SolidWorks was undertaken. A mean cell loading velocity of ~50 µm/s and a perfusion velocity of ~5 µm/s were nominally chosen for the simulation. As shown in figure 5.4.2, cell loading with a mean velocity of 50 µm/s resulted in a shear stress maxima of 0.7 dyn/cm^2. Perfusion and co-culture conditions where the flow velocity is reduced to 5 µm/s resulted in shear stresses of 0.07 dyn/cm^2. It has been reported that shear stresses values found *in vivo* are ~0.025 dyn/cm^2 (Di Carlo D *et al* 2006b, Kobel S *et al* 2010) which is lower than the values resulting in the fluidic co-culture system. However, shear stress levels of 0.07 dyn/cm^2 were suitable for cell co-culture and cell viability is investigated in section 5.4.6. It is important to note however that such microfluidic systems could be used to generate shear stress gradients across single cells with high precision. Although this is not the subject of this chapter, valuable information could be gained by investigating cytoskeletal architecture disruption under shear stress gradients. Previous groups have demonstrated for example that shear stress is an essential cue required for the development of the cardiovascular system (Topper JN *et al* 1998, Reneman RS *et al* 2006).
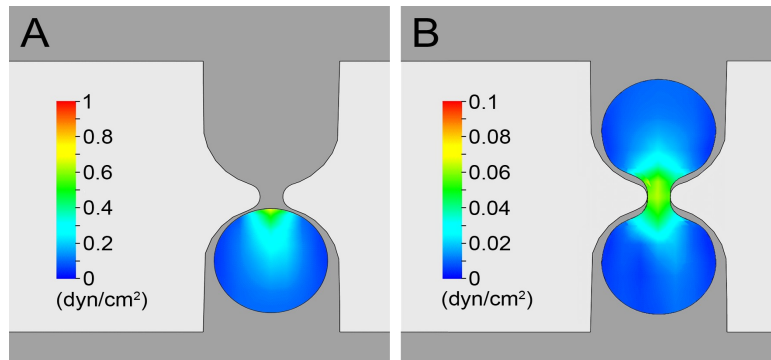
Figure 5.4.2: During secondary cell arraying with a mean velocity of 50 µm/s the previously arrayed cells experience moderate shear stress with a maxima of 0.7 dyn/cm^2 at the interface of the mirrored trap pair (A). Cellular couples perfused with a mean velocity of 5 µm/s experience minimal shear stress (a maxima of 0.07 dyn/cm^2) at the interface (B).

Due to the continuous flow, microfluidic perfusion systems can cause the depletion of soluble factors required for autocrine signalling or paracrine signalling found between cells. Although the elimination of such signals could prove beneficial for the study of juxtacrine signaling alone, a daily perfusion for 1 hour at ~5 µm/s is sufficient to replenish nutrients and maintain soluble factors in place for the remainder of the day. In the context of the presented proof-of-concept experiments, a continuous media perfusion of ~5 µm/s was used.

5.4.3 Flow ratio and trap dimensions

To reduce the possibility of shear induced damage to the cells during loading into the trap structures, the channel height (h = 28 µm) was made almost twice as large as the cells' mean diameter (14.6 µm). However, the height ratio recommended by Tan and Takeuchi was h <1.4. They also used a flow ratio of 3.95 (Tan). However, using h >1.4 requires lower flow ratios for successful sequential cell positioning. Flow ratios ranging from 0.6 to 1.8 were tested and the $Q_1/Q_2 > 1$ requirement for effective microfluidic arraying was confirmed. Figure 5.4.3(a) shows the successful arraying of single SW480 cells using a flow ratio of 1.4. The large variation in cell size (Ø SD ± 3.0 µm) did not significantly impact the level of trapping. As shown in figure 5.4.3(b), flow ratios ≥1.4 resulted in efficient and successful trapping (>98%) whereas flow ratios ≤1.0 resulted in only 25-30% trapping levels. Single cell trapping efficiency is also recorded in figure 5.4.3(b), with levels above 80% for flow ratios of 1.4 (80.6% (SD ± 4.3)) and 1.8 (85.0% (SD ± 2.8)). In addition, trap size variation in relation to cell arraying efficiency was also investigated (figure 5.4.3(c)). Here, a flow ratio of ≥1.4 was used in combination with trap sizes ranging from 15 µm (1 x cell-sized) to 37 µm (2.5 x cell-sized). For all trap dimensions, >99% of traps were occupied indicating that trap dimension has little effect on cell arraying. However, single cell trapping was only 68.6% (SD ± 6.7) for the larger trap size (trap ratio 2.5) when compared to the smaller trap sizes (~80%). The explanation behind this small but significant reduction (*p < 0.001) may be simply attributed to the fact that single cells occupying the larger pockets have greater freedom of positioning

with the possibility of not sufficiently blocking the aperture to divert the streamlines and subsequent cells. As a consequence, two or more cells could be trapped together.
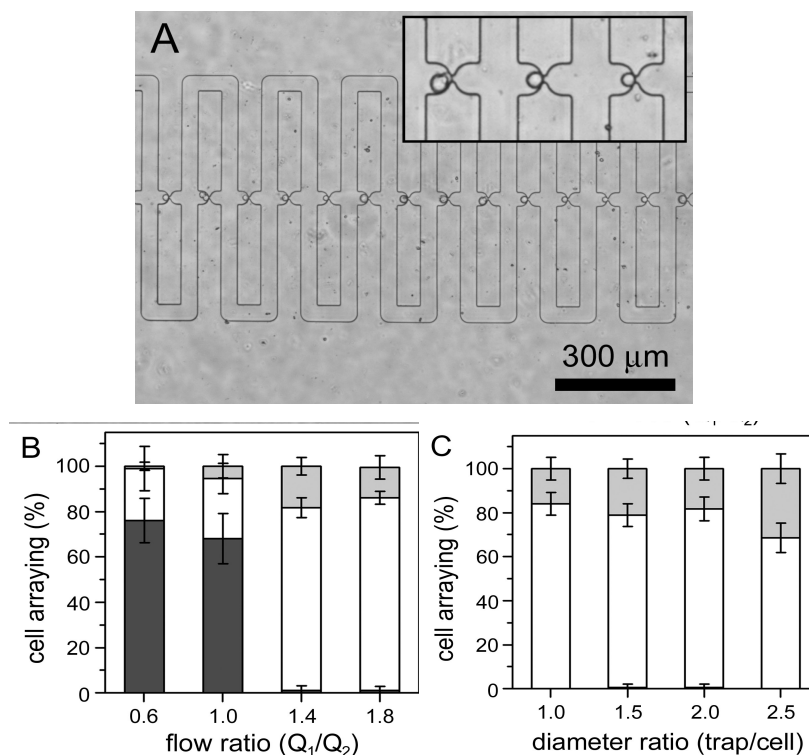
Figure 5.4.3: Highly efficient single cell arraying (A). In this image, 13 single cells are arrayed along with a sole doublet. Inset, enlarged view also demonstrating that the fluidic system was largely insensitive to variations in cell size, with individual trap:cell diameter values ranging from 1.5 to 2.2. The flow ratio significantly impacted the efficiency of single cell arraying (B). Devices with a trap:cell diameter of 1.8 were used. Flow ratios ≤1.0 resulted in large numbers of empty traps (dark grey). Flow ratios ≥1.4 enabled efficient single cell (white) arraying, with few traps containing multiple cells (light grey). The trap diameter had a small effect on single and multiple cell arraying (C). Devices producing a flow ratio of 1.4 were used.

5.4.4 Single cell coupling

In order for the cells to act as living valves they must remain viable after initial trapping. This will allow the cells to flatten and restore the $Q_1 > Q_2$ condition necessary for coupling the second cell type using a reversed flow. Figure 5.4.4 shows the single cell coupling process. Here MCF-7 cells are first trapped as single cells (a) and incubated for 4 hours to adopt a flat morphology typical of cells cultured on standard tissue culture substrates (b). Once the cell is in a flattened morphology the microstructure aperture is re-opened allowing a second cell to be trapped in the sister pocket (c) and over several hours of incubation, neighbouring single cells are able to physically contact each other (d).
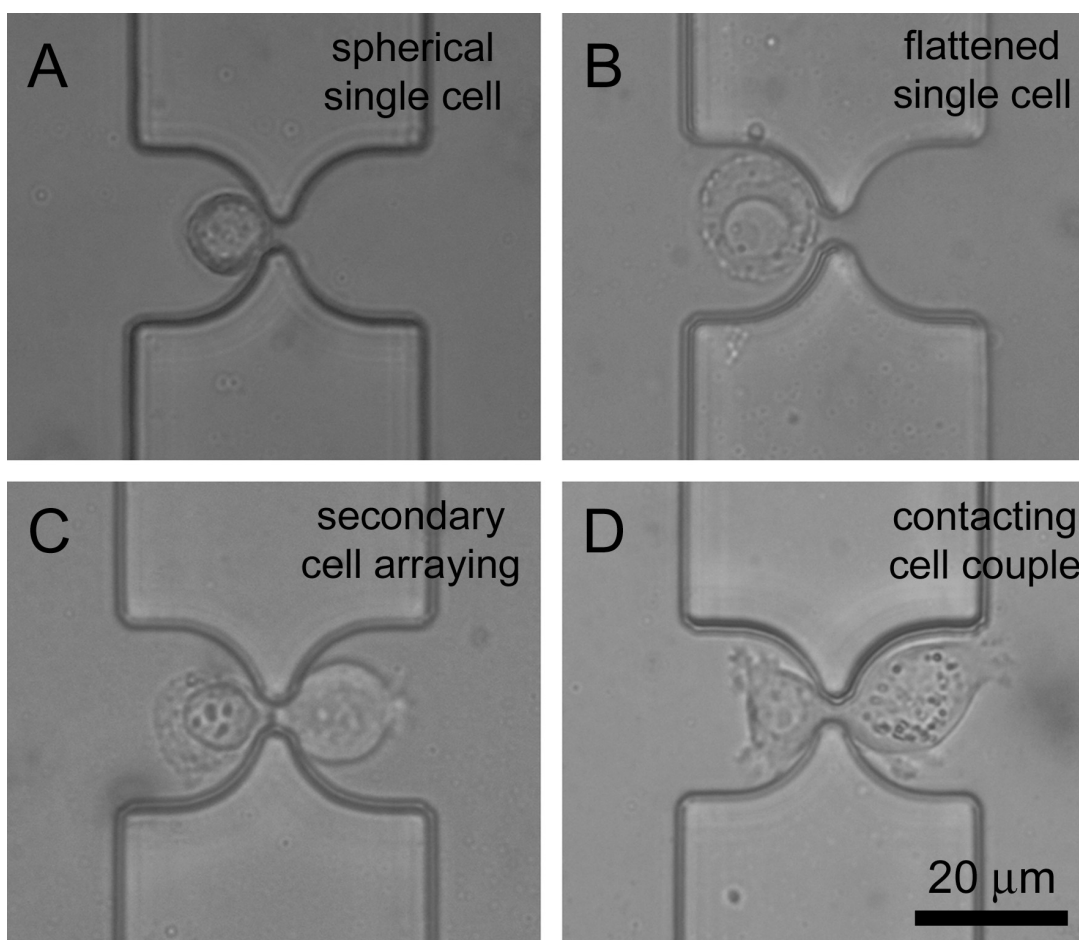
Figure 5.4.4: The cellular valving approach for single cell co-culture. Single cell arraying (A) and cellular adhesion, transforming to a flattened morphology to act as a valve in the open state (B). Introduction of the second cell (C) and following further culture the cell flattens and contacts the first cell (D).

The concept of using cellular valving in a microfluidic system is therefore demonstrated for the first time. The only prerequisite is that at least one cell type is able to adhere and flatten to act as the microfluidic valve. Since many cell types do exhibit these characteristics, the method could be widely applied to study co-cultures at the single cell level. In addition, cells of different sizes can also be studied with the only requirement that the aperture is smaller than the smallest cell type.

Importantly, the Tan and Takeuchi microfluidic architecture involves pairing cells within recessed trap structures such that the bypass channels are not blocked. This is not the case for systems involving the pairing of cells across a single channel, which naturally occlude the channels and can lead to the accumulation of further cells and eventual channel blockage (Lee PJ *et al* 2005).

The trapping of dead and non-adherent cells was another issue found when arraying single cells inside the microfluidic device. Indeed, about 10% of cells were trapped in a dead state and were unable to attach and spread. Moreover, the reversal of the flow for the second cell trapping was observed to direct the dead cells into the empty traps immediately across the microfluidic channel, blocking the trap and producing a pairs with one viable cell and one dead cell. To tackle this problem and avoid the trapping of dead cells, it is possible to exploit the differential times of cell adhesion and cell spreading (flattening). Characteristically, a cell response to a substrate is first to attach and then to spread. Following 2 hours of cell trapping, viable cells will have attached without flattening whereas dead cells will remain trapped and unattached. Since no cells have flattened at this stage, the cellular valves remain in a closed state and dead cells can then be pushed away from the system with a gentle reversal flow (~5 µm/s). Following a further 4 hours of incubation, the viable cells flatten and switch the cellular valve to the open position. This allows a second cell type to be introduced and trapped in the sister pocket ensuring that at least one co-culture cell partner is viable.

5.4.5 Cell migration inside the microchannels

Co-culture experiments require that cells maintain their positions for periods of time long enough (hours to days) for contact mode of communications to occur between the cell pairs. Therefore, using the presented microfluidic device, the cells must remain trapped within the pockets for as long as possible. During chip fabrication and device assembly, the underlying PDMS surface is plasma activated (oxidized) transforming it into a hydrophilic surface. Immediate introduction of the cell culture media keeps the PDMS in this hydrophilic state which is permissive to cell adhesion and migration as previously discussed in Chapter 2 (Delamarche E *et al* 1998, Frimat JP *et al* 2009). Unfortunately, the cells are not restricted to the pockets, and can migrate throughout the whole microfluidic chip surface during culture. As a consequence, following 24 hours of incubation, some cells had migrated from the pockets into the channel (figure 5.4.5(a)) with cells migrating up to the corners of the circuits by day 4 (figure 5.4.5(b)).
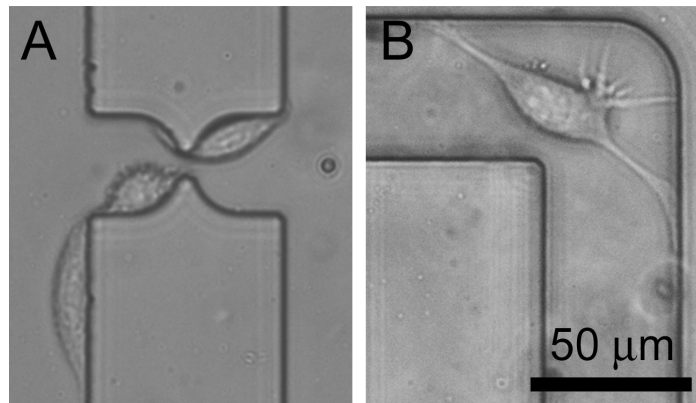
Figure 5.4.5: Without patterning the cell adhesion microenvironment, within 24 hours SW480 cells can migrate outside the trap (A) and along the serpentine channel following 4 days of culture (B).

In order to study single cell co-culture, migration events must be prevented or dramatically reduced. The knowledge gained from Chapter two on plasma oxidation patterning helped towards tackling this issue. Patterning cells within the

traps can be done by using our plasma stencilling approach. The concept is very simple. Following device assembly and plasma bonding, the device is left overnight in a dry state (instead of immediate wetting) for the diffusive return of oligomers to the surface (Kim J *et al* 2000). This allows the PDMS to return to its native hydrophobic state which provides a biologically inert background which resists cell adhesion (Frimat JP *et al* 2010, Hirschhaeuser F *et al* 2010, Hardelauf H *et al* 2010). When the chip is in this state the cells will be trapped but will not be able to attached and spread as the PDMS is hydrophobic. In order to selectively render the traps hydrophilic for cell adhesion, a plasma (same Tesla generator as described in Chapter two) was routed inside the microfluidic chip prior to cell loading. Similar to aqueous flows, the plasma takes the linear path of least resistance (R_1, figure 5.2.1), selectively oxidizing only the surfaces of the pockets to produce a hydrophilic state which supports cell adhesion. In this manner, only the pocket regions are suitable for cell adhesion while the remainder of the bypass circuit remains hydrophobic and resists cell migration. Cell migration outside the traps was decreased 6-fold by the use of this simple step with 96% of cells remaining within the traps for a period of 48 hours. With the efficient maintenance of cell positioning within the traps by plasma stencilling, a coupling efficiency of 66.9% (SD ± 8.5) could be obtained when using a flow ratio of 1.4 and a trap diameter of 30 µm. In comparison, a coupling efficiency of only 50.3% (SD ± 11.7) was recorded when plasma stencilling was not used.

5.4.6 Heterotypic coupling and gap junction formation

To fully demonstrate the heterotypic single cell coupling capability of the device, unlabelled cells were coupled to cells labeled with the fluorescent product of calcein AM metabolism. Figure 5.4.6(A) shows a row of six heterotypic single cell co-cultures. To confirm that communication is occurring between the cell pair candidates, the formation of gap junctions were investigated by labeling the connexin 43 protein within the connexon structures. Connexins are an intercellular network of protein channels that facilitates the cell-to-cell passage of

ions, hormones, and neurotransmitters and their presence is a general indication that the cells are able to communicate via contact modes. Following staining, successful Cx43 identification was observed and is shown in figure 5.4.6 (B and C). Here, the single cells were co-cultured for 24 hours and serves to demonstrate that on-chip conditions are suitable for the maintenance of viable cells with the formation of contact structures necessary for communication between single cells.
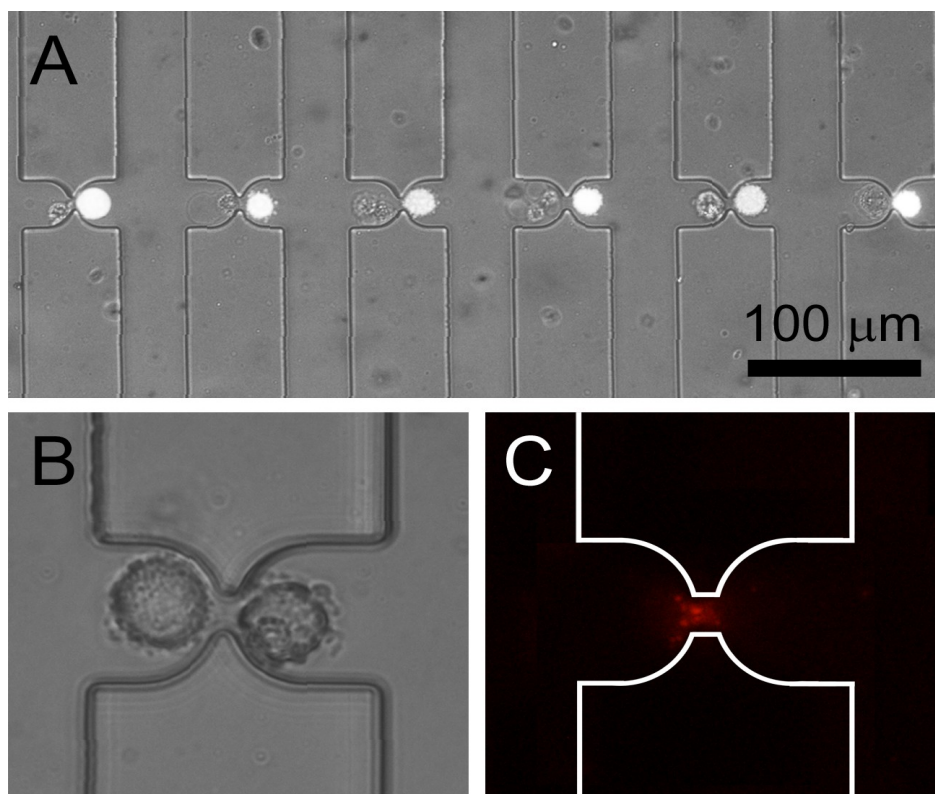
Figure 5.4.6: Heterotypic single cell co-culture. Unlabelled single SW480 cells co-cultured with single SW480 cells metabolically-labelled with the fluorescent product of calcein AM (A). A single cell couple (B), and the same couple immunostained for connexin 43 (red, C).

In an effort to fully optimize the device, the effect of trap size on cell coupling efficiency was also analyzed. Cell coupling was observed to be more efficient for larger traps then smaller traps. Figure 5.4.7 shows that coupling rates

of ~70% could only be obtained with the larger 30 and 37-μm-diameter traps (trap to cell ratios of 2 and 2.5 respectively), with the 37-μm-diameter traps showing the highest level of cell coupling (70.0% (SD ± 7.4)). Skelly AM and co-workers have reported similar values for their microfluidic reverse parking method (Skelley AM *et al* 2009). Smaller sized traps did not confer the same level of coupling efficiency, with 43.0% (SD ± 9.2) of coupling for the 20 μm-diameter traps and only 27.8% (SD ± 7.4) of coupling for the 15-μm-diameter traps. This could be explained by the fact that the area presented to the cells within the smaller traps is insufficient for complete cellular flattening and valving. Therefore fluidic streamlines remain diverted and the adjacent trap is not able to trap the second cell type, resulting in the overall coupling efficiency being decreased.
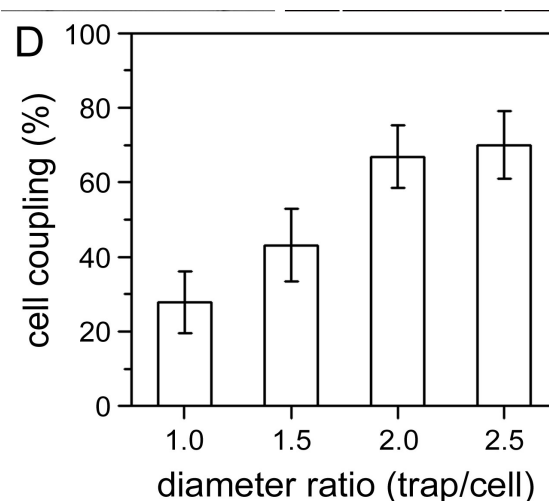
Figure 5.4.7: The effect of trap size on coupling efficiency. A trap:cell diameter ratio of ≥2.0 was required for efficient (~70%) cell coupling.

To demonstrate that the microflow conditions support sustained viability and growth, long term cell cultivation was performed and cell division was examined. HT29 proliferation during 5 days of on chip culture with continuous perfusion is shown in figure 5.4.8. Here, cell division occurs rapidly, with multi-cell clusters forming along the channels indicating sequential rounds of cellular division. This indicates that the chip provides excellent culture conditions and strongly suggests that the shear stresses are not damaging to the cells. For

comparison, the single cell trapping device reported by Kobel S *et al* (2010) could only maintain cell viability above 80% for 12 hours. However with cell division the single cell co-culture condition is no longer satisfied. Therefore, the rate of cell proliferation defines a window for single cell co-culture experiments. One suggestion to increase this experimental window would be to either biochemically-induce cell cycle synchronization or pre-select cells within the same cell cycle state by fluorescent activated cell sorting (FACS).
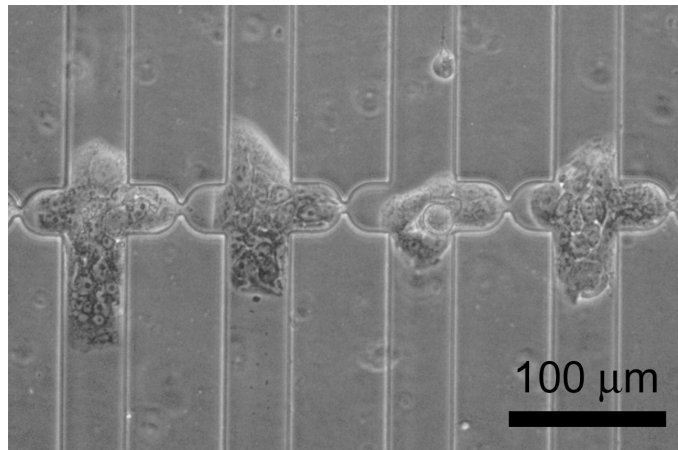
Figure 5.4.8: HT29 cells cultured on the microfluidic array for 5 days. The conditions support rapid proliferation, with multiple cell division events (3–4) during this period of culture.

5.5 Conclusions and outlook

In this chapter a novel cellular valving concept is introduced within a differential resistance microfluidic circuit for efficient single cell coupling. The research demonstrates that the device allows the culture of viable cells for the formation of cell-cell contacts in the context of single cell co-cultures. Intercellular communication was identified by positive staining of connexin 43. The cellular valving concept allows the coupling of both homotypic and heterotypic single

cells and requires that one or more of the cell types is adherent and able to flatten. The harvesting of individual cells for off-chip analysis still requires further developments but the presented method shows great potential in increasing our understanding of communication events occurring at the single cell level between heterogenous cell populations. Beyond this application, the research validates the concept of using the natural behaviour of cells for mechanical operations within microengineered environments.

For truly high throughput analysis, the device could be redesigned to include more traps. Device design could include bifurcation into 64 channels, each with 100 cell pair traps which could examine 6400 heterotypic single cell communication events. However, the harvesting of single cells prior to cell loading remains problematic. Insufficient cellular disaggregation was found even following 45 minutes of accutase treatment. One suggestion would be to perform a pre-selection of single cells using a FACS so that only monodisperse cell collections can be harvested and loaded inside the device. Alternatively, the integration of an upstream size-based cell aggregate separation method such as pinched-flow fractionation (Yamada *et al* 2004) for the selection of single cell populations prior to arraying is another solution.

The use of PDMS as the material of choice in microfluidic chip fabrication has been criticized due to its adsorption properties. Indeed, using PDMS leads to a loss by adsorption of soluble factors produced by the cells which are necessary for the development of normal cell behaviour (Regehr KJ *et al* 2009). This problem could be overcome by using biochemically inert materials such as glass with fabrication instead by methods such as deep reactive ion etching (DRIE) to fabricate a glass device instead of PDMS. The analysis of biological reactions on microfluidic chip is often impractical for the majority of methods available to biologists. Harvesting cells is particularly challenging when operating a closed microfluidic platform. Tan and Takeuchi have used a laser-induced technique to form microbubbles within the traps to eject trapped particles into the flow for collection and particle-based combinatorial compound libraries screening. Harvesting single cells with the knowledge of their individual co-culture histories

for off-chip analysis would be hugely beneficial. Indeed the bi-directional configuration of the circuit can be used to separate a cell pair following a period of co-culture. Trypsin or accutase could be introduced inside the circuit and used to detach the individual cells from the surface. Once in suspension the cell switches its morphology back to the spherical form, diverting the majority of the flow into the bypass channel. Laser-induced microbubble method could then be used to sequentially eject individual cells into the flow for retrieval at the outlet. Sequential cell ejection is essential as otherwise unoccupied traps will be able to trap cells due to the differential fluidic resistance circuit principles. Another solution to retrieve the cells following co-culture exposure is to tilt the device for gravity-driven cell removing following cell detachment. Here only one cell type could be recovered as once the first cell population has vacated, the now emptied pockets are available for trapping. To attain the 100% coupling necessary to prevent re-trapping within otherwise vacant traps, further optimization is required.

6

Conclusions

In modern cell biology there is an onus on the development of standardized, quantitative and high throughput analysis methods. In this thesis, new cell patterning methods are presented and the development of spatially standardized and quantitative cell biology assays are described.

Plasma stencilling methods were successfully developed and used to pattern 10 different cell types, including two poorly adherent cell lines, on hydrophobic PDMS, methylated glass and polystyrene substrates. The described methods are simple, involving a Tesla generator or dielectric barrier discharges (DBD) systems operating at atmospheric pressure and without gas supplies. This streamlined and versatile approach does not require printing molecules, but instead uses cell repellent hydrophobic substrates with selective plasma oxidisation for the differential assembly of serum proteins. Plasma stencilling is highly effective, reproducibly generating clearly defined cell patterns that are stable during long term cultivation. By using different stencil configurations and materials a variety of patterns including cellular arrays can be produced. Lastly, plasma stencilling complements PDMS–PDMS bonding to enable the inclusion of cell patterns within microfluidic systems. In summary, these plasma stencilling methods are simple, rapid, effective and these potentially universal cell line patterning techniques are ideally suited for adoption by the biology community.

Thin film PDMS patterning is another cell patterning approach that was successfully developed to pattern cell repellent thin film PDMS layers on glass and polystyrene substrates. Two techniques are presented: PDMS microcontact printing (µCP) and PDMS micro-embossing (µE). These straightforward and

inexpensive techniques can be used directly for patterning cells on the exposed regions of the substrate, thereby providing an adhesive surface that is identical to standard tissue culture surfaces. The thin film PDMS micropatterning techniques are cheap, simple, efficiently producing patterns over large areas as well as being of sufficiently high resolution to enable the shape of single cells to be controlled. thin film PDMS µE offers higher resolution, while thin film PDMS µCP offers excellent reproducibility and was also used to pattern 10 human cell lines as well as primary mouse hepatocytes and neurons. In addition to this widespread applicability, cell patterns remained stable during lengthy cultivation. Taken together, these features make the thin film PDMS µCP method accessible and desirable to biologists and microengineers alike. In conclusion, PDMS micropatterning is an effective capability that can be used to tackle outstanding challenges in the life sciences.

To establish PDMS patterning as a valuable tool for cell biology research, two spatially standardized bioanalytical platforms were developed. The first assay has involved the production of cellular arrays for the scalable production and analysis of 3-D tumour spheroids. In this study, thin film PDMS µCP was successfully used to pattern HT29 cells (as well as BT474 cells and NCI-H1792 cells) for the parallel and mass production of 3D spheroids. Large spheroids which were genuinely spherical and densely aggregated (equivalent to *in vivo* tissues) could be produced by this approach. The use of thin film PDMS µCP for the production of spheroid arrays shows that uniformly-sized tumour spheroids can be produced with high pattern occupancy (>98%) and low non-specific binding. This approach is ideal for spheroid mass production and thousands of spheroids can be cultivated in an industry standard 6-well plate with the robust character of the spheroids enabling harvesting with high efficiency (>99%).

In addition, a novel spatially standardized analytical display for high throughput neurotoxicity screening, termed the network formation assay (NFA), is also presented. The NFA combines the benefits of the neurite outgrowth assay with microarray principles to provide a spatially standardized analytical platform for the rapid, sensitive and reproducible assessment of the neurotoxic effects of

test substances. The NFA meets the urgent challenge of providing new *in vitro* methods with improved predictive value for the high throughput hazard classification of a massive catalogue of untested or inadequately tested substances. To demonstrate the NFA the human SH-SY5Y neuroblastoma cell line was patterned by thin film PDMS printing. A hexagonal geometry was used, where each cell adhesion node is located at an equal distance from neighbouring nodes. This arrangement standardizes the neurite outgrowth length to eliminate the extremely intensive task of length measurements. The array format also defines assay coordinates, and enables the neurites to be readily visualised. Together these features transform the neurite outgrowth assay into a reliable format for high throughput analysis. Moreover, interconnection, the basis of memory and learning, is a higher functional potential indicator than outgrowth alone. This new and simple assay enabled the reproducible, rapid and sensitive assessment of the inhibitory effects of acrylamide and pathway specific neurotoxicants. Straightforward developments are required for the widespread adoption of the assay to progress the neurotoxic hazard assessment effort as well as impact the field of neurodevelopmental biology. Currently, the NFA is being further developed for inclusion within microtitre plates, and by tailoring surface chemistries for use with gold standard *ex vivo* murine neurons and with neuronal precursor cells. In summary, these demonstrations and developments will promote the widespread adoption of the NFA to aid the neurotoxicity testing hazard assessment effort.

Furthermore, a novel cellular valving concept for use within a differential resistance microfluidic circuit for efficient single cell coupling is presented. The microfluidic conditions support the culture of viable cells and the formation of cell–cell contacts required for intercellular communication. The method is suitable for both homotypic and heterotypic single cell co-culture experiments, requires that one or more of the cell types is adherent and can be applied to differently sized cell type combinations. Simple developments are required for assay optimisation and the retrieval of individual cells for experiments requiring off-chip analysis. In summary, the microfluidic arraying technique has great potential to

advance co-culture research at the level of a pair of single cells and could be useful for the examination of single cell events to discern the behavioural heterogeneity of individuals within the tissue population. Beyond this application, the research also validates the concept of using the natural behaviour of cells for mechanical operations within microengineered environments.

The simple surface chemistry and microfluidic cell patterning techniques developed here are a first step to bring biologists closer to handling and designing these spatially organized bio-systems. In the future, microtechnologies will be increasingly available to biologists for the spatial control of cells, and will make cell biology more accurate, reproducible and quantitative. This spatially standardized cell biology vision places cell micropatterning as an invaluable and everyday part of quantitative cell biology, ultimately resulting in a change in the way scientists think about the experimental possibilities in cell biology. The ability to spatially organize cellular culture has the benefit of better mimicking the spatial organisation of cells found in living tissues and allows the generations of more accurate and efficient assays to address unmet challenges in cell biology. Therefore, microarrays and microfluidics can be used to spatially control cell biology, allowing high throughput and quantitative data to be recorded in a reproducible fashion and with automated image analysis capabilities. In addition, the level of complexity of *in vitro* cell biology experiments will increase from simple co-cultures to multiple cell types which are spatially ordered to represent more meaningful model or experimental systems. Temporal control is another dimension worthy of investigation and coupled to spatial organisation can be used to gain a deeper understanding of cell biology. The combination of spatial organisation, complexity control and temporal control over cellular events is the next key step for achieving more advanced *in vitro* systems that accurately preserve authentic *in-vivo* cellular behaviour. Figure 6.1 summarises this vision where an increase in the ability to control the spatial, temporal and complexity aspects increases the potential to obtain large quantities of high quality data. The

parallel nature of microtechnologies enables this information to be obtained in a high throughput manner. In turn, these advancements can lead to a more complete understanding of cell biology.
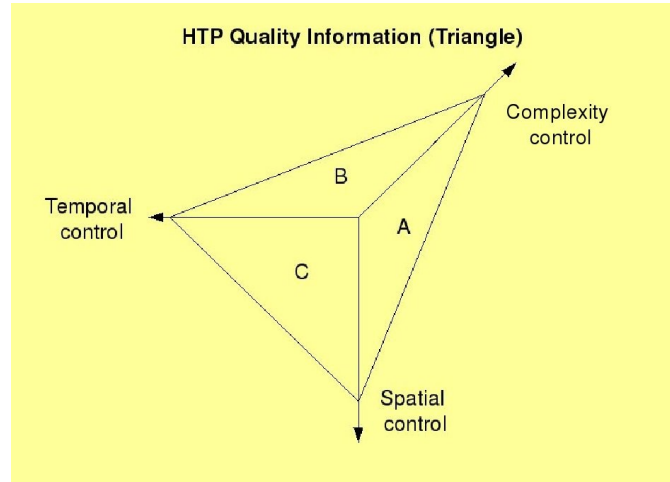
Figure 6.1: The effect of spatial, temporal and complexity control of experiments to obtain high quality cell biology information in a high throughput manner. Taken together, spatial, temporal and complexity control produce a 3-D information space (AxBxC) and microtechnologies can be used to access this information in a high quality and a high throughput manner.

In essence, the ability to spatially organise cell culture allows biologists to design more complex *in vitro* experiments and gain a better understanding of *in vivo* critical biological events. Taken together, this thesis demonstrates that it is possible to exploit cell micropatterning technologies for the realization of spatially standardized, highly reproducible and quantitative cell biology assays for both fundamental research and commercial applications.

References

Adem A, Mattsson MEK, Nordberg A and Påhlman S. Muscarinic receptors in human SH-SY5Y neuroblastoma cell line: regulation by phorbol ester and retinoic acid-induced differentiation. Dev. Brain. Res., 1987, 33, 2, 235–242.

Adlerz L, Beckman M, Holback S, Tehranian R, Toro VC and Iverfeldt K. Accumulation of the precursor-like protein APLP2 and reduction of APLP1 in retinoic acid-differentiated human neuroblastoma cells upon curcumin-induced neurite retraction. Mol. Brain Res., 2003, 119, 62–72.

Alvarez M, Long H, Onyia J, Hock J, Xu W and Bidwell JP. Rat osteoblast and osteosarcoma nuclear matrix proteins bind with sequence specificity to the rat type I collagen promoter. Endocrinology, 1997, 138(1), 482-9.

Akselrod GM, Timp W, Mirsaidov U, Zhao Q, Li C, Timp R, Timp K, Matsudaira P and G Timp. Laser-guided assembly of heterotypic three-dimensional living cell microarrays. Biophys. J. 2006, 91(9), 3465-73.

Anderson JR, Chiu DT, Jackman RJ, Cherniavskaya O, McDonald JC, Wu H, Whitesides SH and Whitesides GM. Fabrication of topologically complex 3-D microfluidic systems in PDMS by rapid prototyping. Anal Chem, 2000, 72(14), 3158-64.

Armstrong N, Hardin J and McClay DR. Cell-cell interactions regulate skeleton formation in the sea urchin embryo. Development, 1993, 199, 833-40.

Ashkin A, Dziedzic JM and Yamane T. Optical trapping and manipulation of single cells using infrared-laser beams. Nature, 1987, 330, 769–71.

Ashurst, WR; Yau, C; Carraro, C,Maboudian R and Dugger MT. Dichlorodimethylsilane as an anti-stiction monolayer for MEMS: A comparison to the octadecyltrichlosilane self-assembled monolayer. J mic mecha sys, 2001, 10(1) 41-49

Azioune A, Storch M, Bornens M, Théry M and Piel M. Simple and rapid process for single cell micro-patterning. Lab Chip, 2009, 9, 1640–42.

Ban J, Bonifazi P, Pinato G, Broccard FD, Studer L, Torre V and Ruaro ME. Embryonic stem cell-derived neurons form functional networks in vitro. Stem Cells, 2007, 25, 738–49.

Barbucci R, Torricelli P, Fini M, Pasqui D, Favia P, Sardella E, d'Agostino R and Giardino R. Proliferative and re-differentiative effects of photo-immobilized micro-patterned hyaluronan surfaces on chondrocyte cells. Biomaterials, 2005, 26, 7596-605.

Barron JA, Krizman DB and Ringeisen BR. Laser printing of single cells: statistical analysis, cell viability, and stress. Ann. Biomed. Eng., 2005, 2, 121-30.

Beamson G, Briggs D (1992) High resolution XPS of organic polymers: The Scienta ESCA 300 Database. Wiley, Chichester.

Beebe DJ, Mensing GA and Walker GM. Physics and applications of microfluidics in biology. Annu. Rev. Biomed. Eng., 2002, 4, 261-86.

Bernard A, Delamarche E, Michel B, Scmid H, Bosshard HR and Biebuyck H. Printing patterns of proteins. Langmuir, 1998, 14, 225-29.

Bhatia SN, Balis UJ, Yarmush ML and Toner M. Effect of cell-cell interactions in preservation of cellular phenotype: cocultivation of hepatocytes and nonparenchymal cells. FASEB J. 1999, 13(14), 1883-900.

Bhatia SN, Yarmush ML and Toner M. Controlling Cell Interactions by Micropatterning in Co-Cultures: Hepatocytes and 3T3 Fibroblasts. J. Biomed. Mater. Res., 1997, 34, 189–99.

Bidwell JP, Alvarez M, Feister H, Onyia J and Hock J. Nuclear matrix proteins and osteoblast gene expression. J. Bone Miner. Res., 1998, 13(2), 155-67.

Bietsch A and Michel B. Conformal contact and pattern stability of stamps used for soft lithography. J. Appl. Phys., 2000, 88, 4310-18.

Bosetti M, Boccafoschi F, Leigheb M and Cannas MF. Effect of different growth factors on human osteoblasts activities: a possible application in bone regeneration for tissue engineering. Biomol. Eng., 2007, 24(6), 613-8.

Brodkin KR, Garcia AJ and Levenston ME. Chondrocyte phenotypes on different extracellular matrix monolayers. Biomaterials, 2004, 24, 5929-38.

Brohim RM, Foresman PA, Hildebrandt PK and Rodeheaver GT. Early tissue reaction to textured breast implant surfaces. Ann. Plast. Surg., 1992, 4, 354-62.

Brzoska JB, Benazouz L and Rondelez F. Silanization of solid substrates- A step toward reproducibility. Langmuir, 1994, 10, 4367–73.

Burdick MM, McCarty OJT, Jadhav S, Konstantopoulos K. Cell-cell interactions in inflammation and cancer metastasis. 2001, Eng. Med. Bio. IEEE, 20(3), 86-91.

Bużańska L, Ruiz A, Zychowicz M, Rauscher H, Ceriotti L, Rossi F, Colpo P, Domańska-Janik K and Coecke S. Patterned growth and differentiation of human cord blood-derived neural stem cells on bio-functionalized surfaces, Acta Neurobiol. Exp., 2009, 69, 24–36.

Carroll GT, Wang D, Turro NJ and Koberstein JT. Photochemical micropatterning of carbohydrates on a surface. Langmuir, 2006, 22(6), 2899-905.

Chai J, Li B and Kwok DY. Selective surface modification and patterning by a micro-plasma discharge. Appl Phys Lett, 2005, 86:034107–107.4.

Chaudhury MK and Whitesides GM. Correlation Between Surface Free Energy and Surface Constitution. Science, 1992, 255, 1230–32.

Chen HY, McClelland AA, Chen Z, Lahann J. Solventless adhesive bonding using reactive polymer coatings. Anal Chem 2008, 80, 4119–24.

Chen CS, Mrksich M, Huang S, Whitesides GM and Ingber DE. Micropatterned surfaces for control of cell shape, position, and function. Biotechnol. Prog., 1998, 14, 356-63.

Chen CS, Mrksich M, Huang S, Whitesides GM and Ingber DE. Geometric control of cell life and death. Science, 1997, 276, 1425.

Chen SJ, Chien FC, Lin GY and Lee KC. Enhancement of the resolution of surface plasmon resonance biosensors by control of the size and distribution of nanoparticles. Opt. Lett., 2004, 29(12), 1390-2.

Christman KL, Requa MV, Enriquez-Rios VD, Ward SC and Bradley KA, Turner KL and Maynard HD. Submicron streptavidin patterns for protein assembly. Langmuir, 2006, 15;22(17), 7444-50.

Coecke S, Goldberg AM, Allen S, Buzanska L, Calamandrei G, Crofton K, Hareng L, Hartung T, Knaut H, Honegger P, Jacobs M, Lein P, Li A, Mundy W, Owen D, Schneider S, Silbergeld E, Reum T, Trnovec T, Monnet-Tschudi F, Bal-Price A. Workgroup report: incorporating in vitro alternative methods for developmental neurotoxicity into international hazard and risk assessment strategies. Environ. Health Perspect., 2007, 115(6):924-31.

Conrad PG, Nishimura PT, Aherne D, Schwartz BJ, Wu DM, Fang N, Zhang X, Roberts MJ and Shea RJ. Functional molecularly imprinted polymer microstructures fabricated using microstereolithography. Adv. Mater., 2003, 15(18), 1541.

Corey JM, Wheeler BC and Brewer GJ.Micrometer resolution silane-based patterning of hippocampal neurons: critical variables in photoresist and laser ablation processes for substrate fabrication. IEEE Trans. Biomed. Eng., 1996, 43 (9), 944–55.

Cornish T, Branch DW, Wheeler BC and Campanelli JT. Microcontact printing: a versatile technique for the study of synaptogenic molecules. Mol. Cell Neurosci., 2002, 20, 140–53.

Craighead H. Future lab-on-a-chip technologies for interrogating individual molecules. Nature, 2006, 442, 387–93.

Curtis SG and Forrester JV. The competitive effects of serum proteins on cell adhesion. J Cell Sci, 1984, 71, 17–35

Dang SM, Gerecht-Nir S, Chen J, Itskovitz-Eldor J and Zandstra PW. Controlled, Scalable Embryonic Stem cell differentiation culture. Stem Cell, 2004, 22, 275-82.

Danino AM, Basmacioglu P, Saito S, Rocher F, Blanchet-Bardon C, Revol M and Servant JM. Comparison of the capsular response to the Biocell RTV and Mentor 1600 Siltex breast implant surface texturing: a scanning electron microscopic study. Plast. Reconstr. Surg., 2001,108(7), 2047-52.

Das KP, Freudenrich TM and Mundy WR. Assessment of PC12 cell differentiation and neurite growth: a comparison of morphological and neurochemical measures. Neurotoxicol. Teratol., 2004, 26, 397–406.

Delamarche E, Bernard A, Schmid H, Bietsch A, Michel B and Biebuyck H. Microfluidic networks for chemical patterning of substrate: design and application to bioassays. J. Am. Chem. Soc., 1998, 120, 500–8.

deMello AJ. Control and detection of chemical reactions in microfluidic systems. Nature, 2006, 442, 394.

De Silva MN, Desai R and Odde DJ. Micro-Patterning of Animal Cells on PDMS Substrates in the Presence of Serum without Use of Adhesion Inhibitors. Biomed. Microdev., 2004, 6, 219–22.

De Silva MN, Paulsen J, Renn MJ and Odde DJ. Two-step cell patterning on planar and complex surface by precision spraying of polymers. Biotech. Bioeng., 2006, 93, 919–27.

Detrait E, Lhoest J-B, Knoops B, Bertrand P and van den Bosch de Aguilar P.Orientation of cell adhesion and growth on patterned heterogeneous polystyrene surface. J. Neurosci. Meth., 1998, 84, 193–204.

Dewez JL, Schneider YJ and Rouxhet PG. Coupled influence of substratum hydrophilicity and surfactant on epithelial cell adhesion. J. Biomed. Mat. Res., 1996, 30(3), 373–83.

Diao J, Young L, Kim S, Fogarty EA, Heilman SM, Zhou P, Shuler ML, Wu M, DeLisa MP. A three-channel microfluidic device for generating static linear gradients and its application to the quantitative analysis of bacterial chemotaxis. Lab Chip, 2006, 3, 381-8.

Di Carlo D, Wu LY and Lee LP. Dynamic single cell culture array. Lab Chip, 2006, 6, 1445–49.

Di Carlo D, Aghdam N and Lee LP. Single-cell enzyme concentrations, kinetics, and inhibition analysis using high-density hydrodynamic cell isolation arrays. Anal. Chem., 2006, 78(14), 4925–30.

Dillmore WS, Yousaf MN and Mrksich M. A photochemical method for patterning the immobilization of ligands and cells to self- assembled monolayers. Langmuir, 2004, 20, 7223–31.

Douglas ES, Chandra RA, Bertozzi CR, Matthies RA and Francis MB. Self-assembled cellular microarrays patterned using DNA barcodes. Lab Chip, 2007, 7, 1442–48.

El-Ali J, Peter K, Sorger PK and Jensen KF. Cells on chips. Nature, 2006, 442, 403–11.

Faley SL, Copland M, Wlodkowic D, Kolch W, Seale KT, Wikswo JP and Cooper JM. Microfluidic single cell arrays to interrogate signalling dynamics of individual, patient-derived hematopoietic stem cells. Lab Chip, 2009, 9, 2659–64.

Faley SL, Seale K, Hughey J, Schaffer DK, van Compernolle S, McKinney B, Baudenbacher F, Unutmaz D and Wikswo JP. Microfluidic platform for real-time signaling analysis of multiple single T cells in parallel. Lab Chip, 2008, 8, 1700–12.

Falconnet D, Csucs G, Grandin HM and Textor M. Surface engineering approaches to micropattern surfaces for cell-based assays. Biomaterials, 2006, 27, 3044-63.

Favia P, Sardella E, Gristina R and d'Agostino R. Novel plasma processes for biomaterials: micro-scale patteming of biomedical polymers. Surf. Coat. Technol., 2003, 169, 707–11.

Fink J, Thery M, Azioune A, Dupont R, Chatelain F, Bornensa M and Piel M. Comparative study and improvement of current cell micro-patterning techniques. Lab Chip, 2007, 7, 672–80.

Fiorini GS and Chiu DT. Disposable microfluidic devices: fabrication, function, and application. BioTechniques, 2005, 38, 429–46.

Fodor SP, Read JL, Pirrung MC, Stryer L, Lu AT and Solas D. Light-directed, spatially addressable parallel chemical synthesis. Science, 1991, 15(251), 767-73.

Folch A, Jo BH, Hurtado O, Beebe DJ and Toner M. Microfabricated elastomeric stencils for micropatterning cell cultures. J. Biomed. Mater. Res., 2000, 52, 346.

Folch A and Toner M. Microengineering of cellular interactions. Annu. Rev. Biomed. Eng., 2000, 2, 227–56.

Folch A and Toner M. Cellular Micropatterns on Biocompatible Materials. Biotechnol. Prog., 1998, 14, 388–92.

Forsby A and Blaauboer B. Integration of in vitro neurotoxicity data with biokinetic modelling for the estimation of in vivo neurotoxicity. Hum. Exp. Toxicol., 2007, 26, 333–38.

Francisco H, Yellen BB, Halverson DS, Friedman G and Gallo G. Regulation of Axon Guidance and Extension by 3-Dimensional Constraints. Biomaterials, 2007, 28, 3398–407.

Franzke J. The micro-discharge family (dark, corona, and glow-discharge) for analytical applications realized by dielectric barriers. Anal. Bioanal. Chem., 2009, 395, 549–57.

Friedrich J, Ebner R and Kunz-Schughart LA. Experimental anti-tumor therapy in 3-D: Spheroids—old hat or new challenge? Int. J. Radiat. Biol., 2007, 83, 849–71.

Friedrich J, Seidel C, Ebner R and Kunz-Schughart LA.Spheroid-based drug screen: considerations and practical approach. Nature Protoc., 2009, 4, 309–24.

Frimat JP, Mariani MM, Kettler R, Jacob P, Franzke J and West J. Directed Organization of cellular patterns. Proceedings of Nanotech2008, Montreux, Switzerland, 2008.

Frimat JP, Menne H, Michels A, Kittel S, Kettler R, Borgmann S, Franzke J and West J. Plasma stencilling for cell patterning. Anal. Bioanal. Chem., 2009, 395(3), 601–09.

Frimat JP, Sisnaiske J, Subbiah S, Menne H, Godoy P, Lampen P, Leist M, Franzke J, Hengstler JG, van Thriel C and West J. The network formation assay: a spatially standardized neurite outgrowth analytical display for neurotoxicity screening. Lab Chip, 2010, 10(6), 701–09.

Fukuda J, Sakai Y and Nakazawa K. Novel hepatocyte culture system developed using microfabrication and collagen/polyethylene glycol microcontact printing. Biomaterials, 2006, 27, 1061–70.

Gallego-Perez D, Higuita-Castro N, Sharma S, Reen RK, Palmer AF, Gooch KJ, Lee LJ, Lannutti JJ and Hansford DJ. High throughput assembly of spatially controlled 3D cell clusters on a micro/nanoplatform. Lab Chip, 2010, 10, 775–82.

Gartner ZJ and Bertozzi CR. Programmed assembly of 3-dimensional microtissues with defined cellular connectivity. Proc. Natl. Acad. Sci. U.S.A., 2009, 106(12), 4606–10.

Gelse K, Poschl E and Aigner T. Collagens structure, function, and biosynthesis. Adv. Drug Delivery Rev., 2003, 55, 1531-46.

Goessl A, Bowen-Pope DF and Hoffman AS. Control of shape and size of vascular smooth muscle cells in vitro by plasma lithography. J. Biomed. Mater. Res., 2001, 57, 15–24.

Goessl A, Garrison MD, Lhoest JB and Hoffman AS. Plasma lithography—thin-film patterning of polymeric biomaterials by RF plasma polymerization I: Surface preparation and analysis. J. Biomater. Sci—Polym. Ed., 2001, 12, 721–38.

Graber DJ, Zieziulewicz TJ, Lawrence DA, Shain W and Turner JN. Antigen binding specificity of antibodies patterned by microcontact printing. Langmuir, 2003, 19, 5431–34.

Gregoire FM, Smas CM and Sul HS. Understanding adipocyte differentiation. Physiol. Rev., 1998, 78(3), 783-809.

Hamilton DW and Brunette DM. The effect of substratum topography on osteoblast adhesion mediated signal transduction and phosphorylation. Biomaterials, 2007, 28(10), 1806-19.

Hamilton DW, Chehroudi B and Brunette DM. Comparative response of epithelial cells and osteoblasts to microfabricated tapered pit topographies in vitro and in vivo. Biomaterials, 2007, 28(14), 2281-93.

Hardelauf H, Frimat JP, Stewart JD, Schormann W, Chiang YY, Lampen P, Franzke J, Hengstler JG, Cadenas C, Kunz-Schughart LA and West J. Microarrays for the scalable production of metabolically-relevant tumour sheroids: A tool for modulating chemosensitivity traits. Submitted

Healy KE, Lom B and Hockberger PE. Spatial distribution of mammalian cells dictated by material surface chemistry. Biotechnol. Bioeng., 1994, 43, 792–800.

Healy KE, Thomas CH, Rezania A, Kim JE, McKeown PJ, Lom B and Hockberger PE. Kinetics of bone cell organisation and mineralization on materials with patterned surface chemistry. Biomaterials, 1996, 17, 195-208.

Heming R, Michels A, Olenici SB, Tombrink S and Franzke J. Electrical generators driving microhollow and dielectric barrier discharges applied for analytical chemistry. Anal. Bioanal. Chem., 2009, 395(3), 611-18

Herbert CB, McLernon TL, Hypolite CL, Adams DN, Pikus L, Huang CC, Fields GB, Letourneau PC, Distefano MD and Hu WS. Micropatterning gradients and controlling surface densities of photoactivatable biomolecules on self-assembled mono-layers of oligo(ethylene glycol) alkanethiolates. Chem. Biol., 1997, 4, 731–7. DELETE?

Hill CS, Wynne J and Treisman R. The Rho family GTPases RhoA, Rac1, and CDC42Hs regulate transcriptional activation by SRF. Cell, 1995, 81(7), 1159-70.

Hillborg H, Ankner JF, Gedde UW, Smith GD, Yasuda HK and Wikstrom K. "Crosslinked polydimethylsiloxane exposed to oxygen plasma studied by neutron reflectometry and other surface specific techniques".Polymer, 2000, 41: 6851–63.

Hirschhaeuser H, Menne H, Dittfeld C, West J, Mueller-Klieser W and Kunz-Schughart LA. Multicellular tumor spheroids: An underestimated tool is catching up again. J. Biotechnol., 2010, 148(1), 3-15

Ho CT, Lin RZ, Chang WY, Chang HY, Liu CH. Rapid heterogeneous liver-cell on-chip patterning via the enhanced field-induced dielectrophoresis trap. Lab Chip, 2007, 8, 81.

Hovis JS and Boxer SG. Patterning and composition arrays of supported lipid bilayers by microcontact printing. Langmuir, 2001, 17, 3400–5.

Huang W, Yang S, Shao J and Li YP. Signaling and transcriptional regulation in osteoblast commitment and differentiation. Front. Biosci., 2007, 1(12), 3068-92.

Hui EE and Bhatia SN. Micromechanical control of cell–cell interactions. Proc. Natl. Acad. Sci. U. S. A., 2007, 104(14), 5722–26.

Hung PJ and Park JK. A novel high aspect ratio microfluidic design to provide a stable and uniform microenvironment for cell growth in a high-throughput mammalian cell culture array. Lab Chip, 2005, 5, 44–48.

Hung PJ Lee PJ, Sabounchi P, Lin R and Lee LP. Continuous perfusion microfluidic cell culture array for high-throughput cell-based assays. Biotechnol. Bioeng., 2005, 89, 1–8.

Hunt TP, Issadore D, Westervelt RM. Integrated circuit/microfluidic chip to programmably trap and move cells and droplets with dielectrophoresis. Lab Chip, 2007, 8, 81-7.

Hynes RO. Integrins: bidirectional, allosteric signalling machines. Cell, 2002, 110, 673-87.

Hypolite CL, McLernon TL, Adams DN, Chapman KE, Herbert CB, Huang CC, Distefano MD and Hu WS. Formation of microscale gradients of protein using heterobifunctional photolinkers. Bioconjugate Chem., 1997, 8, 658–63.

Hyun J, Zhu Y, Liebmann-Vinson A, Beebe TP and Chilkoti A. Microstamping on an activated polymer surface: patterning biotin and streptavidin onto common polymeric biomaterials. Langmuir, 2001, 17, 6358–67.

Inaba R, Khademhosseini A, Suzuki H and Fukuda J. Electrochemical desorption of self-assembled monolayers for engineering cellular tissues. Biomaterials, 2009, 30, 3573–79.

Ingram M, Techy GB, Saroufeem R, Yazan O, Narayan KS, Goodwin TJ and Spaulding GF, Three-dimensional growth patterns of various human tumor cell lines in simulated microgravity of a NASA bioreactor. In Vitro Cell. Dev. Biol. Anim., 1997, 33, 459–66.

Ivascu A and Kubbies M. Rapid generation of single-tumor spheroids for high-throughput cell function and toxicity analysis. J. Biomol. Screen, 2006, 11, 922–32.

James CD, Davis RC, Kam L, Craighead HG, Isaacson M, Turner JN and Shain W. Patterned protein layers on solid substrates by thin stamp microcontact printing. Langmuir, 1998, 14, 741-44.

Janasek DJ, Franzke J and Manz A. Scaling and the design of miniaturized chemical analysis systems. Nature, 2006, 442, 374–80.

Jiang S, Schultz MJ, Chen Q, Moore JS and Granick S. Solvent-free synthesis of Janus colloidal particles. Langmuir, 2008, 24(18), 10073-7.

Kaji H, Kawashima T, Nishizawa M. Patterning cellular motility using an electrochemical technique and a geometrically confined environment. Langmuir, 2006, 25, 10784–87.

Kane RS, Takayama S, Ostuni E, Ingber DE and Whitesides GM. Patterning proteins and cells using soft lithography. Biomaterials, 1999, 20, 2363–76.

Kallury KMR, Krull UJ and Thompson M. X-ray photoelecton spectroscopy of silica surfaces treated with polyfunctional silanes. Anal. Chem., 1988, 60, 169–72.

Karp JM, Yeh J, Eng G, Fukuda J, Blumling J, Suh KY, Cheng J, Mahdavi A, Borenstein J, Langer R and Khademhosseini A. Controlling size, shape and homogeneity of embryoid bodies using poly(ethylene glycol) microwells. Lab Chip, 2007, 7, 786–94.

Keefer EW, Gramowski A, Stenger DA, Pancrazio JJ and Gross GW. Characterization of acute neurotoxic effects of trimethylolpropane phosphate via neuronal network biosensors. Biosens. Bioelectron., 2001, 16, 513–25.

Kelm JM and Fussenegger M. Microscale tissue engineering using gravity-enforced cell assembly. Trends Biotechnol., 2004, 22(4), 195–202.

Kesekowsky BG, Collard DM and Garcia AJ. Surface chemistry modulates fibronectin conformation and directs integrin binding and specificity to control cell adhesion. J. Biomed. Mater. Res. Part A, 2003, 66A, 247-59.

Khine M, Lau A, C. Ionescu-Zanetti, Seo J and Lee LP. A single cell electroporation chip. Lab Chip, 2005, 5, 38–43.

Kidoaki S and Matsuda T. Adhesion Forces of the Blood Plasma Proteins on Self-Assembled Monolayer Surfaces of Alkanethiolates with Different Functional Groups Measured by an Atomic Force Microscope. Langmuir, 1999, 15(22), 7639–46.

Kikuchi K, Sumaru K, Edahiro JI, Ooshima Y, Suguira S, Takagi T and Katamori T. Stepwise assembly of micropatterned co-cultures using photoresponsive culture surfaces and its application to hepatic tissue arrays. Biotechnol. Bioeng., 2009, 103(3), 552–61.

Kim G, Kim B and Brugger J. All photoplastic microstencil with self-alignment for multiple layer shadow-mask patterning. Sensors Actuators A-Phys., 2003, 107, 132–6.

Kim G, van den Boogaart MAF and Brugger J. Fabrication and application of a full wafer size micro/nanostencil for multiple length-scale surface patterning. Microelectr. Eng., 2003, 67(8), 609–14.

Kim J, Chaudhury MK and Owen MJ. Hydrophobic recovery of polydimethylsiloxane elastomer exposed to partial electrical discharge. J. Colloid Interface Sci. 2000, 226, 231–36.

Kim J and Somorjai GA. Molecular packing of lysozyme, fibrinogen, and bovine serum albumin on hydrophilic and hydrophobic surfaces studied by infrared-visible sum frequency generation and fluorescence microscopy. J. Am. Chem. Soc., 2003, 125, 3150–58.

Kim YT, Karthikeyan K, Chirvi S and Davé DP. Neuro-optical microfluidic platform to study injury and regeneration of single axons. Lab Chip, 2009, 7, 9(17), 2576-81.

Klein CI, Scholl M and Maelicke A. A neuronal network in vitro: formation and organisation on biofunctionalized surfaces. J. Mater. Sci-Mater. Med., 1999, 10, 721-27.

Kleinfeld D, Kahler KH, Hockberger PE. Controlled outgrowth of dissociated neurons on patterned substrates. J. Neuroscience, 1988, 8(11), 4098–120.

Knight JB, Vishwanath A, Brody JP, Austin RH: Hydrodynamic focusing on a silicon chip: mixing nanoliters in microseconds. Phys. Rev. Lett., 1998, 80, 3863-66.

Kobel S, Valero A, Latt J, Renaud P and Lutolf M. Optimization of microfluidic single cell trapping for long-term on-chip culture. Lab Chip, 2010, 10(7), 857-63.

Kojima R, Yoshimoto K, Takahashi E, Ichino M, Miyoshi H and Nagasaki Y. Spheroid array of fetal mouse liver cells constructed on a PEG-gel micropatterned surface: upregulation of hepatic functions by co-culture with nonparenchymal liver cells. Lab Chip, 2009, 9, 1991–93.

Kumar A and Whitesides GM. Features of gold having micrometer to centimeter dimensions can be formed through a combination of stamping with an elastomeric stamp and an alkanethiol ink followed by chemical etching. Appl. Phys. Lett., 1993, 63(14), 2002-04.

Lahann J, Balcells M, Rodon T, Lee J, Choi IS, Jensen KF and Langer R. Reactive polymer coatings: a platform for patterning proteins and mammalian cells onto a broad range of materials. Langmuir, 2002, 18, 3632–8.

Lanigan PMP, Chan K, Ninkovic T, Templer RH, French PMW, de Mello AJ, Willison KR, Parker PJ, Neil MAA, Ces O and D.R Klug DR. Spatially selective sampling of single cells using optically trapped fusogenic emulsion droplets: a new single-cell proteomic tool. J. R. Soc. Interf., 2008, 5, S161–68.

Lauer L, Klein C and Offenhausser A. Spot compliant neuronal networks by structure optimized micro-contact printing. Biomaterials, 2001, 22, 1925-32.

Lee PJ, Hung PJ, Shaw R, Jan L and Lee LP. Microfluidic application-specific integrated device for monitoring direct cell-cell communication via gap junctions between individual cell pairs. Appl. Phys. Lett., 2005, 86, 223902-3.

Lehnert D, Wehrle-Haller B, David C, Weiland U, Ballestrem C, Imhof BA and Bastmeyer M. Cell behaviour on micropatterned substrata: limits of extracellular matrix geometry for spreading and adhesion. J. Cell. Sci., 2004, 117, 41-52.

Leikina E, Mertts MV, Kuznetsova N and Leikin S. Type I collagen is thermally unstable at body temperature. Proc. Natl. Acad. Sci. U. S. A., 2002, 99(3), 1314-18.

Lein P, Silbergeld E, Locke P and Goldberg AM. In vitro and other alternative approaches to developmental neurotoxicity testing (DNT). Environ. Toxicol. Pharmacol., 2005, 19, 735–44.

Lein P, Locke P and Goldberg A. Meeting report: alternatives for developmental neurotoxicity testing. Environ. Health Perspect., 2007, 115(5), 764–68.

Leist M, Kadereit S and Schildknecht S.vFood for thought... on the real success of 3R approach. ALTEX, 2008, 25(1), 17–24.

Liu D, McIlvain HB, Fennell M, Dunlop J, Wood A, Zaleska MM, Graziani EI and Pong K. Screening of immunophilin ligands by quantitative analysis of neurofilament expression and neurite outgrowth in cultured neurons and cells. J. Neurosci. Methods, 2007, 163, 310–20.

Luk YY, Kato M and Mrksich M. Self-assembeled monolayers of alkanethiolates presenting mannitol groups are inert to protein adsorption and cell attachement. Langmuir, 2000, 16, 9604-9608.

Lunin VV, Rode SV and Samoilovich VG. Changes in the IR internal reflection and absorption spectra of AK 60/40 polyamide films after the action of a glow discharge plasma. Phy. Chem. Surf. Phe., 2008, 82(13), 2305-08.

Maas-Szabowski N, Stärker A and Fusenig NE. Epidermal tissue regeneration and stromal interaction in HaCaT cells is initaiated by TGF-α. J. Cell Sci., 2003, 116, 2937-48.

Maheshwari G, Brown G, Luffenburger DA, Wells A and Griffith LG. Cell adhesion and motility depend on nanoscale RGD clustering. J. Cell Sci., 2000, 113(10), 1677-86.

Maniotis AJ, Chen CS and Ingber DE. Demonstration of mechanical connections between integrins, cytoskeletal filaments, and nucleoplasm that stabilize nuclear structure. Proc. Natl. Acad. Sci. U. S. A., 1997, 94(3), 849-54.

Matsunaga T, Hosokawa M, Arakaki A, Taguchi T, Mori T, Tanaka T, Takeyama H. High-efficiency single-cell entrapment and fluorescence in situ hybridization analysis using a poly(dimethylsiloxane) microfluidic device integrated with a black poly(ethylene terephthalate) micromesh. Anal. Chem., 2008, 80(13), 5139-45.

McBeath R, Pirone DM, Nelson CM, Bhadriraj K and Chen CS. Cell shape, cytoskeletal tension and RhoA regulate stem cell lineage commitment. Dev. Cell, 2004, 6, 483-95.

McDonald MP, Spalding GC and Dholakia K. Microfluidic sorting in an optical lattice. Nature, 2003, 426, 421-24.

Michael KE, Vernekar VN, Keselowsky BG, Meredith JC, Latour RA and Garcia AJ. Adsorption-induced conformational changes in fibronectin due to interactions with well-defined surface chemistry. Langmuir, 2003, 19, 8033-40.

Millet LJ, Stewart ME, Sweedler JV, Nuzzo RG and Gillette MU. Microfluidic devices for culturing primary mammalian neurons at low densities. Lab Chip, 2007, 7, 987–94.

Mori R, Sakai Y and Nakazawa K. Micropatterned organoid culture of rat hepatocytes and HepG2 cells. J. Biosci. Bioeng., 2008, 106(3), 237–42.

Morin F, Nishimura N, Griscom L, Lepioufle B, Fujita H, Takamura Y and Tamiya E. Constraining the connectivity of neuronal networks cultured on microelectrode arrays with microfluidic techniques: a step towards neuron-based functional chips. Biosens. Bioelectron., 2006, 21, 1093–100.

Morooka T and Nishida E. Requirement of p38 mitogen-activated protein kinase for neuronal differentiation in PC12 cells. J. Biol. Chem., 1998, 273 (38), 24285–88.

Moses PR, Weir LM, Lennox JC, Finklea HO, Lenhard JR and Murray RW. X-ray photoelectron spectroscopy of alkylaminesilanes bound to metal oxide electrodes. Anal. Chem., 1978, 50, 576-85.

Mourzina Y, Kaiaguine D, Schulte P and Offenhäusser A. Patterning chemical stimulation of reconstructed neuronal networks. Anal. Chim. Acta, 2006, 575, 281–89.

Mrksich M, Dike LE, Tien J, Ingber DE and Whitesides GM. Using microcontact printing to pattern the attachment of mammalian cells to self-assembled monolayers of alkanethiolates on transparent films of gold and silver. Exp. Cell Res., 1997, 235, 305-13.

Nakazawa K, Izumi Y, Fukuda J and Yasuda T. Hepatocyte spheroid culture on a polydimethylsiloxane chip having microcavities. J. Biomater. Sci. Polymer Edn., 2006, 17(8), 859–73.

Nahmias YK, Gao BZ and Odde DJ. Dimensionless parameters for the design of optical traps and laser guidance systems. Appl. Opt., 2004, 43(20), 3999-4006.

Nelson CM, Raghavan S, Tan JL and Chen CS. Degradation of micropatterned surfaces by cell-dependent and -independent processes. Langmuir, 2003, 19, 1493-99.

Nishimura T, Ishima T, Iyo M and Hashimoto K. Potentiation of nerve growth factor-induced neurite outgrowth by fluvoxamine: role of sigma-1 receptors, IP3 receptors and cellular signaling pathways. PLoS ONE, 2008, 3(7), e2558.

Nordin-Andersson M, Forsby A, Heldring N, DeJongh J, Kjellstrand P and Walum E. Neurite degeneration in differentiated human neuroblastoma cells. Toxicol. In Vitro, 1998, 12, 557–60.

Nordin-Andersson M, Walum E, Kjellstrand P and Forsby A. Acrylamide-induced effects on general and neurospecific cellular functions during exposure and recovery. Cell Biol. Toxicol., 2003, 19, 43–51.

Odde DJ and Renn MJ. Laser-guided direct writing of living cells. Biotechnol. Bioeng., 2000, 67, 312–8.

Ostuni E, Kane R, Chen CS, Ingber DE, Whitesides GM (2000). Patterning Mammalian Cells Using Elastomeric Membranes. Langmuir, 2000, 16, 7811–19.

Otsuka H, Hirano A, Nagasaki Y, Okano T, Horiike Y and Kataoka K. Two-dimensional multiarray formation of hepatocyte spheroids on a microfabricated PEG-brush surface. ChemBioChem, 2004, 5, 850–55.

Påhlman S, Ruusala AI, Abrahamsson L, Mattsson ME and Esscher T. Retinoic acid-induced differentiation of cultured human neuroblastoma cells: a comparison with phorbolester-induced differentiation. Cell Differ., 1984, 14(2), 135–44.

Påhlman S, Mamaeva S, Meyerson G, Mattsson ME, Bjelfman C, Örtoft E and Hammerling U. Human neuroblastoma cells in culture: a model for neuronal cell differentiation and function. Acta Physiol. Scand. Suppl., 1990, 592, 25–37.

Patolsky F, Timko BP, Yu GH, Fang Y, Zheng G, Greytak AB, and Lieber CM, Detection, stimulation, and inhibition of neuronal signals with high-density nanowire transistor arrays. Science, 2006, 313, 1100–04.

Patrito N, McCague C, Norton PR, Petersen NO. Spatially controlled cell adhesion via micropatterned surface modification of poly(dimethylsiloxane). Langmuir, 2006, 23(2), 715–19.

Pardo L, Wilson WC and Boland TJ. Characterization of patterned self-assembled monolayers and protein arrays generated by the ink-jet method. Langmuir, 2003, 19, 1462–6.

Park J, Cho CH, Parashurama N, Li Y, Berthiaume F, Toner M, Tilles AW and Yarmush ML. Microfabrication-based modulation of embryonic stem cell differentiation. Lab Chip, 2007, 7, 1018–28.

Pease AC, Solas D, Sullivan EJ, Cronin MT, Holmes CP and Fodor SP. Light-generated oligonucleotide arrays for rapid DNA sequence analysis. Proc. Natl. Acad. Sci. U. S. A., 1994, 91(11), 5022-6.

Pittenger MF, Mackay AM, Beck SC, Jaiswal RK, Douglas R, Mosca JD, Moorman MA, Simonetti DW, Craig S and Marshak DR. Multilineage potential of adult human mesenchymal stem cells. Science, 1999, 284(5411), 143-7.

Psaltis D, Quake SR and Yang C. Developing optofluidic technology through the fusion of microfluidics and optics. Nature, 2006, 442, 381–86.

Radio NM and Mundy WR. Developmental neurotoxicity testing in vitro: models for assessing chemical effects on neurite outgrowth. Neurotoxicology, 2008, 29, 361–75.

Radio NM, Breier JM, Shafer TJ and Mundy WR. Assessment of chemical effects on neurite outgrowth in PC12 cells using high content screening. Toxicol. Sci., 2008, 105 (1), 106–18.

Rajagopalan P, Marganski WA, Brown XQ and Wong JY. Direct comparison of the spread area, contractility, and migration of balb/c 3T3 fibroblast adhered to fibronectin- and RGD-modified substrata. Biophys. J., 2004, 87(4), 2818-27.

Ramm P, Alexandrov Y, Cholewinski A, Cybuch Y, Nadon R and Soltys BJ. Automated screening of neurite outgrowth. J. Biomol. Screen, 2003, 8, 7–18.

Ravula SK, McClain MA, Wang MS, Glass JD and Frazier AB. A multielectrode microcompartment culture platform for studying signal transduction in the nervous system. Lab Chip, 2006, 6, 1530–36

Regehr KJ, Domenech M, Koepsel JT, Carver KC, Ellison-Zelski SJ, Murphy WL, Schuler LA, Alarid ET and Beebe DJ. Biological implications of polydimethylsiloxane-based microfluidic cell culture. Lab Chip, 2009, 9(15), 2132-9.

Ren XD, Kiosses WB and Schwartz MA. Regulation of the small GTP-binding protein Rho by cell adhesion and the cytoskeleton. EMBO J., 1999, 18(3), 578-85.

Reneman RS, Arts T and Hoeks AP. Wall shear stress-An important determinant of endothelial cell function and structure-in the arterial system in vivo. Discrepancies with theory. J. Vasc. Res., 2006, 43, 251-69.

Reyes DR, Perruccio EM, Becerra SP, Locascio LE and Gaitan M. Micropatterning neuronal cells on polyelectrolyte multilayers. Langmuir, 2004, 20 (20), 8805–11.

Rhee SW, Taylor AM, Tu CH, Cribbs DH, Cotman CW and Jeon NL. Patterned cell culture inside microfluidic devices. Lab Chip, 2005, 5, 102–07.

Roach P, Farrar D, Perry CC. Interpretation of protein adsorption: surface-induced conformational changes. J. Am. Chem. Soc., 2005, 127, 8168–73.

Romanova EV, Fosser KA, Rubakhin SS, Nuzzo RG and Sweedler JV. Engineering the morphology and electrophysiological parameters of cultured neurons by microfluidic surface patterning. FASEB J., 2004, 18(11), 1267–69.

Roth EA, Xu T, Das M, Gregory C, Hickman JJ and Boland T. Inkjet printing for high-throughput cell patterning. Biomaterials, 2004, 25, 3707–15.

Rozsnyai BF, Bloom SD and Resler DA. Computation of spectral arrays in hot plasmas using the Lanczos algorithm. Phys. Rev. A, 1991, 44(10), 6791-99.

Rowat AC, Bird JC, Agresti JJ, Rando OJ and Weitz DA. Tracking lineages of single cells in lines using a microfluidic device. Proc. Natl. Acad. Sci. U.S.A., 2009, 106(43), 18149–54.

Ruiz A, Bużańska L, Gilliland D, Rauscher H, Sirghi L, Sobanski T, Zychowicz M, Ceriotti L, Bretagnol F, Coecke S, Colpo P and Rossi F. Micro-stamped surfaces for the patterned growth of neural stem cells. Biomaterials, 2008, 29, 4766–74.

Ruoslahti E and Vaheri A. Cell-to-cell contact and extracellular matrix. Curr. Opin. Cell Biol., 1997, 9(5), 605-7.

Sakai Y and Nakazawa K. Technique for the control of spheroid diameter using microfabricated chips. Acta Biomaterialia, 2007, 3, 1033–40.

Sandau KB, Callsen D and Brüne B. Protection against Nitric Oxide-Induced Apoptosis in Rat Mesangial Cells demands mitogen activated protein kinases and reduced glutathione. 1999, Molecular Pharmacology, 56, 4, 744-51.

Sanjana NE and Fuller SB. A fast flexible ink-jet printing method for patterning dissociated neurons in culture. J. Neurosci. Methods, 2004, 136, 151–63.

Schaffner P and Dard MM. Structure and function of RGD peptides involved in bone biology. Cellular Mol. Life Sci., 2002, 60, 119-32.

Scholl M, Sprossler C, Denyer M, Krause M, Nakajima K, Maelicke A, W. Knoll and A. Offenhäusser. Ordered networks of rat hippocampal neurons attached to silicon oxide surfaces. J. Neurosci. Methods, 2000, 104, 65–75.

Sethuraman A, Han M, Kane RS, Belfort G. Effect of surface wettability on the adhesion of proteins. Langmuir, 2004, 20, 7779–88.

Sigal GB, Mrksich M, Whitesides GM. Effect of Surface Wettability on the Adsorption of Proteins and Detergents. J. Am. Chem. Soc., 1998, 120, 3464–73.

Sigal GB, Bamdad C, Barberis A, Strominger J and Whitesides GM. A self-assembled monolayer for the binding and study of histidine-tagged proteins by surface plasmon resonance. Anal Chem., 1996, 68(3), 490-7.

Sikavitsas VI, Temenoff JS and Mikos AG. Biomaterials and bone mechanotransduction. Biomaterials, 2001, 22(19), 2581-93.

Singer A and Hodes RJ. Mechanisms of T cell-B cell interaction. 1983, Ann. Rev. Immunol, 1, 211-41.

Singhvi R, Kumar A, Lopez GP, Stephanopoulos GN, Wang DI, Whitesides and Ingber DE. Engineering cell shape and function. Science, 1994, 264, 696-98.

Skelley AM, Kirak O, Suh H, Jaenisch R and Voldman J. Microfluidic control of cell pairing and fusion. Nat. Methods, 2009, 6(2), 147–52.

Sordella R, Jiang W, Chen GC, Curto M and Settleman J. Modulation of Rho GTPase signaling regulates a switch between adipogenesis and myogenesis. Cell, 2003, 113(2), 147-58.

Stone HA, Stroock AD and Ajdari A. Engineering flows in small devices: microfluidics towards a lab-on-a-chip. Annu. Rev. Fluid. Mech., 2004, 36, 381.

Suh KY, Kim YS and Lee HH. Capillary Force Lithography. Adv. Mat. 2001, 13, 1386–89.

Sutherland RM. Cell and environment interactions in tumor microregions: the multicell spheroid model. Science, 1988, 240, 177–84.

Suzuki I, Sugio Y, Jimbo Y and Yasuda K. Stepwise pattern modification of neuronal network in photo-thermally-etched agarose architecture on multi-electrode array chip for individual-cell-based electrophysiological measurement. Lab Chip, 2005, 5 (3), 241–47.

Takano H, Komuro I, Oka T, Shiojima I, Hiroi Y, Mizuno T and Yazaki Y. The Rho family G proteins play a critical role in muscle differentiation. Mol. Cell Biol., 1998, 18(3), 1580-89.

Takayama S, Ostuni E, LeDuc P and Whitesides GM. Selective chemical treatment of cellular microdomains using multiple laminar streams. Chem. Biol., 2003, 10, 123.

Tamura T, Sakai Y and Nakazawa K. Two-dimensional microarray of HepG2 spheroids using collagen/polyethylene glycol micropatterned chip. J. Mater. Sci. Mater. Med., 2008, 19, 2071–77.

Tan HML, Fukuda H, Akagi T, Ichiki T. Surface modification of poly(dimethylsiloxane) for controlling biological cells' adhesion using a scanning radical microjet. Thin Solid Films, 2007, 515(12), 5172–78.

Tan W and Desai TA. Layer-by-layer microfluidics for biomimetic three-dimensional structures. Biomaterials, 2004, 25(7-8), 1355-64.

Tan WH and Takeuchi S. A trap-and-release integrated microfluidic system for dynamic microarray applications. Proc. Natl. Acad. Sci. U.S.A., 2007, 104(4), 1146–51.

Taylor AM, Rhee SW, Tu CH, Cribbs DH, Cotman CW and Jeon NL. Microfluidic Multicompartment Device for Neuroscience Research. Langmuir, 2003, 19(5), 1551–56.

Taylor AM, Blurton-Jones M, Rhee SW, Cribbs DH, Cotman CW and Jeon NL. A microfluidic culture platform for CNS axonal injury, regeneration and transport. Nature Methods, 2005, 2 (8), 599–605.

Templin MF, Stoll D, Schrenk M, Traub PC, Vöhringer CF and Joos TO. Protein microarray technology. Trends Biotechnol., 2002, 20(4), 160-66.

Teshima T, Ishihara H, Iwai K, Adachi A and Takeuchi S. A dynamic microarray device for paired bead-based analysis.Lab Chip, 2010, 10(18), 2443-8.

Timmins NE and Nielsen LK. Generation of multicellular tumor spheroids by the hanging-drop method. Methods Mol. Med., 2007, 140, 141–51.

Théry M, Pepin A, Dressaire E, Chen Y and Bornens M. Cell distribution of stress fibres in response to the geometry of the adhesive environment. Cell Motil. Cytoskeleton, 2006, 63, 341–55. (a)

Théry M, Racine V, Piel M, Pepin A, Dimitrov A, Chen Y, Sibarita JB and Bornens M. Anisotropy of cell adhesive microenvironment governs cell internal organization and orientation of polarity. Proc. Natl. Acad. Sci. U. S. A., 2006, 103, 19771–76. (b)

Théry M, Racine V, Pepin A, Piel M, Chen Y, Sibarita JB and Bornens M. The extracellular matrix guides the orientation of the cell division axis. Nat. Cell Biol., 2005, 7, 947–53.

Thomas CA, Springer PA, Loeb GE, Berwald-Netter Y and Okun LM. A miniature microelectrode array to monitor the bioelectric activity of cultured cells. Exp. Cell Res., 1972, 74, 61–66.

Thomas CH, Collier JH, Sfeir CS and Healy KE. Engineering gene expression and protein synthesis by modulation of nuclear shape. Proc. Natl. Acad. Sci. U. S. A., 2002, 99(4), 1972-77.

Thomas CH, Lhoest JB, Castner DG, McFarland CD and Healy KE. Surfaces designed to control the projected area and shape of individual cells. J. Biomech. Eng—Trans ASME, 1999, 121, 40–8.

Topper JN, Cai J, Stavrakis G, Anderson KR, Woolf EA, Sampson BA, Schoen FJ, Falb D and Gimbrone MA Jr. Human prostaglandin transporter gene (hPGT) is regulated by fluid mechanical stimuli in cultured endothelial cells and expressed in vascular endothelium in vivo. Circulation. 1998, 98(22), 2396-403.

Tourovskaia A, Barber T, Wickes BT, Hirdes D, Grin B, Castner DG, Healy KE and Folch A. Micropatterns of Chemisorbed Cell Adhesion-Repellent Films Using Oxygen Plasma Etching and Elastomeric Masks. Langmuir 2003, 19(11), 4754–64.

Trau, M.; Murray, B. S.; Grant, K.; Grieser, F. An ellipsometric study of thin films on silica plates formed by alkylchlorosilylation reagents. J. Colloid Interface Sci.1992, 148, 182–89.

Tscherter A, Heuschkel MO, Renaud P and Streit J. Spatiotemporal characterization of rhythmic activity in rat spinal cord slice cultures. Eur. J. Neurosci., 2001, 14, 179–90.

Tsuang YH, Lin FH, Sun JS, Hang YS and Liu HC. In vitro cell behavior of osteoblasts on Pyrost bone substitute. Anat. Rec., 1997, 247(2), 164-9.

Turcu F, Tratsk-Nitz K, Thanos S, Schuhmann W and Hieduschka P. Ink-jet printing for micropattern generation of laminin for neuronal adhesion. J. Neurosci. Methods, 2003, 131, 141–8.

Underwood PA, Steele JG and Dalton BA. Effects of polystyrene surface chemistry on the biological activity of solid phase fibronectin and vitronectin, analysed with monoclonal antibodies. J. Cell Sci., 1993, 104, 793–803.

Ungrin MD, Joshi C, Nica A, Bauwens C and Zandstra PW. Reproducible, ultra high-throughput formation of multicellular organization from single cell suspension-derived human embryonic stem cell aggregates. PLoS ONE, 2008, 3(2), e1565.

Valero A, Post JN, van Nieuwkasteele JW, Ter Braak PM, Kruijer W and van den Berg A. Gene transfer and protein dynamics in stem cells using single cell electroporation in a microfluidic device. Lab Chip, 2008, 8, 62–67.

van Kooten TG and von Recum AF. Cell adhesion to textured silicone surfaces: the influence of time of adhesion and texture on focal contact and fibronectin fibril formation. Tissue Eng., 1999, 5, 223–40.

van Vliet E, Stoppini L, Balestrino M, Eskes C, Griesinger C, Sobanski T, Whelan M, Hartung T and Coecke S. Electrophysiological recording of re-aggregating brain cell cultures on multi-electrode arrays to detect acute neurotoxic effects. Neurotoxicolog, 2007, 6, 1136-46.

Vutskits L, Gascon E, Tassonyi E and Kiss JZ. Effect of ketamine on dendritic arbor development and survival of immature GABAergic neurons in vitro. Toxicol. Sci., 2006, 91(2), 540–49.

Wang W, Itaka K, Ohba S, Nishiyama N, Chung U, Yamasaki Y and Katoaka K. 3D spheroid culture system on micropatterned substrates for improved differentiation efficiency of multipotent mesenchymal stem cells. Biomaterials, 2009, 30, 2705–15.

Welsh CF, Roovers K, Villanueva J, Liu Y, Schwartz MA and Assoian RK. Timing of cyclin D1 expression within G1 phase is controlled by Rho. Nat. Cell Biol., 2001, 3(11), 950-7.

West J, Michels A, Kittel S, Jacob P and Franzke J. Microplasma writing for surface-directed millifluidics. Lab Chip, 2007, 7(8), 981–83.

Wheeler BC, Corey JM, Brewer GJ and Branch DW. Microcontact printing for precise control of nerve cell growth in culture. J. Biomech. Eng—Trans. ASME, 1999, 121, 73–8.

Whitesides GM, Ostuni E, Takayama S, Jiang X and Ingber DE. Soft Lithography in Biology and Biochemistry. Ann. Rev. Biomed. Eng., 2001, 3, 335-73.

Wilson CJ, Clegg RE, Leavesley DI and Pearcy MJ. Mediation of biomaterial-cell interactions by adsorbed proteins: a review. Tissue Eng., 2005, 11, 1–18.

Wlodkowic D, Faley S, Zagnoni M, Wikswo JP and Cooper JM.
Microfluidic single-cell array cytometry for the analysis of tumor apoptosis. Anal. Chem., 2009, 81, 5517–23.

Wright D, Rajalingam B, Karp JM, Selvarasah S, Ling Y, Yeh J, Langer R, Dokmeci MR and Khademhosseini A. Reusable, reversibly sealable parylene membranes for cell and protein patterning. J. Biomed. Mat. Res., 2008, 85A, 530–38.

Wright D, Rajalingam B, Selvarasah S, Dokmeci MR and Khademhosseini A. Generation of static and dynamic patterned co-cultures using microfabricated parylene-C stencils. Lab Chip, 2007, 7, 1272–79.

Xia YN and Whitesides GM. Soft Lithography. Angew. Chem. Int. Ed., 1998, 37, 550-75.

Xia YN and Whitesides GM. Soft lithography. Ann. Rev. Mater. Sci., 1998, 28, 153-184.

Xu JL, Khor KA, Lu YW, Chen WN and Kumar R. Osteoblast interactions with various hydroxyapatite based biomaterials consolidated using a spark plasma sintering technique. J. Biomed. Mater. Res. B Appl. Biomater., 2008, 84(1), 224-30.

Yager P, Edwards T, Fu E, Helton K, Nelson K, Tam MR and Weigl BH. Microfluidic diagnostic technologies for global public health. Nature, 2006, 442, 412–18.

Yamato M, Konno C, Koike S, Isoi Y, Shimizu T, Kikuchi A, Makino K and Okano T. Nanofabrication for micropatterned cell arrays by combining electron beam-irradiated polymer grafting and localized laser ablation. J. Biomed. Mater. Res. Part A, 2003, 67A, 1065–71.

Yang M, Li CW and Yang J. Cell docking and on-chip monitoring of cellular reactions with a controlled concentration gradient on a microfluidic device. Anal. Chem., 2002, 74(16), 3991–4001.

Yoshimoto K, Ichino M and Nagasaki Y. Inverted pattern formation of cell microarrays on poly(ethylene glycol) (PEG) gel patterned surface and construction of hepatocyte spheroids on unmodified PEG gel microdomains. Lab Chip, 2009, 9(9), 1286–89.

Yousaf MN, Houseman BT and Mrksich M. Using electroactive substrates to pattern the attachment of two different cell populations. Proc. Natl. Acad. Sci. U.S.A., 2001, 98(11), 5992–96.

Yamada M, Nakashima M and Seki M. Pinched flow fractionation: continuous size separation of particles utilizing a laminar flow profile in a pinched microchannel. Anal. Chem., 2004, 76(18), 5465-71.